Visualization and velocity measurement of unsteady flow in a gas generator using cold-flow technique

by

Subrahmanyam Kuppa

Dissertation submitted to the Faculty of the

Virginia Polytechnic Institute and State University

in partial fulfillment of the requirements for the degree of

Doctor of Philosophy

in

Aerospace & Ocean Engineering

APPROVED:

Dr.James F. Marchman III, Chairman

Dr.Joseph A. Schetz

Dr.Antoni K. Jakubowski

Dr.Wayne L. Neu

Dr.Dana A. Walker

December 1989

Blacksburg, Virginia

Visualization and velocity measurement of unsteady flow in a gas generator using cold-flow technique

by

Subrahmanyam Kuppa

Dr.James F. Marchman III, Chairman

Aerospace & Ocean Engineering

(ABSTRACT)

Modeling of internal flow fields with hot, compressible fluids and sometimes combustion using cold flow techniques is discussed. The flow in a gas generator has been modeled using cold air. Experimental set up was designed and fabricated to simulate the unsteady flow with different configurations of inlet tubes. Tests were run for flow visualization and measurement of axial velocity at different frequencies ranging from 4 Hz to 12 Hz.

Flow visualization showed that the incoming flow was a complex jet flow confined to a cylindrical enclosure, while the outgoing flow resembled the venting of a pressurized vessel. The pictures show a complex flow pattern due to the angling of the jet towards the wall for the bent tube configurations and straightened flows with straight tube and other configurations with straighteners.

Velocity measurements were made at an inlet Re of 8.1×10^4 based on maximum velocity and inlet diameter using a single sensor hot wire anemometer at several locations in the plane of the inlet tube at 4 Hz, 8 Hz and 12 Hz for the straight tube and bent tube inlet configurations. The axial velocity near the entrance showed a strong component of the forcing frequency. Phase averaged mean velocities were observed to be well defined during charging and diminished during venting inside the cylinder. The jet flow penetrated most for the 4 Hz and least for the 12 Hz case.

For the straight tube inlet comparison with a steady flow measurement of sudden expansion flow showed a qualitative similarity of the mean axial velocity distribution and centerline velocity decay during the charging phases.

For the bent tube inlet case the contour plots showed the flow tendency towards the wall. Two cells were seen in the contours for the 8 Hz and 12 Hz cases. The deviation of the point of occurrence of maximum velocity in a radial profile was found to be about 6.5°. Entrance velocity profiles showed symmetry for the straight tube inlet while were skewed for the bent tube inlet.

Contour plots of the phase averaged axial turbulence intensity for bent tube cases showed higher values in the core and near the wall in the region of impingement. Axial turbulence intensity measured for the straight tube case showed features as observed in an axisymmetric sudden expansion flow.

Acknowledgements

I wish to express my deep appreciation and gratitude to my advisor, Dr. James F. Marchman III for the the constant encouragement, help and understanding during my stay at Virginia Tech while pursuing the graduate program.

Dr. Joseph A. Schetz not only served on the committee but was also involved in the initial phases of this study. I have immensely benefitted from him both in the class and outside. Thanks are due to Dr. Schetz for that and more.

I also thank Dr. Antoni K. Jakubowski, Dr. Wayne L. Neu and Dr. Dana A. Walker for being on the committee and contributing to the author's education.

Thanks are due to and for able support with workshop and instrumentation expertise. I thank all my fellow graduate students for their help and assistance.

Last, but not the least, I would like to thank Dr. R.H. Woodward Waesche for the invaluable experience I gained through this and other projects.

To my parents,

for their love and support.

Table of Contents

1.0 Introduction **1**

1.1 IC Engine Flow Research 3

1.2 Unsteady Axisymmetric Subsonic jets 4

1.3 Biomedical Flow Research 6

1.4 Present Study 6

2.0 Flow Modeling **9**

2.1 Past studies with partial modeling 9

2.2 Modeling of gas generator flow 13

3.0 Experimental Set-Up and Operation **15**

3.1 Flow Visualization 16

3.1.1 Model - Construction and Assembly 16

3.1.2 Flow Visualization Materials 18

3.2 Velocity Measurements 21

3.2.1 Model - Construction and Assembly 21

3.2.2 Data Acquisition 23

3.2.3 Data Reduction 24
3.2.4 Uncertainties 26
3.3 Operation 27

4.0 Results and Discussion 29
4.1 Flow Visualization Results 29
4.2 Velocity Measurements 33

5.0 Conclusion 43

References 46

Figures 51

Vita 142

List of Illustrations

Figure 1. Basic geometry of the flow problem. 53

Figure 2. D-5 PBCS gas generator system. 54

Figure 3. Flow patterns in the combustion zone of a gas turbine system. 55

Figure 4. Model set up for flow visualization tests. 56

Figure 5. Inlet cap for different inlet tube configurations of the model. 57

Figure 6. Model center section with flanges. 58

Figure 7. Dome on the entrance side of the model. 59

Figure 8. Dome on the side away from entrance side of the model. 60

Figure 9. The 70° and straight inlet tube configurations for the model. 61

Figure 10. Schematics of the different copper entrance configurations used with the model in flow visualization tests. 62

Figure 11. Arrangement for flow visualization with silk tufts. 63

Figure 12. Model set up for velocity measurements. 64

Figure 13. Locations of velocity measurements for straight inlet tube. 65

Figure 14. Locations of velocity measurements for bent inlet tube. 66

Figure 15. Side view of gas generator model with 70° entrance tube. 67

Figure 16. Another side view of gas generator model with 70° entrance tube. 68

Figure 17. Oblique view of gas generator model with 70° entrance tube. 69

Figure 18. Flow pattern obtained with 20° offset entrance tube. 70

Figure 19. Frequency spectrum of the axial velocity on the centerline ; x/d0 = 3.38; at 4 Hz. 71

Figure 20. Frequency spectrum of the axial velocity on the centerline ; x/d0 = 3.38; at 8 Hz. 72

Figure 21. Frequency spectrum of the axial velocity on the centerline ; x/d0 = 3.38; at 12 Hz. 73

Figure 22. Phase averaged mean pressure and velocity traces on the centerline over a cycle at x/d0 = 3.38. 74

Figure 23. Mean velocity contour plots for 4 Hz - 4 psig for straight tube inlet configuration. 75

Figure 24. Mean velocity contour plots for 4 Hz - 4 psig for straight tube inlet configuration. 76

Figure 25. Mean velocity contour plots for 4 Hz - 4 psig for straight tube inlet configuration. 77

Figure 26. Mean velocity contour plots for 4 Hz - 4 psig for straight tube inlet configuration. 78

Figure 27. Mean velocity contour plots for 4 Hz - 4 psig for straight tube inlet configuration. 79

Figure 28. Mean velocity contour plots for 4 Hz - 4 psig for straight tube inlet configuration. 80

Figure 29. Mean velocity contour plots for 4 Hz - 4 psig for straight tube inlet configuration. 81

Figure 30. Mean velocity contour plots for 4 Hz - 4 psig for straight tube inlet configuration. 82

Figure 31. Mean velocity contour plots for 4 Hz - 4 psig for straight tube inlet configuration. 83

Figure 32. Mean velocity contour plots for 8 Hz - 4 psig for straight tube inlet configuration. 84

Figure 33. Mean velocity contour plots for 8 Hz - 4 psig for straight tube inlet configuration. 85

Figure 34. Mean velocity contour plots for 8 Hz - 4 psig for straight tube inlet configuration. 86

Figure 35. Mean velocity contour plots for 8 Hz - 4 psig for straight tube inlet configuration. 87

Figure 36. Mean velocity contour plots for 12 Hz - 4 psig for straight tube inlet configuration. 88

Figure 37. Mean velocity contour plots for 12 Hz - 4 psig for straight tube inlet configuration. 89

Figure 38. Mean velocity contour plots for 12 Hz - 4 psig for straight tube inlet configuration. 90

Figure 39. Mean velocity contour plots for 4 Hz - 4 psig for bent tube inlet configuration. 91

Figure 40. Mean velocity contour plots for 4 Hz - 4 psig for bent tube inlet configuration. 92

Figure 41. Mean velocity contour plots for 4 Hz - 4 psig for bent tube inlet configuration. 93

Figure 42. Mean velocity contour plots for 4 Hz - 4 psig for bent tube inlet configuration. 94

Figure 43. Mean velocity contour plots for 4 Hz - 4 psig for bent tube inlet configuration. 95

Figure 44. Mean velocity contour plots for 4 Hz - 4 psig for bent tube inlet configuration. 96

Figure 45. Mean velocity contour plots for 4 Hz - 4 psig for bent tube inlet configuration. 97

Figure 46. Mean velocity contour plots for 4 Hz - 4 psig for bent tube inlet configuration. 98

Figure 47. Mean velocity contour plots for 4 Hz - 4 psig for bent tube inlet configuration. 99

Figure 48. Mean velocity contour plots for 8 Hz - 4 psig for bent tube inlet configuration. 100

Figure 49. Mean velocity contour plots for 8 Hz - 4 psig for bent tube inlet configuration. 101

Figure 50. Mean velocity contour plots for 8 Hz - 4 psig for bent tube inlet configuration. 102

Figure 51. Mean velocity contour plots for 8 Hz - 4 psig for bent tube inlet configuration. 103

Figure 52. Mean velocity contour plots for 12 Hz - 4 psig for bent tube inlet configuration. 104

Figure 53. Mean velocity contour plots for 12 Hz - 4 psig for bent tube inlet configuration. 105

Figure 54. Mean velocity contour plots for 12 Hz - 4 psig for bent tube inlet configuration. 106

Figure 55. Contours of mean axial velocity (Morrison et al (1988)). 107

Figure 56. Deviation from centerline of the point of maximum velocity in the plane for the case of 4 Hz. 108

Figure 57. Deviation from centerline of the point of maximum velocity in the plane for the case of 8 Hz. 109

Figure 58. Deviation from centerline of the point of maximum velocity in the plane for the case of 12 Hz. 110

Figure 59. Gas generator model entrance velocity profiles for charging phases. For straight tube inlet configuration at 4 Hz - 4 psig. 111

Figure 60. Gas generator model entrance velocity profiles for charging phases. For straight tube inlet configuration at 8 Hz - 4 psig. 112

Figure 61. Gas generator model entrance velocity profiles for charging phases. For straight tube inlet configuration at 12 Hz - 4 psig. 113

Figure 62. Gas generator model entrance velocity profiles for charging phases. For bent tube inlet configuration at 4 Hz - 4 psig. 114

Figure 63. Gas generator model entrance velocity profiles for charging phases. For bent tube inlet configuration at 8 Hz - 4 psig. 115

Figure 64. Gas generator model entrance velocity profiles for charging phases. For bent tube inlet configuration at 12 Hz - 4 psig. 116

Figure 65. Mean velocity profiles for a venting phase. For bent and straight tube inlet configurations at 4 Hz - 4 psig - t/T = 0.250. 117

Figure 66. Centerline velocity decay for charging phases in the straight tube configuration at 4 Hz - 4 psig. 118

Figure 67. Centerline velocity decay for charging phases in the straight tube configuration at 8 Hz - 4 psig. 119

Figure 68. Centerline velocity decay for charging phases in the straight tube configuration at 12 Hz - 4 spig. 120

Figure 69. Axial turbulence contour plots for 4 Hz - 4 psig for bent tube inlet configuration. 121

Figure 70. Axial turbulence contour plots for 4 Hz - 4 psig for bent tube inlet configuration. 122

Figure 71. Axial turbulence contour plots for 4 Hz - 4 psig for bent tube inlet configuration. 123

Figure 72. Axial turbulence contour plots for 4 Hz - 4 psig for bent tube inlet configuration. 124

Figure 73. Axial turbulence contour plots for 4 Hz - 4 psig for bent tube inlet configuration. 125

Figure 74. Axial turbulence contour plots for 4 Hz - 4 psig for bent tube inlet configuration. 126

Figure 75. Axial turbulence contour plots for 4 Hz - 4 psig for bent tube inlet configuration. 127

Figure 76. Axial turbulence contour plots for 4 Hz - 4 psig for bent tube inlet configuration. 128

Figure 77. Axial turbulence contour plots for 4 Hz - 4 psig for bent tube inlet configuration. 129

Figure 78. Axial turbulence contour plots for 8 Hz - 4 psig for bent tube inlet configuration. 130

Figure 79. Axial turbulence contour plots for 8 Hz - 4 psig for bent tube inlet configuration. 131

Figure 80. Axial turbulence contour plots for 8 Hz - 4 psig for bent tube inlet configuration. 132

Figure 81. Axial turbulence contour plots for 8 Hz - 4 psig for bent tube inlet configuration. 133

Figure 82. Axial turbulence contour plots for 12 Hz - 4 psig for bent tube inlet configuration. 134

Figure 83. Axial turbulence contour plots for 12 Hz - 4 psig for bent tube inlet configuration. 135

Figure 84. Axial turbulence contour plots for 12 Hz - 4 psig for bent tube inlet configuration. 136

Figure 85. Phase averaged mean velocity profiles for the bent tube case at 4 Hz and t/T = 0.750. 137

Figure 86. Axial turbulence plots for 4 Hz - 4 psig for straight tube inlet configuration during charging phases. 138

Figure 87. Axial turbulence plots for 4 Hz - 4 psig for straight tube inlet configuration during charging phases. 139

Figure 88. Axial turbulence plots for 8 Hz - 4 psig for straight tube inlet configuration during charging phases. 140

Figure 89. Axial turbulence plots for 12 Hz - 4 psig for straight tube inlet configuration during charging phases. 141

Figure 90. Axial turbulence contour plots for bent tube case for different frequencies. 142

NOMENCLATURE

D0	diameter of pipe at entrance to cylinder
f	pressure (p) , velocity (U), etc.
$\bar{f}$	mean f
$\hat{f}$	ensemble averaged f
$\tilde{f}$	fluctuating component of f
f-	turbulent component of f
Fr	Froude number
M	Mach number
P	probability density function
Re	Reynolds number
S	$\{x,y,z\}$ - space variable
t	time variable
T	period of oscillation
U0, $\hat{U}_0$	maximum of phase averaged mean velocity at entrance.
Up	phase averaged mean turbulent velocity
x	axial co-ordinate

y	axis perpendicular to x in the plane of the entrance tube of the cylinder.
θ	phase angle
UU0	$\frac{\hat{U}}{\hat{U}_0}$ in figures.
UPU0	$\frac{\hat{U}'}{\hat{U}_0}$ in figures.

1.0 Introduction

Some aerospace vehicles use jets issuing from nozzles at chosen places on the vehicle to allow attitude control. When such a device is used, a storage tank for the fluid in use is usually on board the vehicle. Figure 2 shows one such system of storage tanks and nozzles on a test stand. This particular device consists of four gas generator cylinders to supply the fluid for the nozzles at the corners. The gas generators and the nozzles are connected by a complex manifold with valves to regulate the flow. Figure 1 shows one of the gas generators with a tube that leads to the manifold. In order to effectively control the vehicle and use the available fluid efficiently the valves are operated periodically in a chosen sequence. When one of the gas generators is exhausted of the fuel that generates the gas, the gas from the rest of the system would flow into and out of it during operation. This flow resembles the flow into and out of a large reservoir through a small opening. The flow in the reservoir can be altered with different geometries of the tube ending into the opening. In this device the flow is at high temperature

and pressure. It is the purpose of this study to model such flows using cold-flow techniques and study it through flow visualization and velocity measurement.

Flows confined to a restricted volume with injection are commonly encountered in engineering practice. Flow in an internal combustion (I.C.) engine cylinder, air flow in rooms due to forced ventilation, flow of blood in a heart are only a few examples of confined flows interacting with their surrounding environment. Some of these flows are unsteady and are characterized by periodicity, as in the cases of I.C. engine and the heart. It is essential to understand the nature and structure of these flows in order to solve the problems and improve the efficiency of their functioning. Improving efficiency of combustion in the case of the I.C. engine contributes to a more efficient use of petroleum resources for a longer time and thus provide enough time to seek alternatives. Understanding the flow through the different valves and chambers of the blood circulation system has enormous impact in alleviating the disorders with its functioning. The present study addresses the problem of pulsating jets confined to a cylinder. This problem has all the characteristics described in the above cases. However, the geometry is simpler than that of a heart or a piston-cylinder assembly.

Much research has already been done on some of the aforementioned problems. Computational methods have been developed and constantly updated for the solution of certain problems arising in this context. Extensive experimental techniques have also been developed and used to study the unsteady flow in these confined flows.

1.1 IC Engine Flow Research

References 1, 2, 3, 13, 21, 22 and 31 deal with flows in a piston-cylinder combination for I.C. engines. These publications provide useful information regarding experimental techniques to be used in such unsteady flows. Typically, the efforts are concentrated in making velocity measurements using hot wire and laser Doppler anemometry. The departure from steady flow measurements using the above techniques is in the way time series data is processed to obtain the relevant mean and fluctuating quantities.

Liou and Santavicca (1985) made laser Doppler velocimetry measurements in a motored I.C. engine. They calculated turbulence intensity using velocity fluctuation with respect to the ensemble average velocity and also the velocity fluctuation with respect to the cycle resolved bulk velocity. Their whole effort was focussed on the differences in the fluctuation intensities obtained in the methods used. It was observed that the ensemble averaging procedure indicated higher fluctuation intensities than the cycle resolved procedure. All the measurements reported were made at a single point in the cylinder chamber. Arcoumanis et al (1981) made velocity measurements using LDV in a cylinder-piston chamber configuration at various axial stations using the ensemble averaging procedure. They reported axial velocity and fluctuation intensity with different piston configurations and with swirl intake. Similar measurements were reported by Arcoumanis et al (1982), Liou et al (1982) and Asanuma et al (1987).

Rask (1981) compared the window, smooth ensemble and cycle-by-cycle data reduction techniques for cylinder velocities measured by LDV. He found that window and smooth ensemble techniques essentially were same with window averaging technique giving more turbulence due to error introduced by large window size. However, both were deviating from cycle-by-cycle procedure results. In the flows where measurements were being made the cycle-by-cycle variation in the mean velocity was considerable.

Gosman and Watkins (1977) describe a computer prediction method for flow and temperature fields. The model used in the method includes the effects of compressibility, viscosity and turbulence while taking care of the unsteady nature of the flow by ensemble averaging the Reynolds averaged flow equations. However, they did not consider combustion in their model and they reported only axisymmetric problems thus neglecting swirl. The books by Gupta and Lilley (1985) and Khalil (1982) provide some direction to include combustion modeling in the prediction methods and more importantly include a large number references for the interested reader.

1.2 Unsteady Axisymmetric Subsonic jets

References 5, 6, 7, 8, 20, 25 and 29 discuss unsteady axisymmetric jet flows. Bremhorst (1979) presents a good overview of unsteady subsonic turbulent jets. Bremhorst compares the effects of cyclic excitation at different frequencies and

amplitudes. Basic properties such as length and velocity scales, decay of the mean centerline velocity, spreading rate as compared to the steady jet flow were addressed in this study. Bremhorst and Harch (1977), Leister (1977), Parikh and Moffat (1981), Binder and Favre-Marinet (1981), and Meyer and Sava (1982) have all reported experimental results obtained for various configurations of pulsating jets. The properties reported by these researchers are similar to what Bremhorst (1979) reviewed. In fact, some of these results were used in the analysis of Bremhorst (1979). The excitation frequencies in these studies vary from 10 Hz.-20 Hz. in some cases to near 700 Hz. in others. Usually lower frequency excitation was used when the jets were pulsed fully. The measurement of velocity and RMS of fluctuations in these studies were either done by direct time averaging or by ensemble averaging. The ensemble averaging process is similar to the process described in the preceding section of this chapter. Leister (1977) studied a flow geometry that is different from the rest in that the jet was pulsating and also impinging normally on a flat plate. He observed that the pulsing of the jet affected the free jet region and the free shear layer of the wall jet region while the wall boundary layer remained unaffected. It should be noted that the pulsation was partial and the frequency was between 10 Hz. and 20 Hz. for the results reported.

Bradley and Ng (1989) extended the above studies by experimenting with multiple frequency excitation. They applied a phase averaging technique in their measurements. They observed that with multiple frequency excitation more control could be imposed on vortex merging and mixing. They phase averaged

their data at the lower frequency of excitation and over only a few cycles and reported excellent agreement with flow visualization results.

1.3 Biomedical Flow Research

Biomedical research studies of flow through heart valves use the same techniques to measure velocities and fluctuation intensities as mentioned above. Walburn et al (1983) used both LDV and hot film anemometry in aortic valves to evaluate whether ensemble averaging or cycle-by-cycle averaging was proper to use for their purpose. Tiederman et al (1988) also conducted similar studies and used a cycle-by-cycle averaging technique to record turbulent shear stress measurements in heart valves. These studies are mentioned here only to emphasize that there are other areas where unsteady internal flow field analysis is important. The above studies were conducted to investigate if any damage would occur to the blood constituents due to increased turbulence.

1.4 Present Study

In all of the above examples complexity arises from several sources. Firstly, most of the work involves modeling real life problems. This implies modeling complex geometries and sometimes high temperature and high pressure flow

conditions. Secondly, the flows are all unsteady which may be periodic in special cases. Next, there arises the problem of finding the appropriate sensors and related instrumentation that will provide the information necessary to understand the phenomenon at hand. The literature regarding flows confined to a definite volume and unsteady jets may be much more extensive than presented here. The above discussion is aimed at showing the complex nature of these flows and their study.

In this study the focus is on pulsating jets confined to a cylindrical enclosure. This combines some of the complexities discussed in this chapter. The inlet for the jet into the cylinder could be straight or curved to study the differences in the flows. Further, the pulsing of the jet in and out of the cylinder may also be varied. The basic geometry of this flow problem is presented in Figure 1, which will be discussed further in later chapters. Initial interest to investigate this flow was prompted by the need to visualize the flow within a full scale model of the D-5 PBCS gas generator (ARC (1986) , Marchman and Kuppa (1987)). The gas generator is one of four in a system connected via a complex manifold to different nozzles (Figure 2). A gas generator contains fuel which would be combusted to generate the gas for the nozzles. For the particular design of the system, propellent is exhausted in the gas generator during operation. It becomes essentially an open tank or accumulator in the system while the other gas generators are exhausting. The operation of the valves in the system is such that the empty gas generator vents and charges periodically. During such operation

localized heating was observed in the empty gas generator that led to structural problems.

Flow visualization tests were conducted at the Aerospace and Ocean Engineering Department of Virginia Tech to investigate the flow due to the existing configuration of the inlet to the gas generator to confirm that :

1. the curved inlet caused asymmetry of the flow with respect to the cylinder axis,
2. the jet was impinging obliquely on the wall of the cylinder,
   and
3. the pulsating, impinging jet was causing large fluctuations at the wall, thereby increasing the momentum and heat transfer to the wall.

After confirmation of the above, several other configurations of the curved inlet were fabricated and the tests were carried out for each of them. This was done to help eliminate the problem of localized heating and the resulting damage.

In the following chapters the flow modeling and flow visualization tests will be discussed. Further, the experimental set up and operation for both flow visualization and velocity measurements, data acquisition and analysis technique, and results will be presented. Finally, the conclusions that can be drawn from the study will be presented.

2.0 Flow Modeling

As already mentioned the gas flow in the original gas generator is both at a high temperature and high pressure. Under these conditions it is necessary to make certain assumptions and reduce the problem to an experiment that can be done without spending too much time or other resources. In this chapter some past studies conducted using simple models of the equipment which were functioning under the above mentioned conditions will be discussed. These past studies support the simple modeling technique used in the present effort.

2.1 Past studies with partial modeling

Modeling of a flow implies that the simulation of the conditions existing in the original or full scale equipment are not all accounted for in the present experiment. It is seldom feasible to conduct the tests at the same conditions as the

original. It is necessary to model a flow in certain conditions. For example, the temperature and pressure in the original may be too high and require special construction. Also, such equipment and it's operation may be subject to severe safety codes. Such conditions may be difficult to meet in the atmosphere of a university laboratory and may make it difficult to observe and measure the quantities of interest. Under such circumstances engineers need to look for satisfactory model experiments which would permit the desired observations to be made under less severe conditions. Modeling may also be done to circumvent mathematical or computational difficulties as in the case of turbulence modeling. In this chapter only the hardware side will be dealt with.

In order to model a given flow accurately and give interpretable results certain rules need to be followed. These rules may be derived from dimensional analysis or from the governing differential equations. These rules are usually in the form of dimensionless groups and are required to be the same in the model as in the original. These will then ensure that similarity in flows exists and are therefore called similarity conditions. Reynolds number (Re), Froude number (Fr), Mach number (M), etc., are some of these dimensionless groups which are used in flow characterization. Spalding(1962) in his paper on the art of partial modeling of combustion flow fields gives a table of dimensionless groups. In this paper Spalding explains that it is difficult to satisfy all the similarity conditions at the same time. This is very much apparent to any practising researcher. He further makes the following suggestions in his conclusions :

1. The strict requirements of similarity theory are so numerous that complete modeling of combustion processes is practically impossible. For this reason, only partial modeling is practicable.

2. When partial modeling is done taking into account only the major influences, good modeling results. For example, as long as the Reynolds number is sufficiently large to ensure turbulent flow, the Reynolds numbers of the model and the prototype need not be equal for observing certain fluid mechanical processes such as vortices and separated regions.

3. Good judgement is called for from the researchers in selecting the model. The modeling technique chosen depends upon the accuracy of prediction required, and the economics of time and money among other factors. Often the modeling technique which most flagrantly flouts the similarity rules is the most useful one in practice.

Beer and Chigier (1983) echo the aforementioned ideas with regard to aerodynamic modeling of combustion systems.

Flow visualization in combustor models in the past have been done with the same reasoning as discussed above. The methods and results reported in the publications of Poulston and Winter (1956), Winter and Deterding (1956), Winter (1958), Gerrard(1961), Clarke et al (1962), Kennedy(1974), Vanka et al (1983), Schetz et al (1983), Stull et al (1985), Schetz, Guruswamy and Marchman (1985) and Schetz et al (1985) support the validity and utility of partial modeling.

Winter (1956) and Gerrard (1961) describe methods for flow visualization in water in combustion systems. Both of them describe apparatus and techniques for flow visualization, measurement of certain quantities like velocity and scaling to predict the flow conditions at different conditions. They have applied these techniques to combustion problems in gas turbine systems and obtained good results. With their experiments they were able to understand the flow field using partial modeling. The details of the problems they tackled and the results they obtained for them are described in Poulston and Winter (1956), Winter (1958) and Clarke et al (1962). More recently similar work was reported by Kennedy (1974), Schetz et al (1983), Schetz, Guruswamy and Marchman (1985), Schetz et al (1985) and Stull et al (1985). While Kennedy (1974) and Stull et al (1985) reported studies of combustor flow visualization in water, work done here at Virginia Tech by Professor Schetz and co-workers involved both water flow visualization and cold air flow testing. The cold air flow testing enabled measurements with well established techniques and apparatus like five hole pitot probes and hot wire anemometers. Schetz et al (1985) have also developed and used polyaphrons, a new material to aid flow visualization. Polyaphrons are small globules of one liquid encapsulated in a thin film of another whose size, shape, color and density can all be adjusted. Thus tracers which are visible in photographs and are of the same density of the medium can be developed and used. Obtaining the right type of tracer in flow visualization studies is often difficult and several methods have to be tried before satisfactory pictures can be obtained.

2.2 *Modeling of gas generator flow*

In the present study the model internal dimensions and shape are identical to the original hardware. The gas generator modeled is the one in which a local hot spot was observed (ARC (1986)) and in which a structural failure occurred during ground testing of the actual equipment. The temperature inside the original gas generator is in excess of 1000 ° R and the pressure in excess of 400 psia. It was obvious that these conditions can not be duplicated while trying to visualize the flow for the camera. The flow was characterized by unsteadiness due to valve sequencing. The flow occurred in the empty generator in the system only due to the valve sequencing while using the remaining non-empty generators. Hence it was decided that while using a clear acrylic model of the gas generator, the testing would be done with unheated air and at a pressure which was slightly higher than atmospheric pressure. The test conditions were chosen such that no structural failure would take place in the laboratory. The unsteadiness was modelled to reflect the frequencies of pulsing observed in the original equipment.

With the model used it was possible to maintain a reasonably high Reynolds number so that the fluid mechanical processes observed would be similar to the ones in the original generator. Cold air was chosen in place of water or some other fluid due to the ease in obtaining large volumes of pressurized air and producing pulsing with simple equipment. The whole apparatus and the operation used in this modeling are described in a later chapter. Although the comparison of hot compressible flow with the cold flow cannot be generally validated, the present

program of studying the flow was encouraged by the past results discussed earlier. These results indicated that the gross features of combustor flow fields can be characterized through water or cold air flow experiments.

Winter (1958) reports that in his studies the hot and cold flow patterns agree closely, except for the accelerations due to heat release. In the case in hand there is no heat release of the magnitude experienced in combustors. This case is similar to a combustor in the sense of variable density and high pressure and temperature. Unlike the combustor, acceleration of the fluid takes place due to pressure pulsations and is not local. This reasoning is bolstered by the observations of similarity between actual flow patterns in a particular system with and without combustion as reported by Winter (1958) and reproduced here in Figure 3.

3.0 Experimental Set-Up and Operation

In an attempt to understand the behavior of the flow in the gas generator, an experimental program was undertaken with the collaboration of the designers and makers of the gas generator system, viz., Lockheed Missile and Space Company, and Atlantic Research Corporation. This program was in two parts, consisting of flow visualization and velocity measurements. In this chapter the hardware set-up and operation of the system in order to accomplish both of the aforementioned objectives are described separately. Though there is an essential similarity in the two set-ups and their operation, the differences in their objectives necessitates different descriptions. Hence, in this chapter the flow visualization set-up is dealt with first and the velocity measurement set-up after that. For each there is a description of the apparatus used, the procedures followed in conducting the tests, the quantities or results obtained from these tests and the techniques followed to reduce the data for presentation.

3.1 Flow Visualization

The set up of the model for the flow visualization tests is as in Figure 4. The construction of the model, excluding the entrance tubes, is also the same for velocity measurements and therefore will be described only here.

3.1.1 Model - Construction and Assembly

Excluding the entrance tubes, the gas generator model was made in four parts. It was done so to facilitate easy changes in configuration. The entrance tube can be attached to the inlet cap (see Figure 5) so that only this assembly needs to be changed for a different entrance configuration. There is a constant 14 in. outer diameter pipe with flanges on either end, which forms the center portion of the gas generator (Figure 6). The two end pieces (domes) were machined to the correct dimensions from solid pieces of Plexiglas. The solid pieces themselves were formed from gluing several flat plates of Plexiglas together. The inlet dome piece has a central hole to take the inlet cap with the entrance tube. The end dome (i.e. away from the inlet) is without holes. The dome pieces also have flanges, so that they can be attached to the central cylindrical piece. These dome pieces are shown in Figure 7and Figure 8, representing the dome pieces for the entrance side and end side of the model repectively. All the joints were provided with rubber "O-ring" seals to ensure that the cylinder was airtight. The

different configurations for testing were achieved through the assembly of different inlet cap configurations. The different entrance tube configurations used in the flow visualization tests were :

1. A 3 in. (7.62 cm.) radius, 70 ° bend between a 9 in. (22.86 cm.) straight section and 1 in. (2.54 cm.) straight section going to the gas generator cylinder as per the actual device, made out of Plexiglas tubing.

2. A 12 in. (30.48 cm.) straight entrance tube.

3. Copper entrance tubes with 70 °,75 °, 80 °, and 90 ° bends to simulate both normal entrance and distortions in bend and nozzle. For the distorted cases inserts in the dome cap were fabricated to place the nozzle at 0 °,5 °, 10 °, and 20 ° relative to the generator center line for use with 70 °,75 °, 80 °, and 90 ° bend entrance tubes respectively.

4. Copper entrance tubes with 1 in. (2.54 cm.), 2 in. (5.08 cm.), 3 in. (7.62 cm.) and 4 in. (10.16 cm.) straight sections with a 70 ° bend going into the gas generator.

5. Copper entrance tube of 1 in. straight section and 70 ° bend fitted with a ½ in. long splitter vane across the center of the entrance.

All the tubing used in making the entrance tubes had an outer diameter of 1 in. (2.54 cm.). These different inlet tube configurations are shown in Figure 9 to Figure 10.

3.1.2 Flow Visualization Materials

The objective, in part, of this study is to obtain a good picture of the flow inside the gas generator cylinder. In order to obtain a good picture of the flow it is necessary to use materials that have certain qualities. In steady flow testing practice, flow visualization techniques are well established and literature regarding this is available in the publication of Merzkirch (1987). The right type of material would be the one which provides the best picture of the flow being studied. In this study it is necessary to have a tracer material that is visible and will be carried by the fluid. As Winter (1956) identifies, ideally, the tracers should have the following characteristics :

1. They should remain as discrete bodies.

2. They should have the same specific gravity as the fluid.

3. They should be of spherical shape.

4. They should be sufficiently small to follow the flow in fairly fine detail while being sufficiently large for satisfactory observation.

5. They should possess the optical property of reflecting a high proportion of light normal to the incident light.

With the above conditions in perspective, several methods were tried for flow visualization studies including smoke, silk tufts and light weight styrofoam beads. Smoke dissipated very easily due to the large fluctuations and did not provide any useful information. Silk tufts tied to spokes about a center rod were tried next. This arrangement is depicted in the schematic in Figure 11. These provided some information about the effect of the jet and the flow direction, but were probably more intrusive than helpful. The small styrofoam beads provided by far the most useful picture of the flow. The density of the beads is about 1.0 lb/ft^3. They were spherical in shape with the diameter in the range of 0.1 in. These were small and light enough to follow the flow. A problem of static buildup causing the beads to cling to the Plexiglas model, was easily eliminated by the use of commercially available anti-static spray normally used on clothing.

The flow inside the generator is unsteady. Still photography would provide a view of the flow fixed at the time of exposure only. In order to see the dynamic nature of the flow, a time series record of the flow is necessary. This can be accomplished by the use of cinematography or videography. In the present study videography was chosen since the equipment was readily available and a lot of post-processing could be avoided.

Figure 4 shows the full test system schematically for visualization tests. High pressure air was available through a storage tank which was a part of the Supersonic Wind Tunnel System at Virginia Tech. This air was maintained at

at least 60 psi and could be drawn for long periods of time for testing once the tank was pressurized. A Nullmatic pressure regulator (model 40-100) in conjunction with an AMF CUNO filter (model 1A1) was used along with a Fairchild Hiller Air Loaded pressure regulator (model 200) to adjust and maintain the pressure upstream of the entrance to the gas generator. Flow was pulsed into the gas generator using a ASCO, model B-8210, 2 way solenoid valve controlled by a square wave function generator (Hewlett-Packard) which could be set to the desired pulse rate. A solid state relay was present in between the solenoid valve and the function generator. The air supply to the gas generator was regulated using a Bourdon type pressure gauge (US Gauge 0-30 psig) at a station after the pressure regulator and before the solenoid valve. Pressure inside the gas generator cylinder was monitored using a strain gauge type pressure transducer (Statham pressure transducer) connected to a Measurements Group 2310 signal conditioning amplifier. The pressure transducer was mounted on the cylindrical wall with the orifice flush with the inside surface. The bridge amplification was selected such that the amplifier output would directly give the pressure in psig. The pressure transducer along with the bridge amplifier was calibrated using a static pressure testing device.

3.2 Velocity Measurements

The initial visualization tests of the flow in the gas generator indicated it to be highly turbulent and oscillating. A complete study of the flow would require a three dimensional mapping of all velocity components in the cylinder taking into account the unsteady nature of the flow. This would entail enormous expenditure of time and other resources. Therefore, instead of investing all the efforts on a single task, it would be good judgement to make some measurements in the beginning to elevate the level of understanding. From these measurements one may be able to decide what must be done further. The flow visualization and some velocity measurements (Marchman & Kuppa (1987)) have already provided some information about the nature of the flow. On the basis of these results and the aforementioned restrictions it was decided to make the measurements in a plane of symmetry.

3.2.1 Model - Construction and Assembly

In this section the models, facility and the data acquisition technique used in the experiments are described. Two configurations of the entrance into the gas generator were chosen for study. The first entrance tube was straight as shown in Figure 9. The second entrance tube was curved so as to simulate the inlet of the D-5 gas generator. The angle of the bend is 70 °. This configuration is also

shown in Figure 9. For the straight entrance tube the geometry is axisymmetric and hence measurements were made only in one radial plane. In the case of the curved entrance tube the flow has only one plane of symmetry. This plane is the section passing through the axis of the entrance tube.

The model of the gas generator used in the present study was fabricated previously for flow visualization tests. To enable this the model was fabricated with Plexiglas, except for the entrance tube. The straight entrance tube was made of 1 in. outer diameter Plexiglas tube, where as the curved entrance tube was of 1 in. outer diameter copper tube. A commercial copper tubing bender was used to achieve a smooth bend without crimping the pipe. The radius of the bend was 3 ½ in.

Figure 12 shows the full test system schematically for velocity measurements. High pressure air was available through shop air supply. This air is maintained at greater than 75 psi and could be drawn for long periods of time for measurements. A Nullmatic pressure regulator (model 40-100) in conjunction with an AMF CUNO filter (model 1A1) was used along with a Fairchild Hiller Air Loaded pressure regulator (model 200) to adjust and maintain the pressure upstream of the entrance to the gas generator. Flow was pulsed into the gas generator using a ASCO, model B-8210, 2 way solenoid valve controlled by a square wave function generator (Wavetek, model 131, VCG Generator) which could be set to the desired pulse rate. A solid state relay was present between the solenoid valve and the function generator.

3.2.2 Data Acquisition

The air supply to the gas generator was regulated using a Bourdon type pressure gauge (US Gauge 0-30 psig) at a station after the pressure regulator and before the solenoid valve. Pressure inside the gas generator cylinder was monitored using a strain gauge type pressure transducer (Statham pressure transducer) connected to a Measurements Group 2310 signal conditioning amplifier. The pressure transducer was mounted on the cylindrical wall with the orifice flush with the inside surface. The bridge amplification was selected such that the amplifier output would directly give the pressure in psig. The pressure transducer along with the bridge amplifier was calibrated using a static pressure testing device.

Velocity measurements were made using hot wire anemometry. A single wire (TSI model 1210 with a 0.00015 in. tungsten wire) transducer was used in conjunction with a DANTEC anemometer set-up. Two types of probe support accessories were used in the measurements. For measurements away from the entrance a TSI model 1150 single sensor probe support was used. To access the locations at the entrance a TSI model 1152 90° angle adapter was used along with the above. The DANTEC anemometer consisted of a DANTEC 56C17 bridge and a DANTEC 56C01 CTA Unit in a DANTEC 56B12 Main Frame. The hot wire anemometer set-up was calibrated using a TSI model 1125 calibrator. The calibration of the hot wire is sensitive to the gas temperature. Therefore, the calibration was carried out every time before a measurement and was checked

each time. This was to ensure accurate velocity measurements. The correlation coefficient for curve fit obtained through the calibration was at least 0.999. Figure 13 and Figure 14 show the locations used to examine the velocities using the hot wire anemometer. The axis of the cylindrical hot wire sensor was aligned perpendicular to the plane of measurements to measure the axial component of the velocity.

Data acquisition was done using a MetraByte model DASH-16/16F multifunction high speed A/D converter installed in a portable IBM PC. The A/D converter can sample 16 single ended channels or 8 differential channels at high speeds. In the present study only three single ended channels were used for data acquisition. One channel was connected to the function generator to monitor the square wave function being fed to the solenoid valve. The second channel was connected to the amplifier output of the cylinder pressure transducer. The last one was connected to the bridge output from the hot wire anemometer. The details about programming for A/D conversion and related topics are available in reference 10.

3.2.3 Data Reduction

At each data station the hot wire signal was phase averaged over several cycles depending upon the pulsing frequency. The analog to digital sampling rate was fixed such that an integer number of cycles of the pulsing frequency can be obtained for the period of sampling. As mentioned earlier the forcing square wave

signal was sampled along with the velocity signal. This was done to enable the computer to synchronize the data with the forcing signal. The forcing signal was compared to a predetermined trigger condition based on a threshold level and slope. The point on the forcing signal that matches the trigger condition is the "event trigger" and hot wire signals from then on are stored.

The flow in the gas generator is regulated by a periodic forcing of the solenoid valve, hence the upstream conditions are periodic with period T. Consider a characteristic scalar or vector of interest in the experiment $f(S,t)$ where,

f - represents pressure, velocity, etc.

S - $\{x,y,z\}$ - represents space variable

t - time variable

$P(f)$ - Probability density function of f

At a given point in space (S), and for a given phase (θ) (corresponding to the period T, mentioned above) we can get a constant phase, ensemble average of f as,

$$\begin{aligned} \hat{f}(S,\theta) &= E(f) \\ &= \int f\, P(f,S,\theta)\; df \end{aligned} \tag{3.1}$$

Clearly $\hat{f}$ is a function of S and θ. Now, the turbulent part can be obtained as,

$$f' = f - \hat{f} \tag{3.2}$$

For the n^{th} moment of f dependent on S and θ we have,

$$\hat{f}'^{n} = (f - \hat{f})^{n} \qquad for\ n > 1 \tag{3.6}$$

For $n = 2$, we get

$$\hat{f}'^{2} = \hat{f^{2}} - \hat{f}^{2} \tag{3.7}$$

3.2.4 Uncertainties

Uncertainty in the measured and calculated quantities arise from uncertainties in the quantities controlling the experiment and quantities measured in the experiment. It is essential to keep these uncertainties in perspective while looking at the results. The pressure upstream of the gas generator was within $\pm$ 1% of the regulated value according to the manufacturer's specifications. The frequency of the square wave would be maintained within $\pm$ 2% of the set frequency according to the specifications of the function generator manufacturer. This may be on the pessimistic estimation of the uncertainty. The temperature during the series of tests was within $\pm$ 1°C of the temperature at which the hot wire calibration was done. The pressure transducer was calibrated to measure within $\pm$ 0.5% of the measured value under static calibration. The static calibration is assumed to hold good during dynamic measurements as the frequencies of interest are low. The hot wire sensor was calibrated mainly for the higher velocities. The uncertainty at the higher velocities was calculated by the

method of Kline and McClintock (1953) for single sample experiments. Holman(1984) and Moffat(1988) also provide details of this method. The uncertainty in velocity measurement was found to be about $\pm$ 4% at higher velocities. However, this could be higher for velocities of 5 m/s and below. Such velocities usually occurred at the end away from the entrance and near the cylinder wall away from the core of the flow. Aside from the above errors the inability of the single sensor to detect the direction of flow has to be taken into account. In the plane of measurements the velocity in a direction perpendicular to the plane can be assumed to be negligible as this is a plane of symmetry to the geometry. This component of velocity has negligible effect as it is along the direction of the axis of the cylindrical sensor. In the plane of measurements the problem of angularity and flow reversal do arise. The uncertainty due to angularity can be considerable for the bent tube case and near the walls of the cylinder. Also in both the cases flow reversal at a particular time and station could not be taken into account. Use of a two sensor apparatus can resolve the angularity of the flow, but LDV is the proper choice for measurement of velocity in this kind of flow. In spite of these uncertainties the single sensor apparatus was used in order to keep the costs to the minimum. The single sensor would sense the axial component of the velocity near the entrance quite accurately as the angularity of the flow is small. Also, flow reversal may occur only at certain phases in a cycle and may not affect the results at other phases adversely.

3.3 Operation

For flow visualization the model was assembled with the flow visualization material inside the model. Before that the model was cleaned with a glass cleaner for clear visibility of the flow visualization. Lights were also arranged in such a fashion as to eliminate glare in the region of interest. Initially the gas generator was filled up by opening the valve in between the model and the air tank. This initial charge up also provided a brief violent flow in the model which distributed the styrofoam beads well. Then the desired frequency was set on the square wave function generator and the pulse fed to the solenoid valve. The opening and closing of the valve let the air flow out of the system and charging of generator respectively. This action at a set frequency forced a flow in the model and motion of the beads and tufts. This resulting motion of the tufts and beads were recorded using the video camera and recorder.

For the velocity measurements, the operation of the solenoid valve was the same as described above. The hot wire support had a length of 18 in. and could therefore traverse a radial plane of the model from wall to wall. Several holes were made along the axis of the model to enable a traverse of the probe at that axial station. After due calibration and checking of the hot wire sensor, a traverse was made from wall to wall at a given axial station. The data at each station was collected as mentioned in a previous section of this chapter, ensemble averaged and stored in a file on a disk. This data was later plotted and analysed.

4.0 Results and Discussion

The present study attempts to evaluate the effect of different inlet tube configurations on the periodically forced flow inside a gas generator model. In this chapter the tests conducted and the results obtained will be discussed. First the results of flow visualization studies will be presented and discussed. Later the velocity measurements made in the gas generator cylinder for particular configurations of the inlet tube at particular frequencies of forcing will be presented. These results will be discussed in the light of the results obtained through flow visualization.

4.1 Flow Visualization Results

The flow visualization tests were conducted at frequencies of 4 Hz, 6 Hz, 8 Hz, 10 Hz, 12 Hz and 16 Hz. Also for certain observations, just charging and

venting of the gas generator model was done without regard to the frequency. For all these tests videographic recording was done with appropriate observations of the researchers accompanying the video, in audio by Dr. Marchman.

Silk tufts were used with the model as described in item #1 in the list of different entrance tube configurations used in flow visualization tests (see page 17). They provided the first glimpse of the nature of the flow inside the vessel. Tests conducted with the silk tufts revealed a strong center jet angled toward the wall of the cylinder due to the bend in the entrance tube. This flow was present during the period when the air was pulsed into the generator. When the pulsing valve was open, i.e. the air in the vessel was allowed to exhaust, the outward flow did not produce high velocities in the cylinder. The only high velocities were at the entrance into the generator. The relatively small velocities were very much subdued as one moved away from the entrance in the axial direction. This information suggested that the incoming flow was a complex jet flow confined to a cylindrical enclosure, while the outgoing flow resembled the venting of a high pressure reservoir.

Flow visualization tests with the different configurations described earlier were conducted using the small styrofoam beads. These tests were videotaped to provide an image of the unsteady and complex behavior of the flow inside the generator. Here a description of the visualization will be attempted as a complete view of the flow patterns discovered in these tests can be obtained only from viewing the tapes.

Figure 15 to Figure 18 have been obtained from scanning a still video image on a television set screen. Clearly, these pictures show the state of the flow at a certain time. It should be carefully noted that even these pictures are averaged over the short duration of time of exposure and hence are not strictly instantaneous. It should also be noted that averaging over a distance is being performed when viewing from any perspective. All of these pictures have been obtained when using the solenoid valve to generate pulses at the rate of 4 Hz. at a pressure of 4 psi. Figure 15 and Figure 16 are side views of the live generator model with the 70 ° entrance tube. These show the side views of the vessel with the entrance tube to the right and the center jet going downward from right to left. The entrance tube is bent upward. These give some idea of the rotational flow patterns in the vessel as viewed from the side. The basic flow patterns are a big oval clockwise flow degenerating into two clockwise cells as shown in these two figures with a short time interval between them. It should be emphasized that these patterns are unsteady and the observations did not show them to be synchronous with the pulsing. However, it was observed that these patterns did repeat. It was not observed if they repeated at periodic intervals. Figure 17 shows an oblique view of the genarator from a point above and right, but in the same configuration as for Figure 15 and Figure 16 This figure reveals the highly three dimensional nature of the flow. Again, this shows two basic rotational cells of flow.

These still figures can not completely reveal the dynamic nature of the flow which is better observable in the video tapes. The flow centers around two basic

rotational cells which continually break down and then reestablish themselves with a continuous exchange of energy. During this process there is "scrubbing" of the bottom of the generator in approximately the region where high heat transfer rates and surface deterioration were observed in the tests with the live gas generator (reference 10). The flow patterns were more intense when the pulsing of the jet occurred at 4 Hz. than at 8 Hz. or 12 Hz. The jet was in the generator for a longer period at 4 Hz. and hence was able to penetrate more into the generator before the solenoid valve opened to exhaust the generator. This resulted in more violent flow patterns at the lower frequency.

Figure 18 shows a flow pattern obtained when using 20 ° offset entrance tube. A similar flow pattern was observed for the 10 ° offset. Here the jet was deflected to the "top" of the generator and an essential inversion of the flow pattern was observed with a clockwise pattern at the lower right. Tests conducted with a 5 ° offset produced a more stable and uniform flow in the generator, which resembled the straight entrance flow pattern. That is, the flow was basically of a centerline jet without much deflection to the side walls.

Tests with the straight sections of 1 in., 2 in., and 3 in. with the 70 ° entrance tube showed the same patterns as observed in Figure 15 and Figure 16. These extensions did not completely straighten the jet, thereby producing asymmetry which produced the patterns described in Figure 15 and Figure 16 in turn. However, the 4 in. straight section was able to straighten the jet considerably and eliminate the flow patterns as observed above. Finally, the entrance tube with ½ in. long splitter vane across the center of the entrance was used to see if it can

straighten the jet. The flow pattern observed in this case was also similar to that of the straight entrance tube, thus showing that a splitter vane can straighten the jet.

4.2 Velocity Measurements

Tests were run for velocity measurements for the two inlet tube configurations mentioned in the previous chapters. For these tests the pressure ahead of the inlet tube was maintained at 4 psig for frequencies of 4 Hz, 8 Hz and 12 Hz. As mentioned earlier a single hot wire sensor measured the velocity at different radial locations at each axial station. The solenoid valve was held at each frequency and the velocity, cylinder pressure and the wave generator signals were sampled at 96 Hz each for over 20 seconds. The number of traces for ensemble averaging was about 240 for 12 Hz, 160 for 8 Hz and 80 for 4 Hz. Though the number of traces for the 4 Hz case is not sufficiently high, it is hoped that fairly good results may be obtained similar to the experience of Bradley and Ng (1989). Therefore, the number of points over a cycle for 4 Hz were more than for 8 Hz, for which there were more points than for 12 Hz. The locations for velocity measurements are shown in Figure 13 and Figure 14. The radial positions at each axial station were chosen so as to record at closer intervals where velocity and velocity changes are high. A Reynolds number calculated on

the basis of maximum jet entrance velocity and jet entrance diameter was found to be about 8.1×10^4.

In the flow visualization tests it was observed that the flow in the gas generator cylinder was characterized by charging and venting at different frequencies. Hence, in a cycle at any frequency one would expect the velocity profiles at each axial station to be well defined during the charging phase and be diminished in magnitude (to almost negligible) during the venting phase. This is because the gas generator would act as a reservoir during venting.

Figure 19, Figure 20 and Figure 21 show the frequency content of the axial velocity on the centerline. These particular cases are for velocity time series obtained at an axial distance $\frac{x}{D0} = 3.38$ at the three different frequencies for the straight tube. Dominating frequency for each case is very evident and corresponding to the forcing frequency. Even the first and second harmonics are not too difficult to discern in each case. However, the figures are not good enough to seek any more information.

Further in Figure 22 the phase averaged pressure and velocity traces over a cycle are presented. The pressure data presented here is the cylinder pressure as previously mentioned and the velocity data was obtained at the same location as for the aforementioned spectrum figures. The definition of the curves is better for the 4 Hz case rather than for 8 Hz or 12 Hz, due to more number of points per cycle. In this figure the charging and venting phases can be identified by the pressure rise and fall in each case during the cycle. For the 4 Hz case the charging phases are for 3 points from $\frac{t}{T} = 0.00$ to $\frac{t}{T} = 0.0833$ and for 10 points

from $\frac{t}{T} = 0.625$ to $\frac{t}{T} = 1.00$ approximately. For the 8 Hz case the charging phases are for 3 points from $\frac{t}{T} = 0.00$ to $\frac{t}{T} = 0.182$ and for 3 points from $\frac{t}{T} = 0.818$ to $\frac{t}{T} = 1.00$ approximately. And for the 12 Hz case the charging phases are for 3 points from $\frac{t}{T} = 0.00$ to $\frac{t}{T} = 0.286$ and $\frac{t}{T} = 1.00$ approximately. The remaining points are venting phases for each case. The diminished values of velocity during the venting phases clearly show that the cylinder acts as a reservoir during those phases.

Apart from the changes in velocity due to charging and venting, there is an oscillatory behavior of the velocity during the charging phase. This is clear at least for the 4 Hz case where there is more definition. In general the velocity should go down as the cylinder is getting charged until pressure equalization after the initial increase. This is observed in the trace presented here. However, the cause for the oscillatory damping of the velocity may arise from the pulsation of the flow into the cylinder periodically using a square wave to open and shut the valve.

The phase averaged mean velocity values are presented as contour plots in the plane of measurements. In these plots the entrance of the jet is from the left. For plotting convenience the data was plotted on a rectangular grid. These plots cover all the points of measurement except at the entrance to the vessel. The entrance velocity data will be presented separately. These plots were produced for each configuration and at each frequency, shown here as :

1. Figure 23 to Figure 31 ------ 4 Hz, Straight tube.

2. Figure 32 to Figure 35 ------ 8 Hz, Straight tube.

3. Figure 36 to Figure 38 ------ 12 Hz, Straight tube.

4. Figure 39 to Figure 47 ------ 4 Hz, Bent tube.

5. Figure 48 to Figure 51 ------ 8 Hz, Bent tube.

6. Figure 52 to Figure 54 ------ 12 Hz, Bent tube.

These plots confirm the observation from flow visualization that the velocities are well defined during charging and diminished in magnitude during venting. Further, the straight tube configuration plots at each charging phase are similar to those observed in an axisymmetric sudden expansion. Morrison et al(1988) have reported three dimensional LDV measurements for an axisymmetric sudden expansion. The area ratio they dealt with was 121:1. In the present case the area ratio is about 182:1. In their publication they indicate that 121:1 is the highest ratio that has been dealt with in such a study. Though they reported in detail the different components of velocity and turbulence after making elaborate measurements, the interest here is in the axial velocity contour plot reproduced here in Figure 55. The phase averaged mean velocities presented here have been non-dimensionalised by the maximum of the phase averaged mean velocity at the entrance. This occurred at the centerline for the straight tube and elsewhere for the bent tube configuration as will be seen later. The similarity in the figures is evident to the eye, even though the geometries are slightly different. Hence, it can

be said that during charging phases the straight tube configuration behaves much as an axisymmetric sudden expansion.

Aside from this the plots show that the jets have penetrated most for the lower 4 Hz frequency and least for the 12 Hz frequency. This can be seen from the extent to which higher velocities propagated in the axial direction for different phases in each case. The jets penetrate more in the axial direction for the lower frequencies as there is more time for charging the generator cylinder and hence more mass and momentum influx in a cycle. This is seen as higher pressure readings for 4 Hz and 8 Hz over 12 Hz as presented in Figure 22.

In the bent tube case the plots clearly show show a deviation of the core towards the wall during charging phases. During venting, however there is a diminished core present for some phases which shows a tendency of being near the wall (see Figure 40 for example). A similar core can also be seen for the straight tube cases, but on the axis of symmetry. The observations made in the straight tube cases about penetration of the jet hold good for these cases also. However there is a feature, not observed in the straight tube cases or even in the 4 Hz case for the bent tube configuration, in the plots for 8 Hz and 12 Hz cases of the bent tube configuration. Two cells are seen in the contour plots for these cases; one larger with higher velocities near the entrance and one smaller with smaller velocities away from the entrance (see Figures 48 and 52). These may be observable in these cases only due to a couple of reasons. One reason could be that the penetration of the jet is lesser in these two cases and hence the area away from the entrance experiences its own periodic pulses of compression and

expansion. The other plausible reason is that for these two cases the number of traces for averaging was higher than for the 4 Hz case. These higher number of traces might have provided more details of the flow. Since these details were not observed in the straight tube case, it is assumed that the first reason holds good.

The deviation from the centerline can be seen more clearly in Figure 56, Figure 57, and Figure 58. These figures have been produced for the bent tube configuration to show variation with different phases. In these figures the curve at each phase represents the points where the maximum of the phase averaged mean velocity occurs along the axial direction. The deviation from the centerline is evident. The angle of deviation is about 6.5°. The velocity profile at the entrance itself is skewed as will be discussed later. The figures show that the deviation is quite consistent for the different charging phases near the entrance. The scatter in the deviation away from the entrance is due to the smaller values of velocity and also different lengths of penetration at different phases.

Figures 59 to 64 show the velocity profiles at the entrance to the gas generator. These profiles are presented only for those phase values when the gas generator was being charged. This is because the hot wire sensor supported by a probe support with a right angle adapter at the entrance would measure the incoming flow accurately, but not the outgoing flow. The exhausting flow is spoiled by the hot wire probe support before it reaches the hot wire and so is in error. In the above discussion, it is already seen that during the venting phase of the flow the velocities are small in the cylinder. Therefore if the cylinder behaved like a reservoir then the velocity during venting at the entrance should be much

higher than in the cylinder. The entrance profiles during venting, however in error, did show this characteristic. The Figure 65 shows two example profiles, plotted along with the velocities recorded inside the cylinder. One each for the bent tube and straight tube cases.

The mean velocity profiles for the straight tube configuration in Figure 59, Figure 60, and Figure 61 show axisymmetric profiles. These profiles are not flat because flow has already occurred over a length of more than 15 diameters of the inlet tube. Also, there is a curved expansion into the gas generator at the end of the tube. Figure 62, Figure 63, and Figure 64 show the mean velocity profiles for the bent tube configuration. These profiles show a distinct kink which persists even in the profiles in the next two axial stations in some instances. This asymmetry in the velocity profile is attributed mainly to the bend in the inlet tube. Miller(1978) mentioned this characteristic while discussing bends in internal flow systems. The effect is enhanced by the almost sudden expansion of the inlet tube into the gas generator. This particular phenomenon contributes not only to the unsteady vortex motion as observed in the flow visualization tests, but also bends the jet towards the wall of the cylinder.

Further discussion about the straight tube configuration velocity measurements is in order. In Figure 66, Figure 67 and Figure 68 the centerline velocity decay for charging phases are shown. This has been done in order to compare with the data of Morrison et al(1988) mentioned before. The curves for different phases do not fall on each other. When there is little jet penetration as for the cases of $\frac{t}{T} = 0.625$ and $\frac{t}{T} = 0.667$ at 4 Hz the velocity drops off rapidly

in the axial direction (see Figure 66). Similar curves can be seen for 8 Hz and 12 Hz cases in Figures 67 and 68 respectively. However when the flow has penetrated sufficiently, the curves are all at least bunched near each other for 4 Hz and 8 Hz cases. For the 12 Hz case there are not as many curves to make any such remark. These curves compare well with the data of Morrison et al(1988) in the same manner as they compare with each other i.e. they follow the same trend but are not exactly similar to each other.

The phase averaged axial turbulence intensities are presented as contour plots in the plane of measurements in Figures 69 to 84. The orientation and the grid for these plots are identical to the ones used in mean velocity plots. These plots were produced for the bent tube configuration and at each frequency, shown here as :

1. Figure 69 to Figure 77 ------ 4 Hz, Bent tube.

2. Figure 78 to Figure 81 ------ 8 Hz, Bent tube.

3. Figure 82 to Figure 84 ------ 12 Hz, Bent tube.

The turbulence intensity was normalized by the maximum velocity at the entrance ($\hat{U}_0$) as was done for the mean velocity. The largest level of intensity observed about 4 percent of $\hat{U}_0$ and smallest about 0.5 percent of $\hat{U}_0$. In the venting phases the turbulence intensities were diminished along with the mean velocity values and hence there is not much well defined structure observed in the

plots as observed in the charging phases. In this configuration the velocity profile is not symmetric about the axial direction. The shape of the velocity profiles at least near the entrance would be highly skewed as suggested by the entrance mean velocity profiles discussed before. Figure 85 shows the phase averaged mean velocity profiles for the 4 Hz case at $\frac{t}{T} = 0.75$ which shows the velocity profiles near the entrance at $x/D0$ of 3.38 and 6.25 to follow the irregularity seen in the entrance profile. These irregular velocity profiles would then suggest that the turbulence intensities would be higher not only at the edges but also in the core. This is seen in the contour plots of the axial turbulence intensity normalized by $\hat{U}_0$. Moreover the structure also shows affinity towards the wall of the cylinder as the gradients in velocity there would be higher as observed in the mean velocity plots. This is especially clear in the Figure 75 where the plots represent phases phases of $\frac{t}{T} = 0.750$, $\frac{t}{T} = 0.7917$ and $\frac{t}{T} = 0.8333$ for the 4 Hz case. Similar observations can be made for phases of $\frac{t}{T} = 0.9091$ and $\frac{t}{T} = 1.00$ for the 8 Hz case in Figure 81 and $\frac{t}{T} = 0.000$, $\frac{t}{T} = 0.143$ and $\frac{t}{T} = 0.286$ for the 12 Hz case in Figure 82.

Turbulence intensity in the above cases could have been normalized by the average over a cross section of the jet of the phase average velocities. However in the present case it was not possible to define such an area for finding the average of the phase averaged velocities. Contour plots of turbulence intensity normalized by the local phase averaged velocity is presented in Figure 90 for the three frequencies considered at particular phases. Compared to the plots in

Figures 69-84, these do not provide any useful information. Hence this type of normalizing was abandoned.

Figure 86 to Figure 89 show axial turbulence intensities measured for the straight tube case. Here the intensities have been normalized using the maximum of the velocity (centerline) at the given axial station. These plots represent the values obtained for charging phases only as values obtained for venting phases are not as well defined. The maximum intensity measured was about 0.014. There is one case for $\frac{t}{T} = 0.625$ at 4 Hz where as much as 0.4 is seen (Figure 86, center), but this should not be considered here because any intensity measured with hot wire above 0.3 is suspect. This enormity may be due to the sudden change of flow direction from venting to charging. Similar but smaller increases are observed at $\frac{t}{T} = 0.8181$ for 8 Hz and $\frac{t}{T} = 1.00$ for 12 Hz. The intensity is smaller on the centerline for $\frac{x}{D0} = 3.38$ in some cases. This is because the velocity gradient is smaller on the centerline than slightly away. The intensity also shows an increase along the axial direction in cases where the jet has penetrated up to the rear most axial station.

5.0 Conclusion

Complexities of some internal flow problems have been presented. Modeling of internal flow fields with hot, compressible fluids and sometimes combustion using cold flow techniques has been discussed. The flow in a D-5 PBCS gas generator has been modeled using cold air. Experimental set up was designed and fabricated to simulate the unsteady flow with different configurations of inlet tubes. In addition to a model of the original different inlet tube variations were used. Flow field investigation was done with flow visualization and measurement of axial velocity at different frequencies ranging from 4 Hz to 12 Hz.

Flow visualization was done using silk tufts and small styrofoam beads, treated for elimination of static build up. The silk tufts showed that the incoming flow was a complex jet flow confined to a cylindrical enclosure, while the outgoing flow resembled the venting of a pressurized vessel with the 70° inlet tube. The tests with the styrofoam beads have been recorded on videotapes. These pictures show a complex flow pattern due to the angling of the jet towards the wall. The

basic flow patterns observed were a big oval clockwise flow degenerating into two clockwise cells when viewed from the side with the inlet to the right. "Scrubbing" of the wall of the generator was observed at the area of impingement of the jet. Similar patterns were observed with other distorted inlets. A straight tube inlet, a bent tube inlet with a 4 in. straight section and a ½ in. long splitter vane across center of the entrance straightened the jet considerably and eliminated the above flow patterns.

Velocity measurements were made at an inlet Re of 8.1×10^4 using a single sensor hot wire anemometer. The measurements were made at the entrance and at several radial locations along the axis in the plane of the inlet tube at 4 Hz, 8 Hz and 12 Hz for the straight tube and bent tube inlet configurations. Spectral analysis of the axial velocity near the entrance showed that it had a strong component of the forcing frequency. Phase averaging of the time series allowed to identify the charging phases and the venting phases in a cycle for a given frequency. Phase averaged mean velocities were observed to be well defined during charging and diminished during venting inside the cylinder.

For the straight tube inlet comparison with a steady flow measurement of sudden expansion flow was found to be qualitatively similar for the mean axial velocity distribution during the charging phases. The centerline axial velocity decay also showed qualitative similarity during most charging phases. The jet flow penetrated most for the 4 Hz and least for the 12 Hz case.

Similar observations were made for the bent tube inlet case about jet penetration and charging and venting phases. In addition the contour plots

showed the flow tendency towards the wall. Two cells were seen in the contours for the 8 Hz and 12 Hz cases. The deviation of the point of occurrence of maximum velocity in a radial profile was found to be about 6.5° . Entrance velocity profiles showed symmetry for the straight tube inlet while were skewed for the bent tube inlet.

Contour plots of the phase averaged axial turbulence intensity for bent tube cases show higher values in the core due to the skewness of the velocity profile. There is also an occurrence of higher values near the wall in the region of impingement. Axial turbulence intensity measured at two stations for the straight tube case show similar features as observed in an axisymmetric sudden expansion flow.

References

1. Arcoumanis, C., Bicen, A.F. and Whitelaw, J.F., "Measurements in a motored four-stroke reciprocating model engine", *Fluid mechanics of Combustion Systems; Fluids Engineering Conference - ASME*, pp. 21-27, June 1981.

2. Arcoumanis, C., Bicen, A.F. and Whitelaw, J.F., "The application of LDA to four-stroke motored model engines", *Laser anemometry in Fluid Mechanics : Selected papers from the First Intl. Symp. on applications of Laser-Doppler Anemometry*, pp. 165-178, July 1982.

3. Asanuma, T., Iijima, T. and Katayama, K., "Flow characteristics of an unsteady jet ejected into a prechamber spark ignition engine", *Laser Diagnostics and Modelling of Combustion*, pp. 35-44, 1987.

4. Beer, J.M. and Chigier, N.A., *Combustion Aerodynamics*, Robert E. Kreiger Publishing Company, Malabar, FL, pp. 196-211, 1983.

5. Binder, G. and Favre-Marinet, M., "Some characteristics of pulsating or flapping jets", *IUTAM Symposium on Unsteady Turbulent Shear Flows*, Toulouse, France, pp. 370-379, May 1981.

6. Bradley, T.A. and Ng, T.T., "Phase-locking in a jet forced with two frequencies", *Experiments in Fluids*, Vol. 7, pp. 38-48, 1989.

7. Bremhorst, K., "Unsteady subsonic turbulent jets", *Recent Developments in Theoretical and Experimental Fluid Mechanics : compressible and incompressible flows*, pp. 480-500, 1979.

8. Bremhorst, K. and Harch, W.H., "Near field velocity measurements in a fully pulsed subsonic air jet", *Symposium on Turbulent Shear Flows*, pp. 2.41-2.50, April 1977.

9. Clarke, A.E., Gerrard, A.J. and Holliday, L.A., "Some experiences in gas turbine combustion chamber practice using water flow visualization techniques", *Ninth Symposium (International) on Combustion*, pp. 878-891, 1962.

10. *DASH-16/16F Manual*, Metrabyte Corporation, Taunton, MA, 1986.

11. *Final EDT-5 Test Report*, Atlantic Research Corporation, Gainesville, VA, August 1986.

12. Gerrard, A.J., "Methods of flow visualization by means of water", *Experimental Methods in Combustion Research - A Manual*, Edited by J. Surugue, section 2.1.1, pp. 22-44, 1961.

13. Gosman, A.D. and Watkins, A.P., "A computer prediction method for turbulent flow and heat transfer in piston/cylinder assemblies", *Symposium on Turbulent Shear Flows*, pp. 5.23-5.30, April 1977.

14. Gostelow, J.P., "A new approach to the experimental study of turbomachinery flow phenomena", *Transactions of ASME - Journal of Engineering for Power*, pp. 97-105, January 1977.

15. Gupta, A.K. and Lilley, D.G., *Flowfield Modeling and Diagnostics; Energy and Engineering Science Series*, Vol. 4, Tunbridge Wells, Kent, Abacus Press, 1985.

16. Holman, J.P., *Experimental Methods for Engineers*, pp. 50-88, McGraw-Hill Book Company,1984.

17. Kennedy, J.B., "Ramburner flow visualization studies", *Eleventh JANNAF Combustion Meeting*, pp. 415-440, 1974.

18. Khalil, E.E., *Modelling of Furnaces and Combustors; Energy and Engineering Science Series*, Vol. 2, Tunbridge Wells, Kent, Abacus Press, 1982.

19. Kline, S.J. and McClintock, F.A., "Describing uncertainties in single sample experiments", *Mechanical Engineering*, pp. 3-8, January 1953.

20. Leister, P., "Experimental investigation on the turbulence structure of an impinging, pulsating jet", *Symposium on Turbulent Shear Flows*, pp. 3.35-3.44, April 1977.

21. Liou, T.M., Santavicca, D.A. and Bracco, F.V., "Turbulence measurements in a ported IC engine", *Laser Anemometry in Fluid Mechanics : Selected papers from the First Intl. Symp. on applications of Laser-Doppler Anemometry*, pp. 179-194, July 1982.

22. Liou, T.M. and Santavicca, D.A., "Cycle resolved LDV measurements in a motored IC engine", *Transactions of ASME - Journal of Fluids Engineering*, Vol. 107, pp. 232-240, June 1985.

23. Marchman, J.F. and Kuppa, S., *Flow Visualization Tests of the D-5 Gas Generator - Final Project Report*, March 1987.

24. Merzkirch, Wolfgang, *Flow Visualization*, Orlando, Academic Press, 1987.

25. Meyer, P. and Sava, P.G., "Two dimensional laser-Doppler measurements of fluctuations of velocity in an excited jet", *Laser Anemometry in Fluid Mechanics : Selected papers from the First Intl. Symp. on applications of Laser-Doppler Anemometry*, pp. 3-18, July 1982.

26. Miller, D.S., *Internal Flow Systems*, pp. 43-69, Vol. 5, BHRA Fluid Engineering Series, 1978.

27. Moffat, R.J., "Describing uncertainties in experimental results", *Experimental Thermal and Fluid Science*, 1 : 3-17, 1988.

28. Morrison, G.L., Tatterson, G.B. and Long, M.W., "Three-dimensional laser velocimeter investigation of turbulent, incompressible flow in an axisymmetric sudden expansion", *Journal of Propulsion and Power*, Vol. 4, No. 6, pp. 533-540, Nov.-Dec. 1988.

29. Parikh, P.G. and Moffat, R.J., "Mixing improvement in a resonantly pulsed, confined jet", *Fluid Mechanics of Combustion Systems : Fluids Engineering Conference - ASME*, pp. 251-256, June 1981.

30. Poulston, B.V. and Winter, E.F., "Techniques for the study of air flow and fuel droplet distribution in combustion systems", *Sixth Symposium (International) on Combustion*, pp. 833-842, 1956.

31. Rask, R.B., "Comparison of window, smoothed-ensemble, and cycle-by-cycle data reduction techniques for laser Doppler anemometer measurements of in-cylinder velocity", *Fluid Mechanics of Combustion Systems : Fluids Engineering Conference - ASME*, pp. 11-20, June 1981.

32. Schetz, J.A., Hewitt, P.W. and Thomas, R., "Swirl combustor flow visualization studies in a water tunnel", *Journal of Spacecraft and Rockets*, Vol. 20, No. 6, pp. 574-582, November-December 1983.

33. Schetz, J.A., Guruswamy, J.and Marchman J.F., "Effects of an S-inlet on the flow in a dump combustor", *Journal of Spacecraft and Rockets*, Vol. 22, No. 2, pp. 221-224, March-April 1985.

34. Schetz, J.A., Sebba, F. and Thomas, R.H., "Flow visualization studies of a solid fuel ramjet combustor using a new material-polyaphrons", *Twenty second JANNAF Combustion Meeting*, pp. 1-9, October 1985.

35. Sharma, O.P., Butler, T.L., Joslyn, H.D., and Dring, R.P., "Three-dimensional unsteady flow in an axial flow turbine", *Journal of Propulsion and Power*, Vol. 1, No. 1, pp. 29-38, January-February 1985.

36. Spalding, D.B., "The art of partial modeling", *Ninth Symposium (International) on Combustion - Colloquium on Modeling Principles*, pp. 833-843, 1962.

37. Stull, F.D., Craig, R.R., Streby, G.D. and Vanka, S.P., "Investigation of a dual inlet side dump combustor using liquid fuel injection", *Journal of Propulsion and Power*, Vol. 1, No. 1, pp. 83-88, January-February 1985.

38. Tiederman, W.G., Privette, R.M. and Phillips, W.M., "Cycle-to-cycle variation effects on turbulent shear stress measurements in pulsatile flows", *Experiments in Fluids*, Vol. 6, pp. 265-272, 1988.

39. Vanka, S.P., Stull, F.D. and Craig, R.R., "Analytical characterization of flow fields in side-inlet dump combustors", *AIAA/SAE/ASME Nineteenth Joint Propulsion Conference*, AIAA-83-1399, June 1983.

40. Walburn, F.J., Sabbah, H.N. and Stein, P.D., "An experimental evaluation of the use of an ensemble average for the calculation of turbulence in pulsatile flow", *Annals of Biomedical Engineering*, Vol. 11, pp. 385-399, 1983.

41. Winter, E.F. and Deterding, M.A., "Apparatus and techniques for the application of a water flow system to the study of aerodynamic systems", *British Journal of Applied Physics*, Vol. 7, pp. 247-260, July 1956.

42. Winter, E.F., "Flow visualization techniques applied to combustion problems", *Journal of the Royal Aeronautical Society*, Vol. 62, pp. 268-276, April 1958.

PAGE LEFT BLANK INTENTIONALLY

Figures

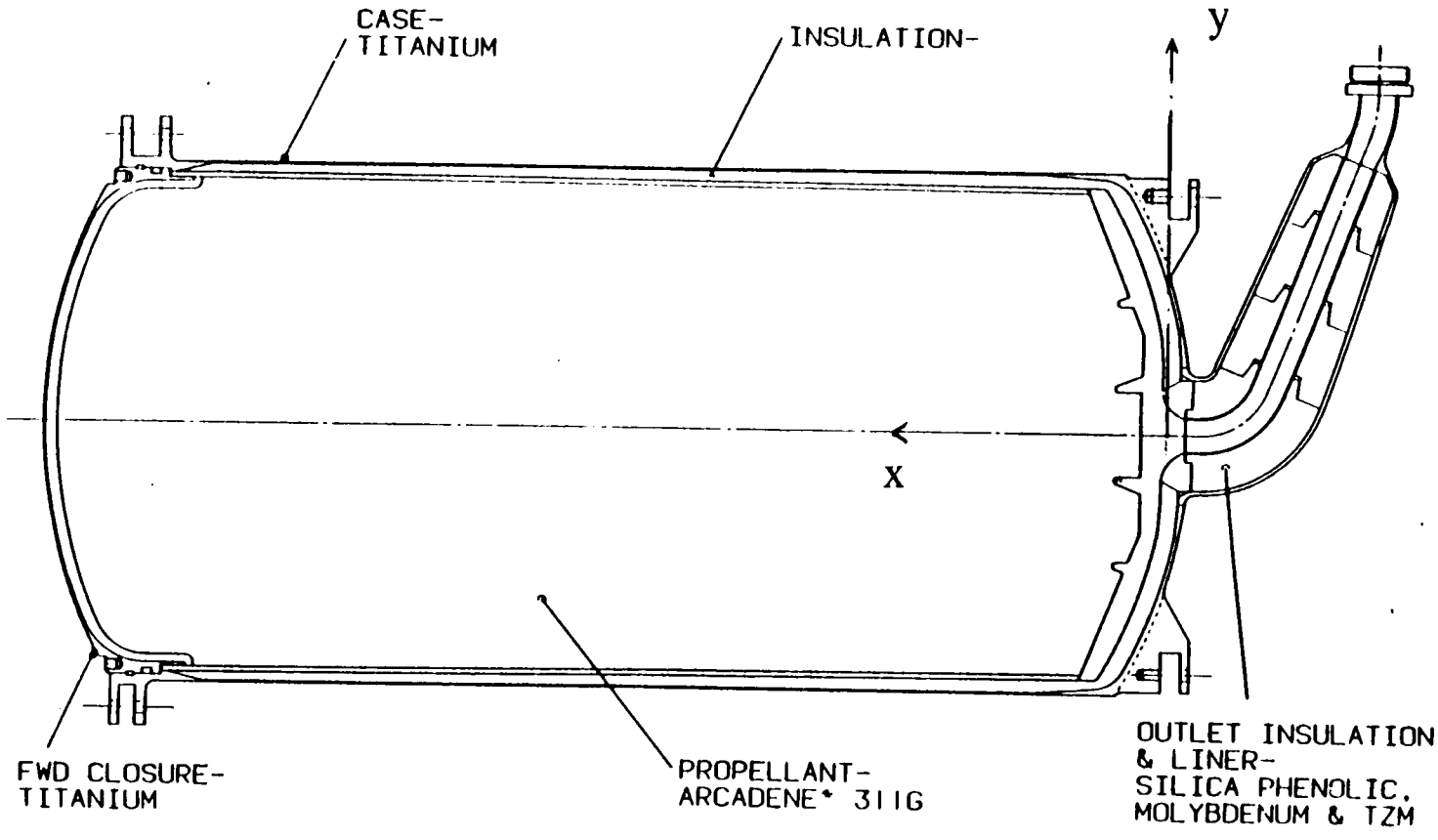

Figure 1. Basic geometry of the flow problem.

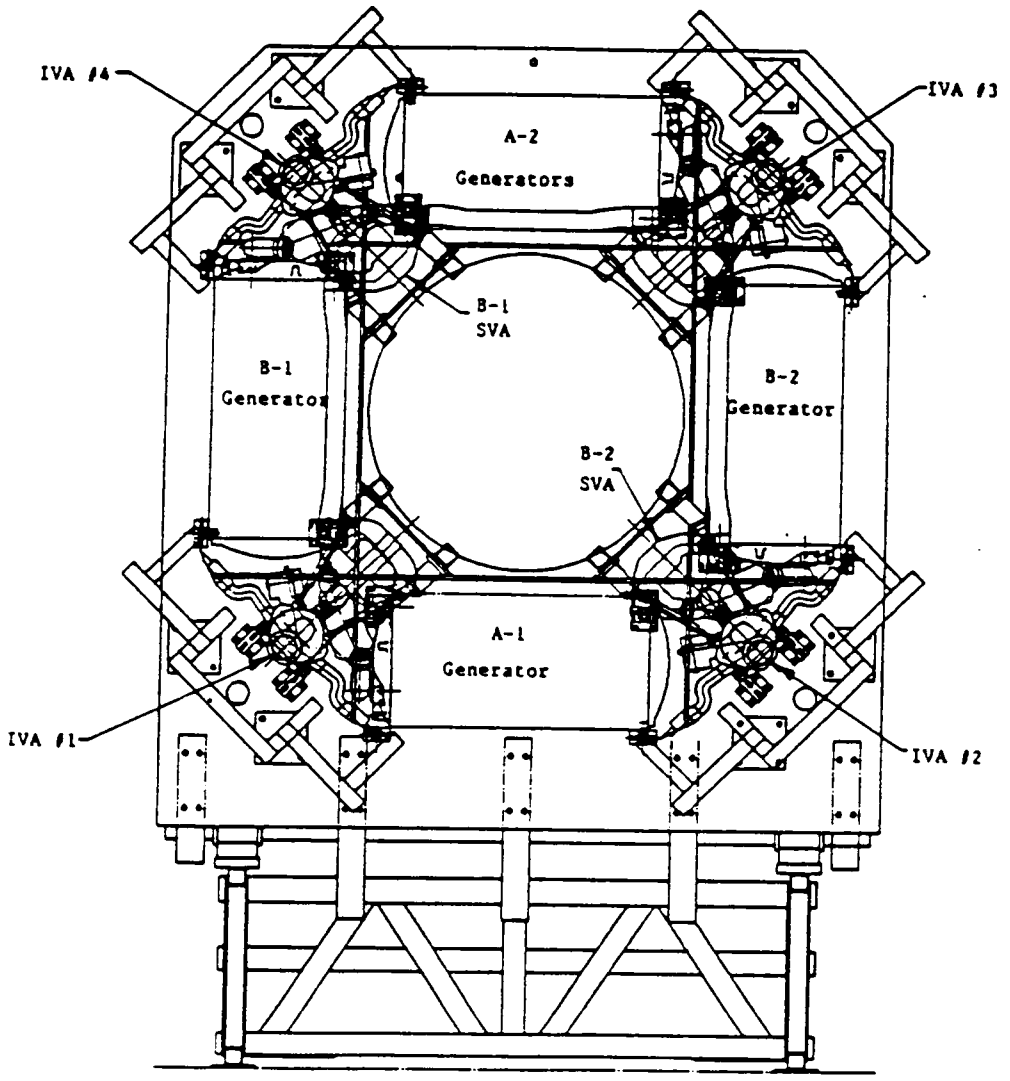

Figure 2. D-5 PBCS gas generator system.

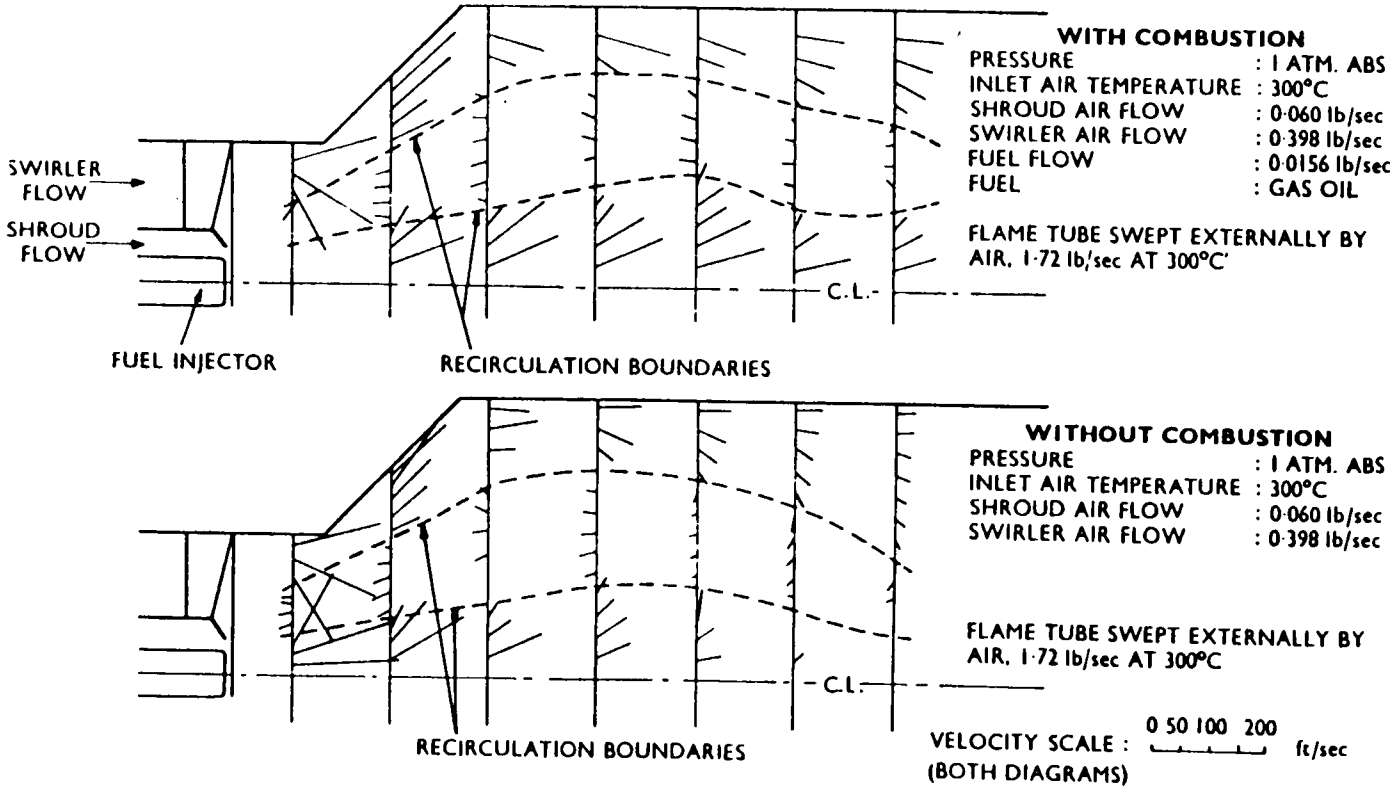

Figure 3. Flow patterns in the combustion zone of a gas turbine system.: The vectors refer to components in the central plane; swirl component not shown.

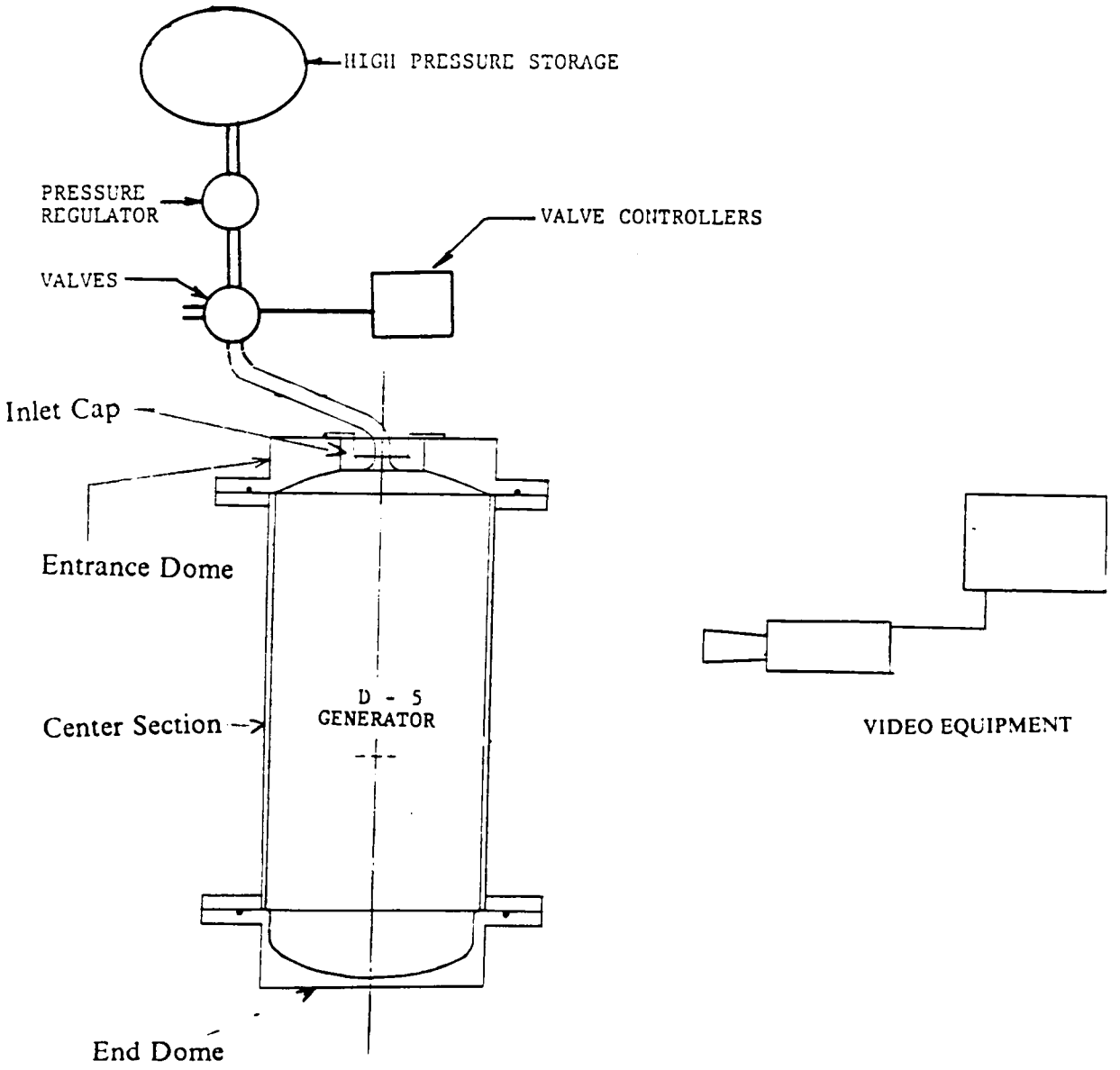

Figure 4. Model set up for flow visualization tests.

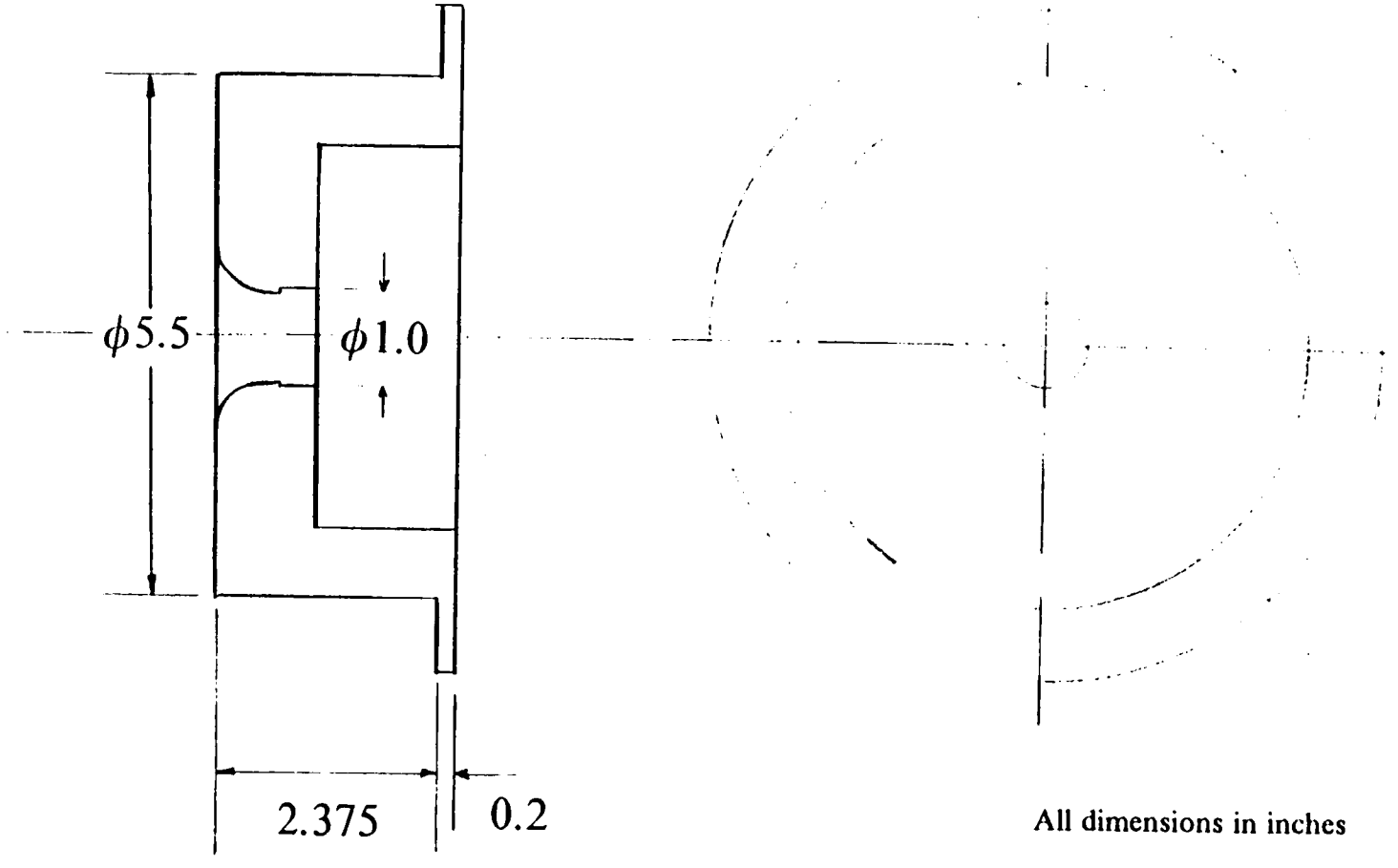

Figure 5. Inlet cap for different inlet tube configurations of the model.

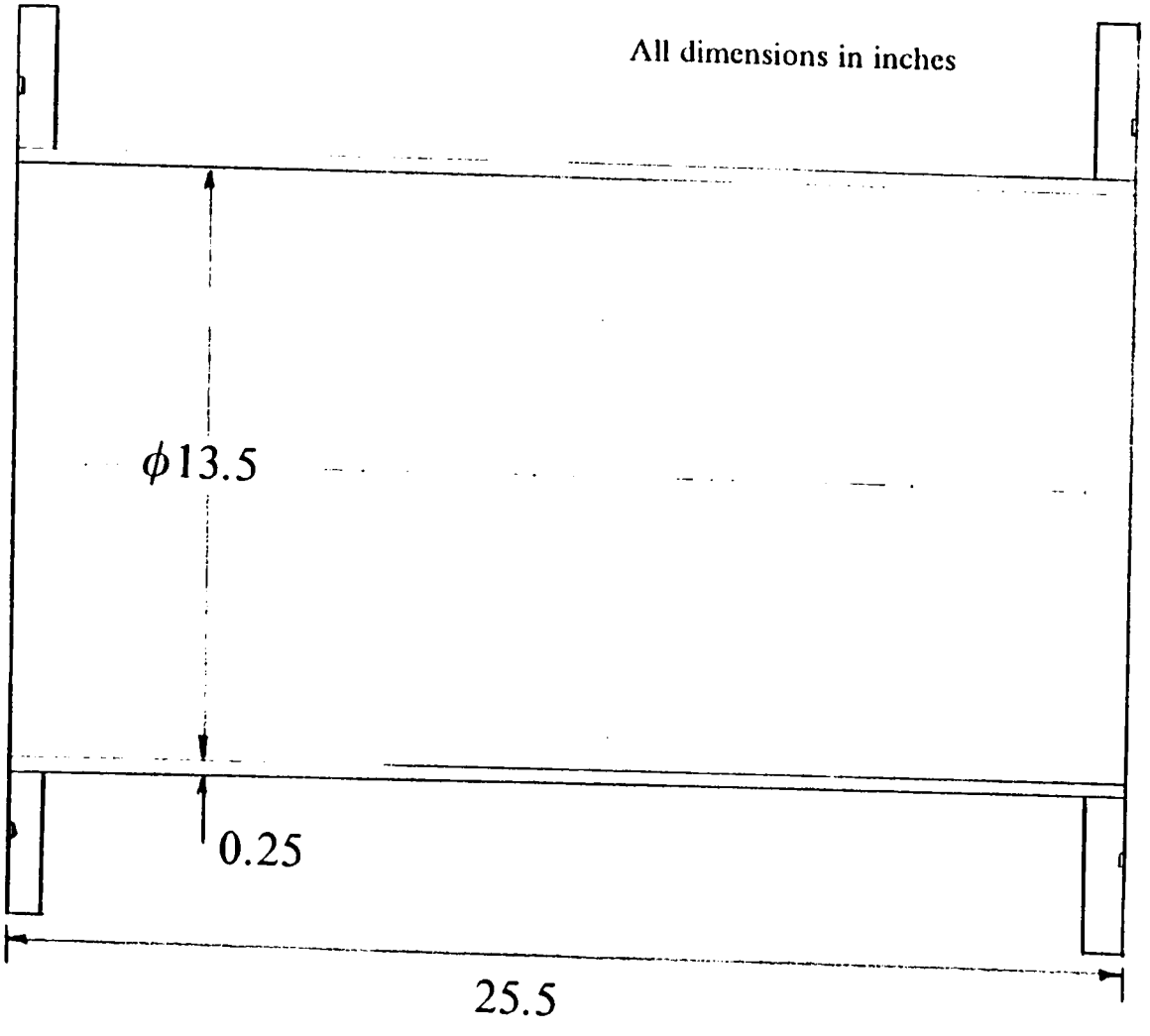

Figure 6. Model center section with flanges.

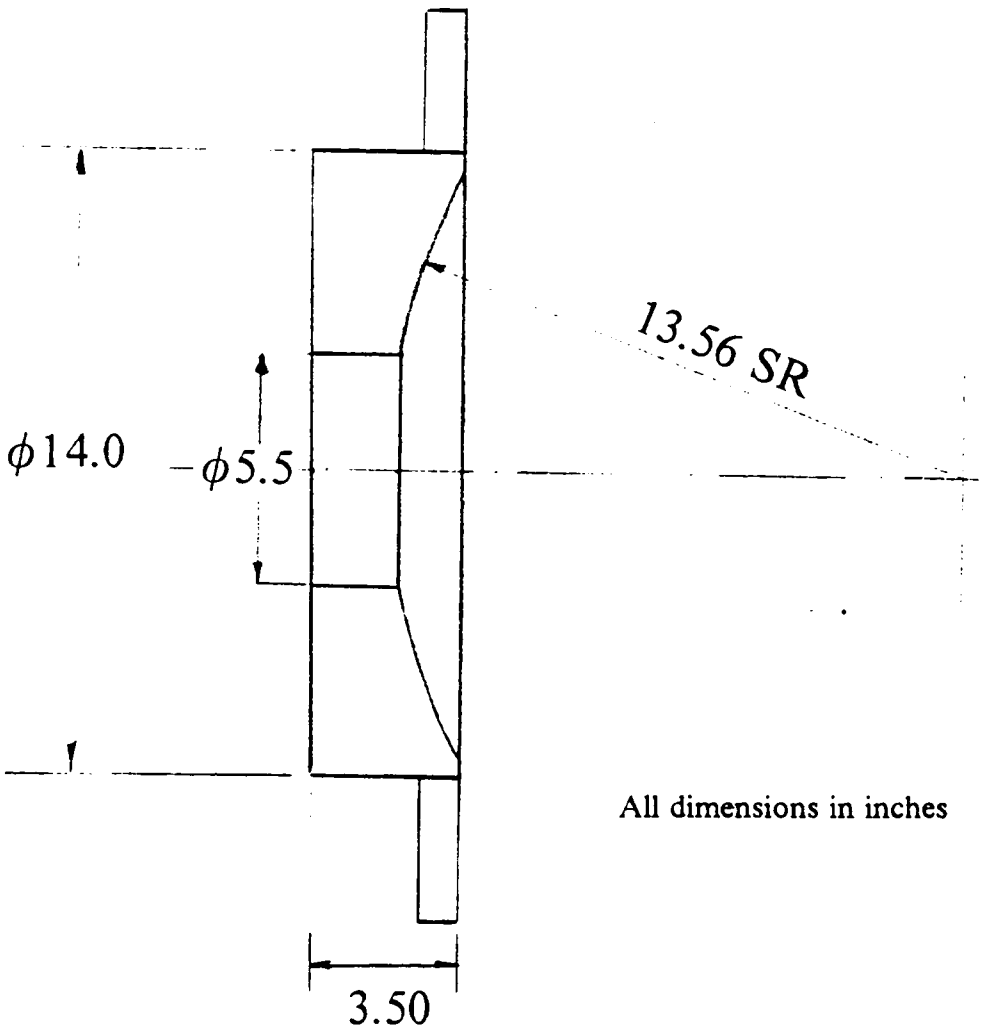

Figure 7. Dome on the entrance side of the model.

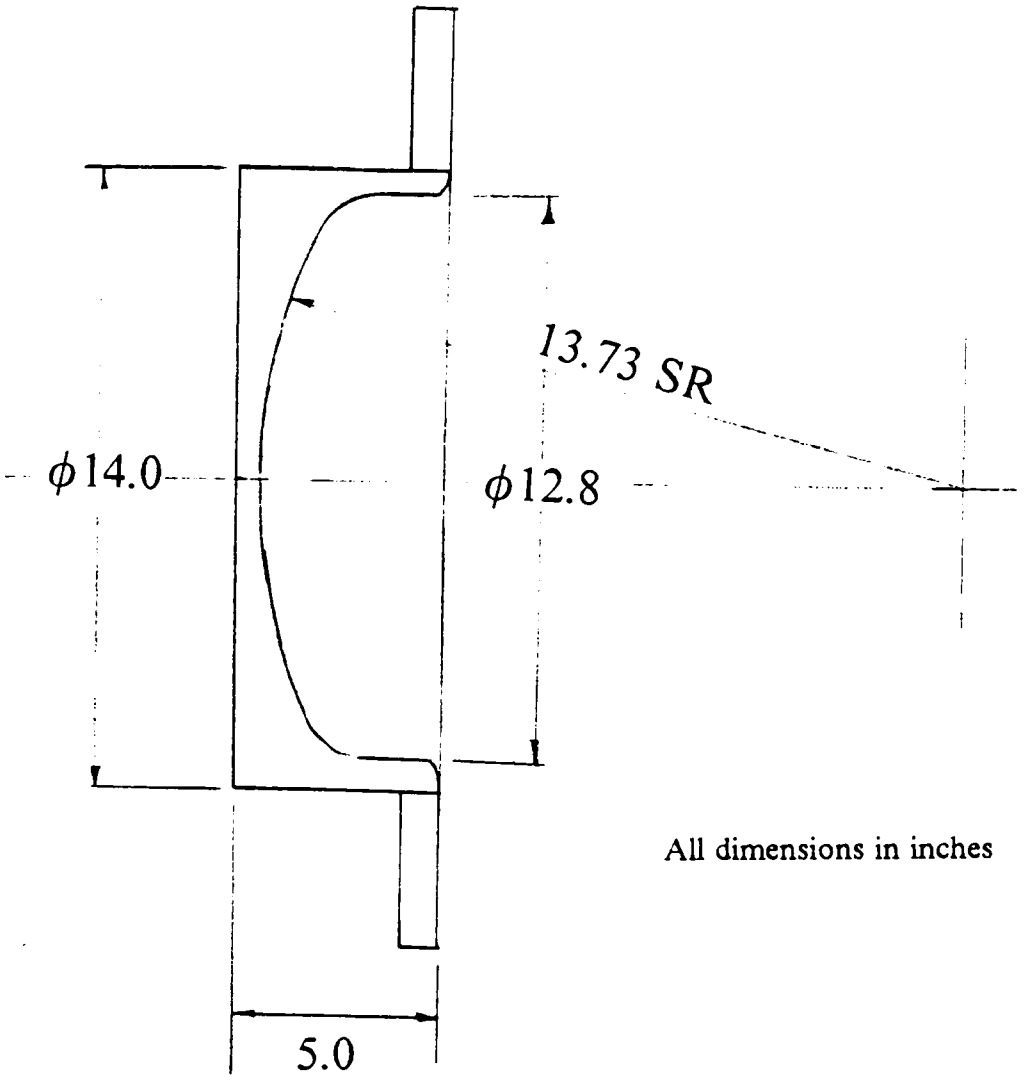

Figure 8. Dome on the side away from entrance side of the model.

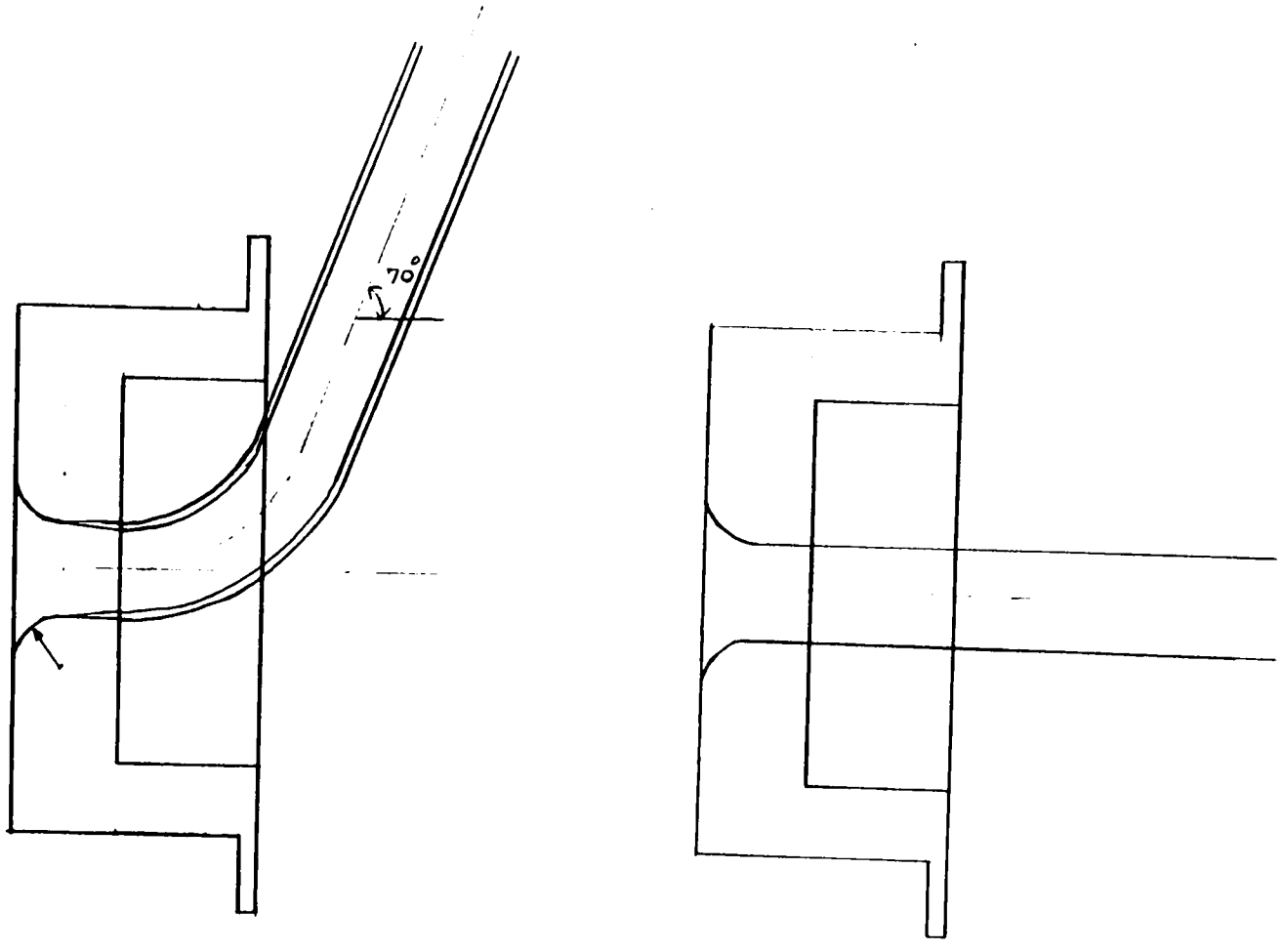

Figure 9. The 70° and straight inlet tube configurations for the model.

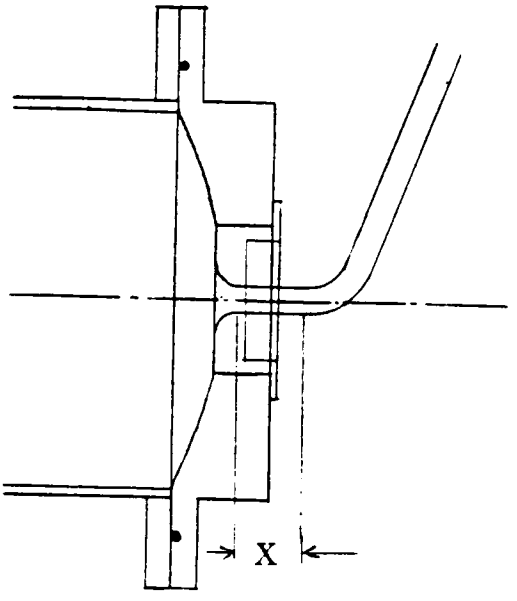

Sketch of extension of the entrance tube's straight section (x = 1″, 2″, 3″, and 4″). Splitter vane used only with x = 1″.

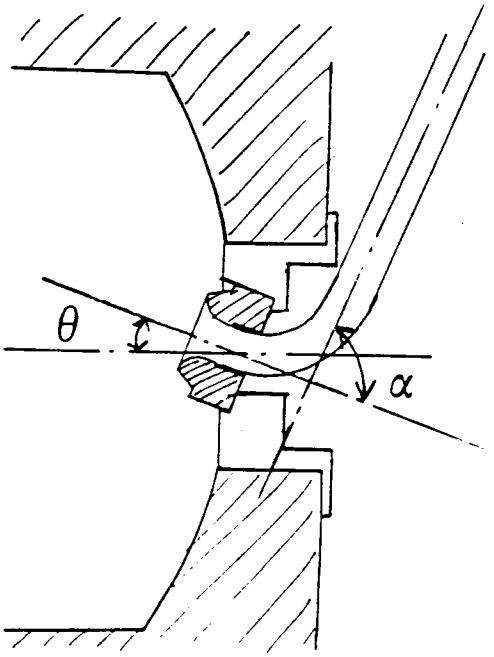

Sketch of simulated distorted entrance tube configuration. For θ = 70° ,75° ,80° and 90° , α = 0°,5° ,10° and 20° respectively.

Figure 10. Schematics of the different copper entrance configurations used with the model in flow visualization tests.

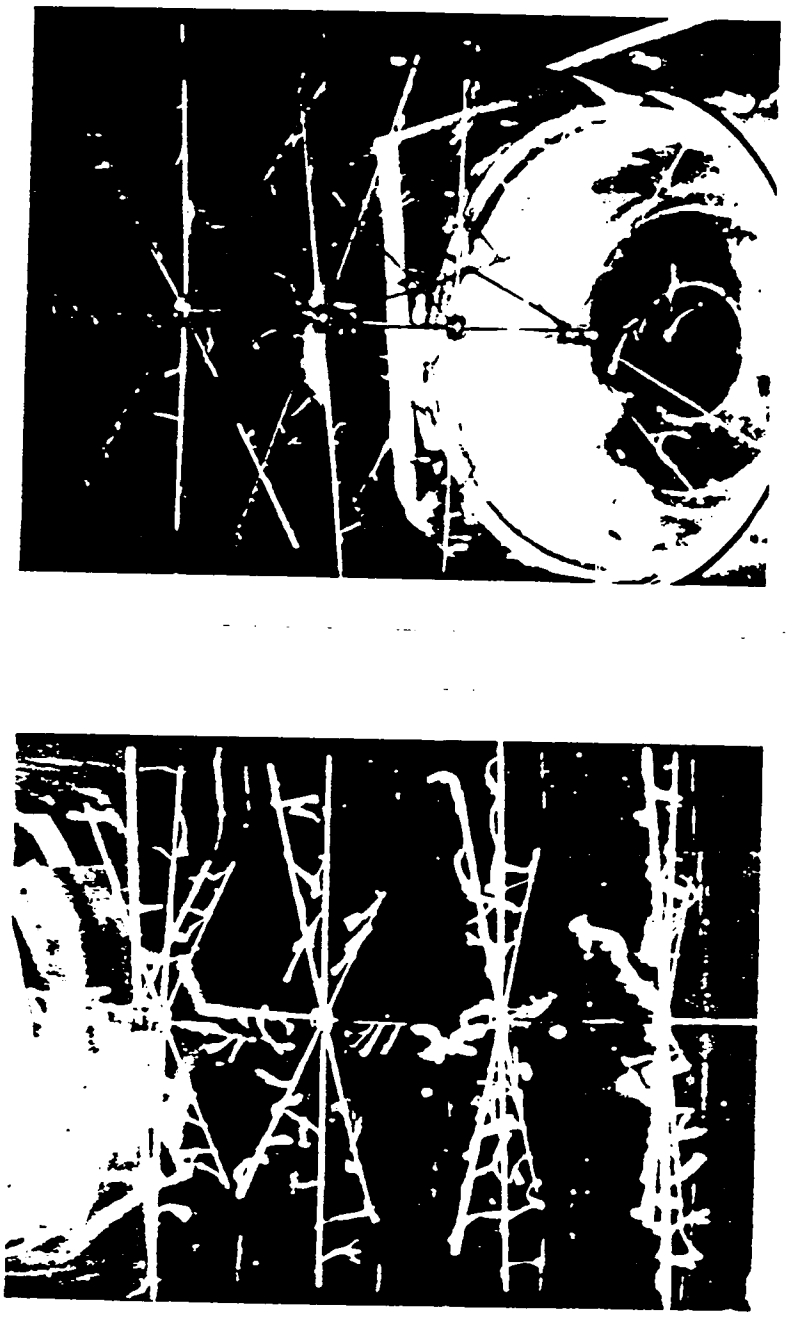

Figure 11. Arrangement for flow visualization with silk tufts.

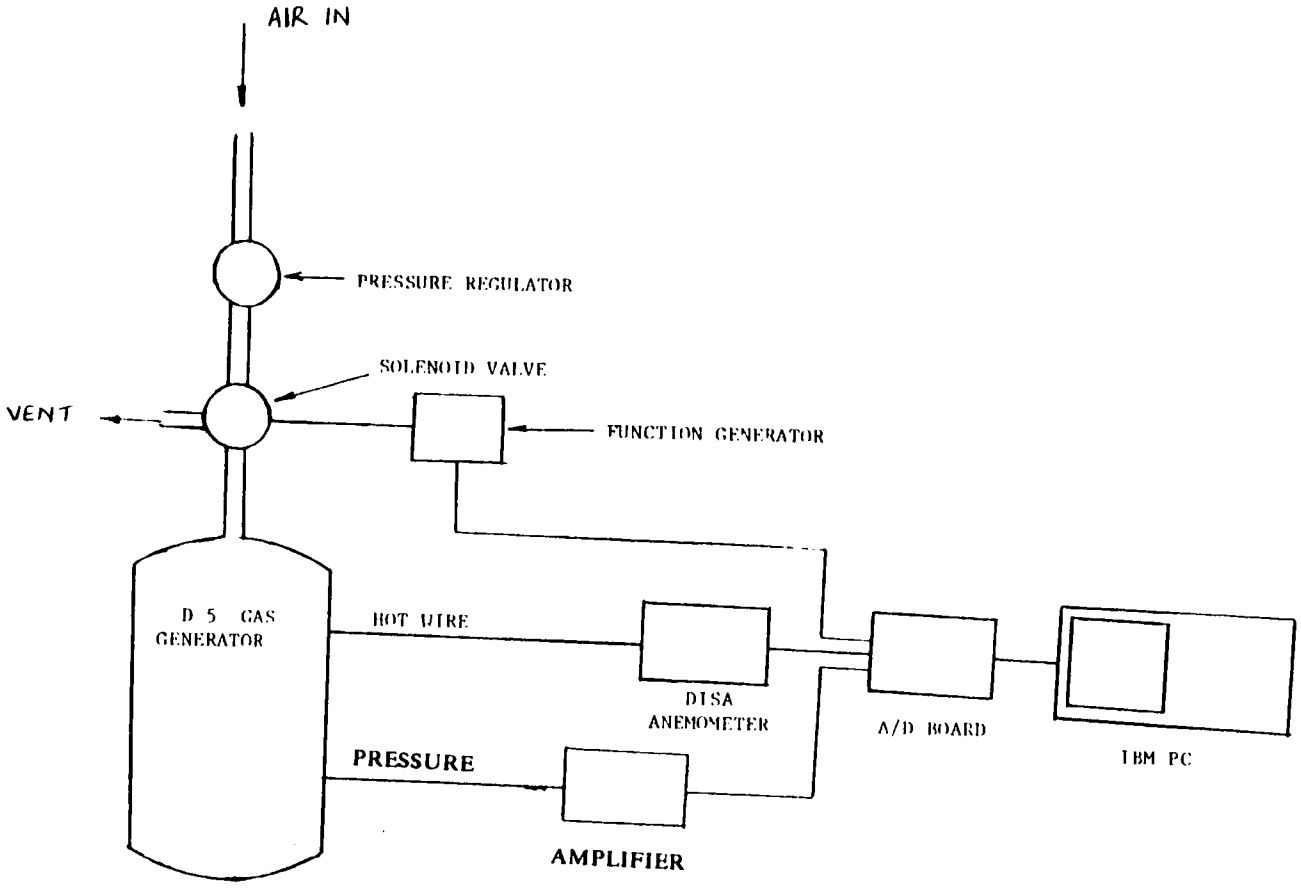

Figure 12. Model set up for velocity measurements.

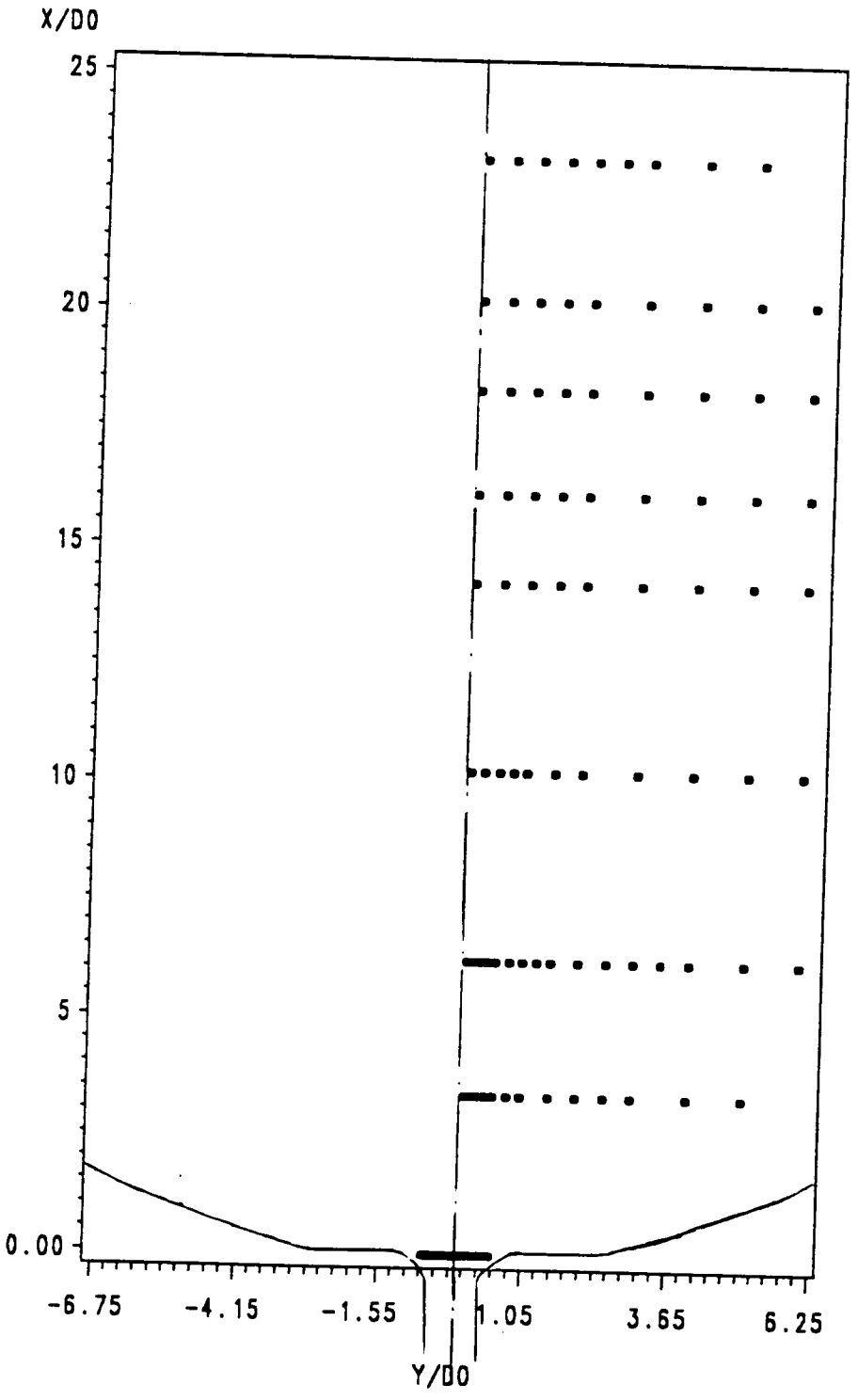

Figure 13. Locations of velocity measurements for straight inlet tube.

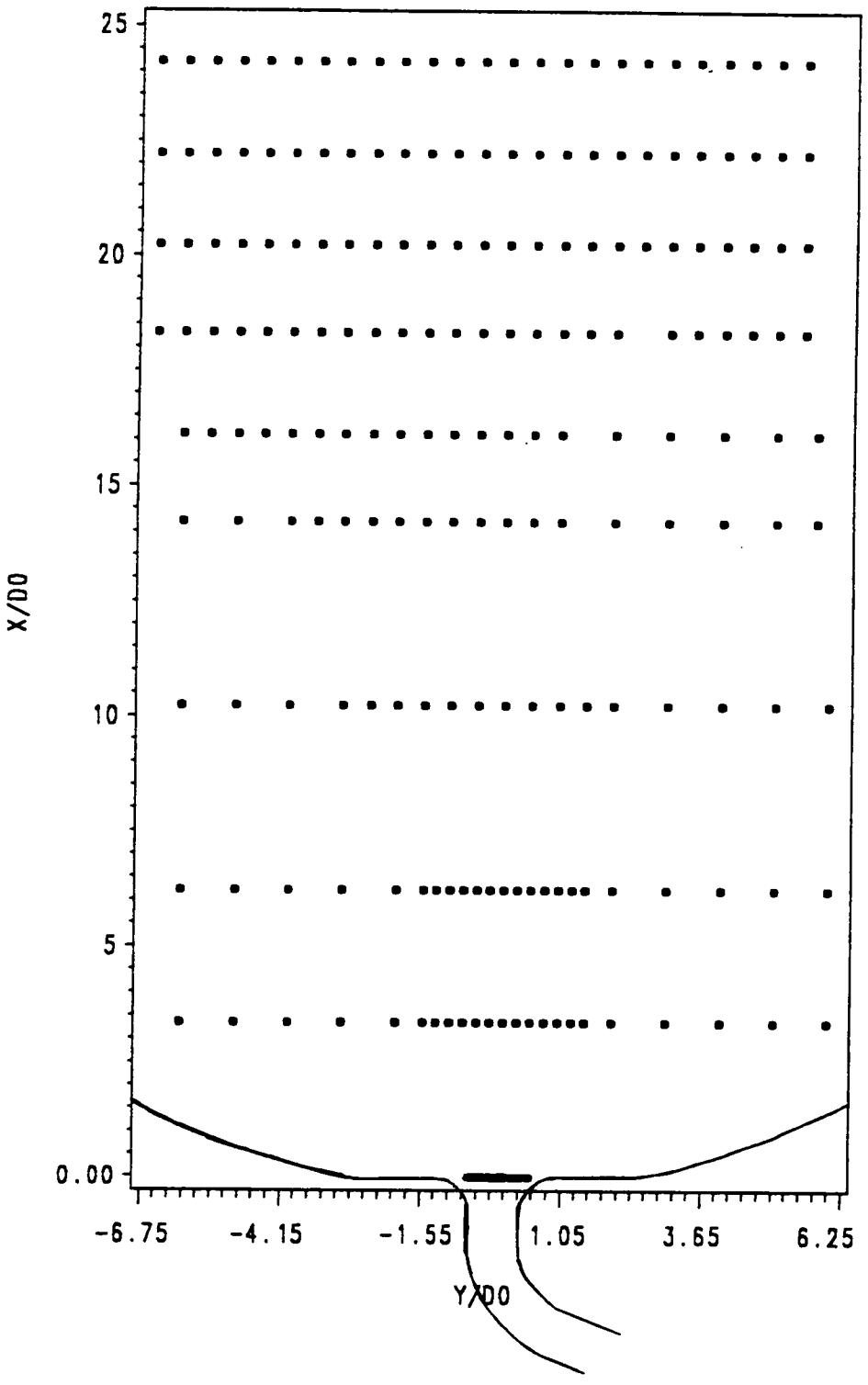

Figure 14. Locations of velocity measurements for bent inlet tube.

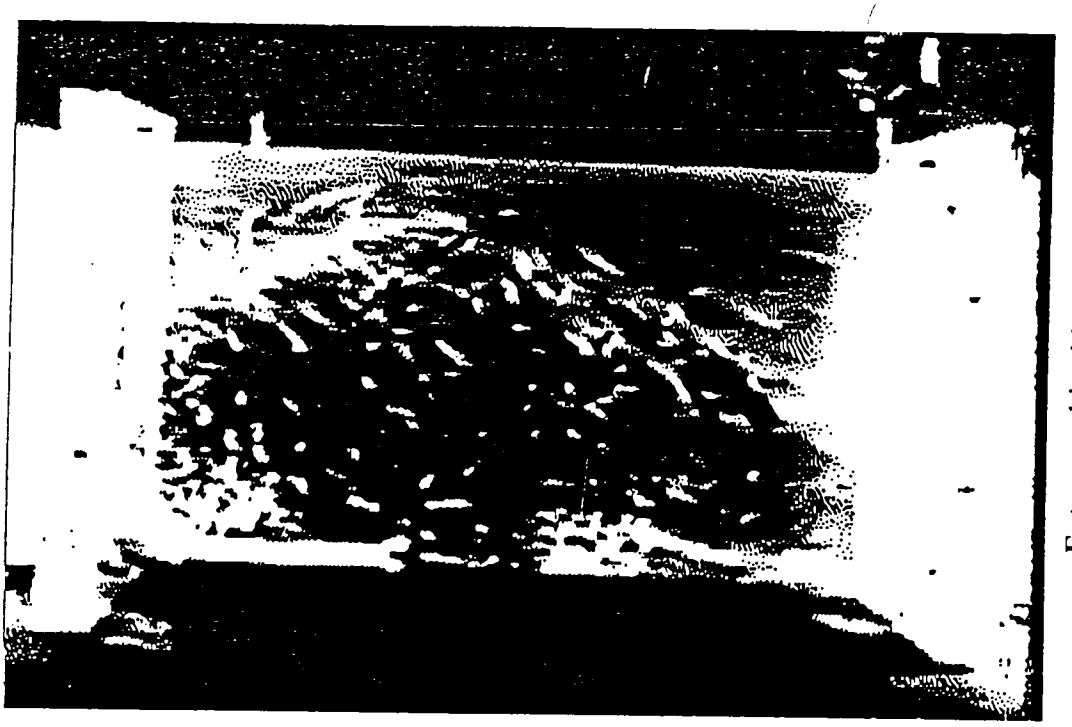

Figure 15. Side view of gas generator model with 70° entrance tube.: 4 Hz - 4 psig.

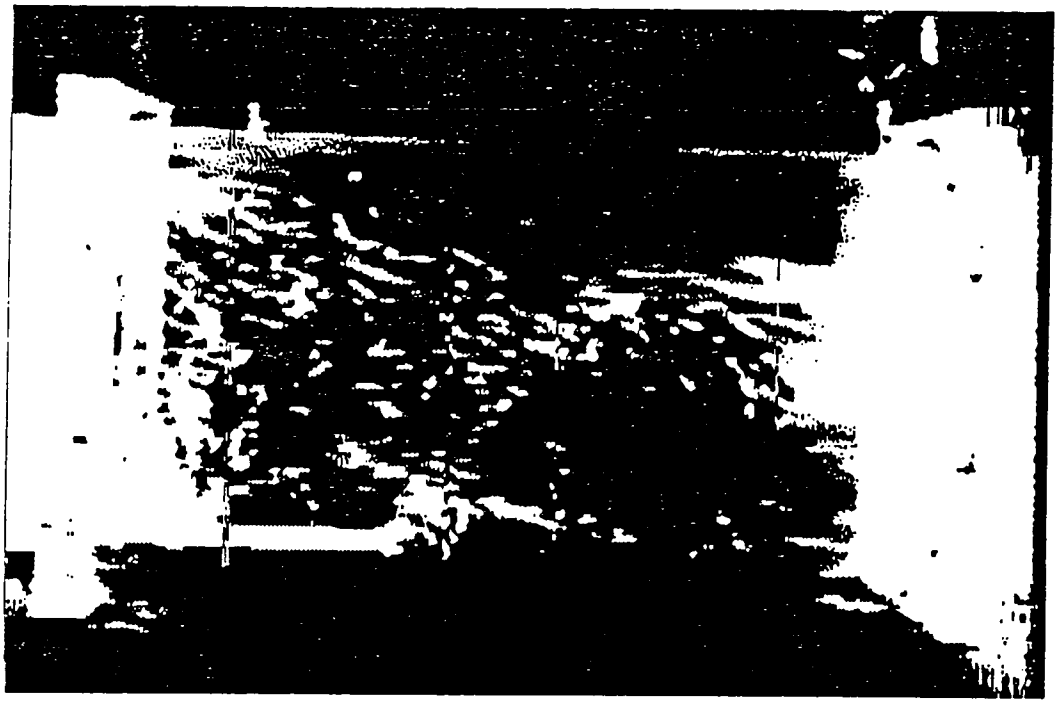

Figure 16. Another side view of gas generator model with 70° entrance tube.: 4 Hz - 4 psig.

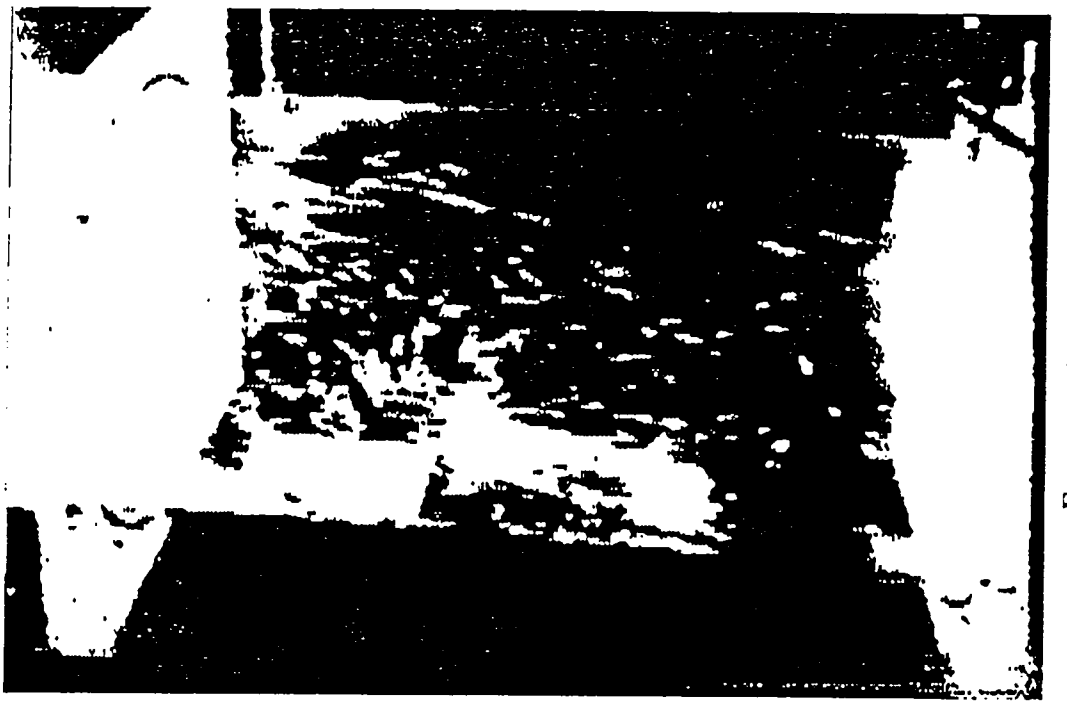

Figure 17. Oblique view of gas generator model with 70° entrance tube.: 4 Hz - 4 psig.

Figure 18. Flow pattern obtained with 20° offset entrance tube.: 4 Hz - 4 psig.

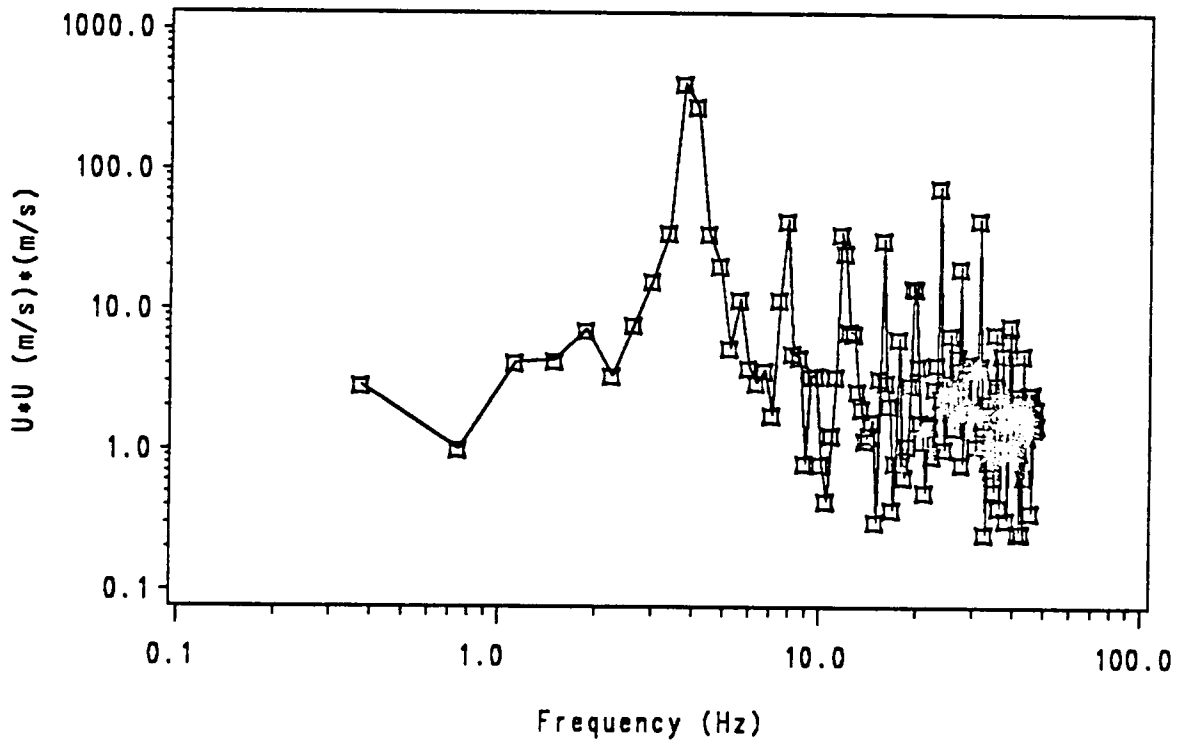

Figure 19. Frequency spectrum of the axial velocity on the centerline ; x/d0 = 3.38; at 4 Hz.

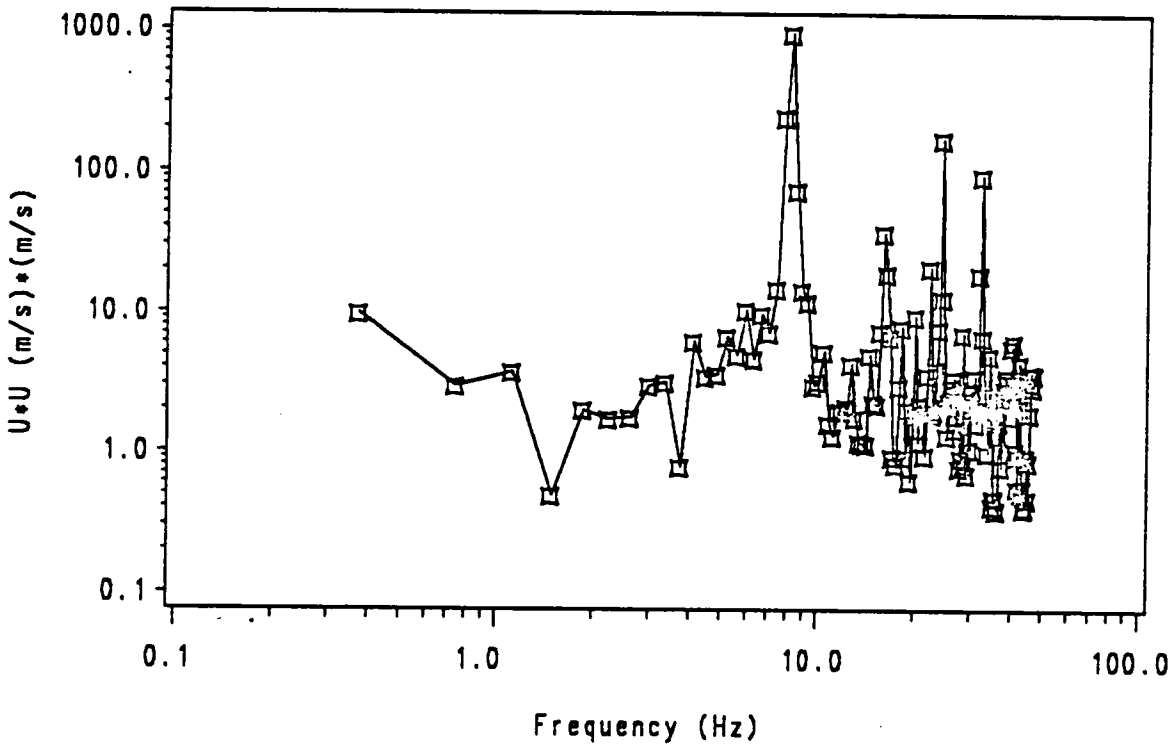

Figure 20. Frequency spectrum of the axial velocity on the centerline ; x/d0 = 3.38; at 8 Hz.

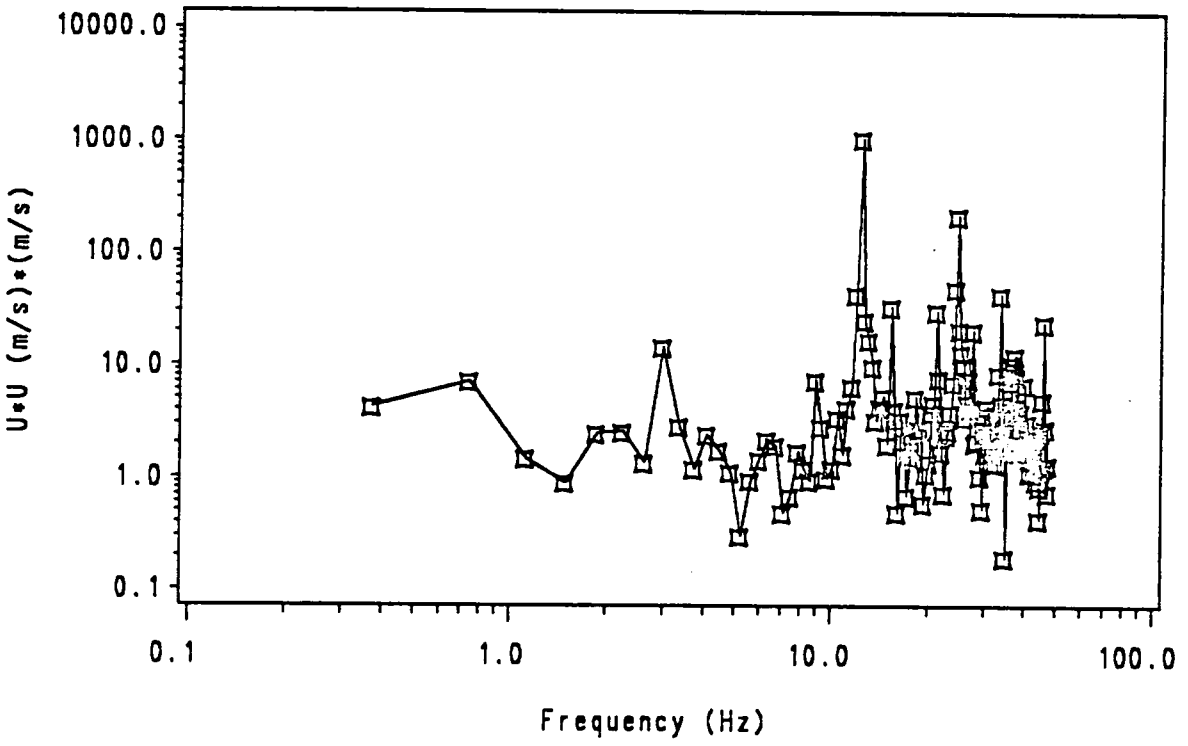

Figure 21. Frequency spectrum of the axial velocity on the centerline ; x/d0 = 3.38; at 12 Hz.

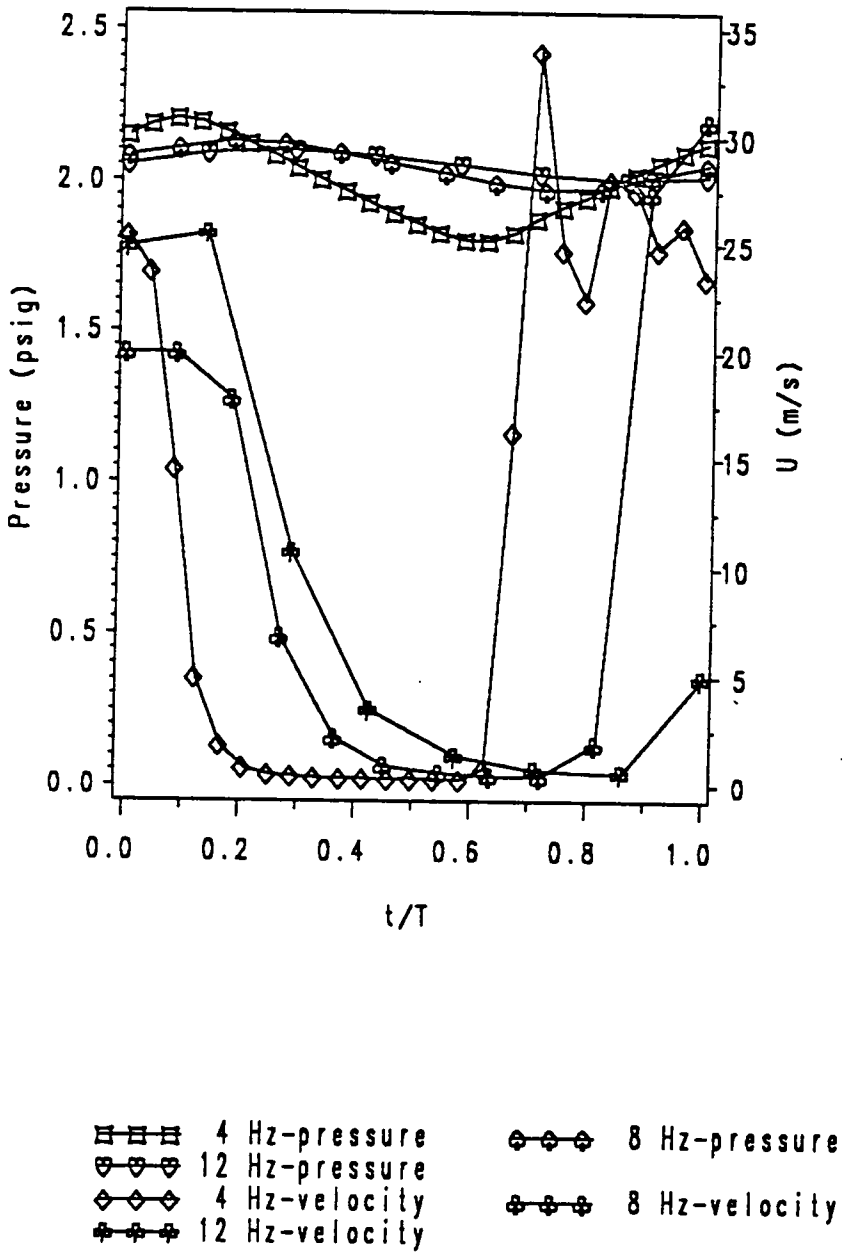

Figure 22. Phase-lock averaged mean pressure and velocity traces on the centerline over a cycle at x/d0 = 3.38.

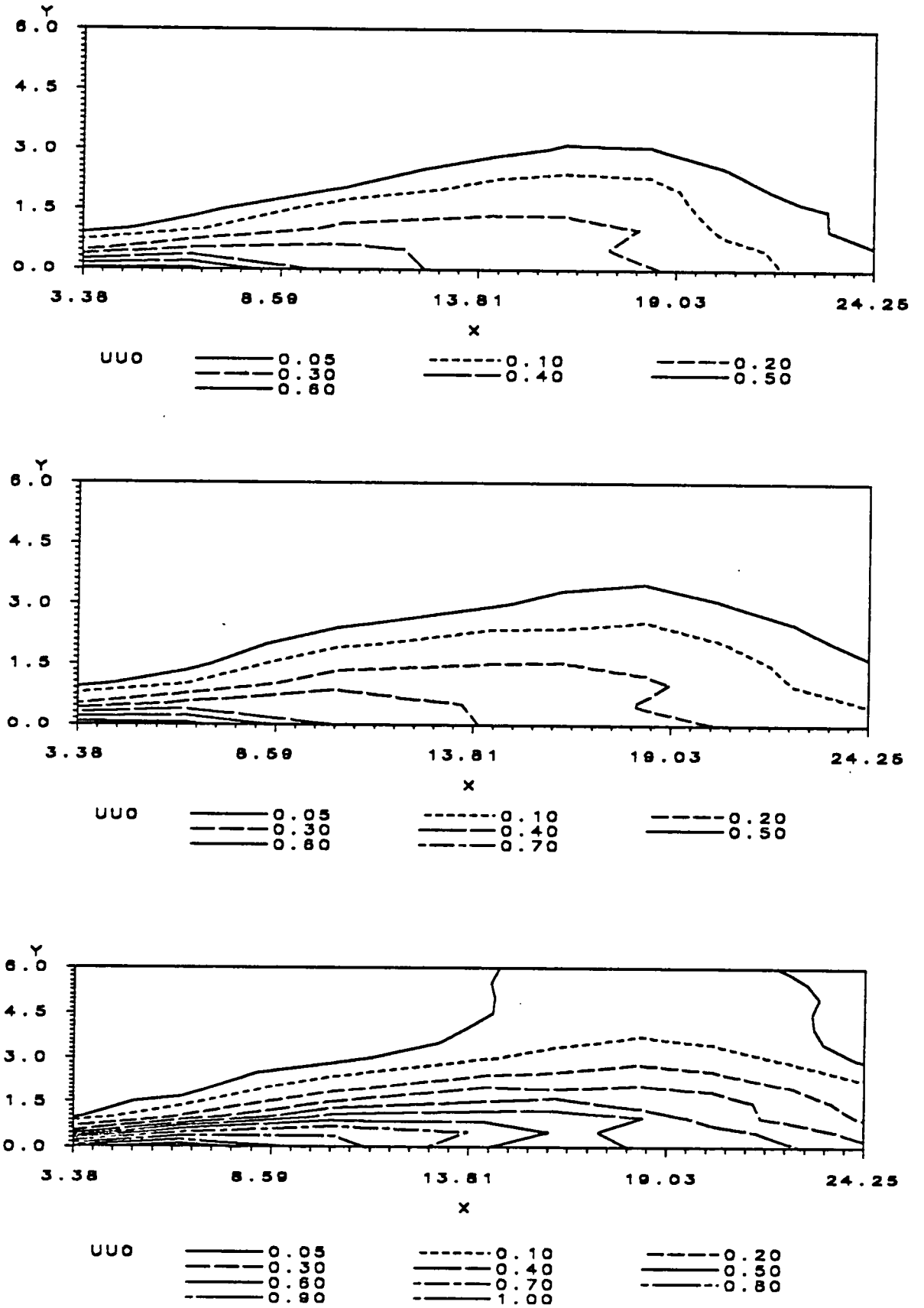

Figure 23. Mean velocity contour plots for 4 Hz - 4 psig for straight tube inlet configuration. Top - t/T = 0.000, center - t/T = 0.042, bottom - t/T = 0.083.

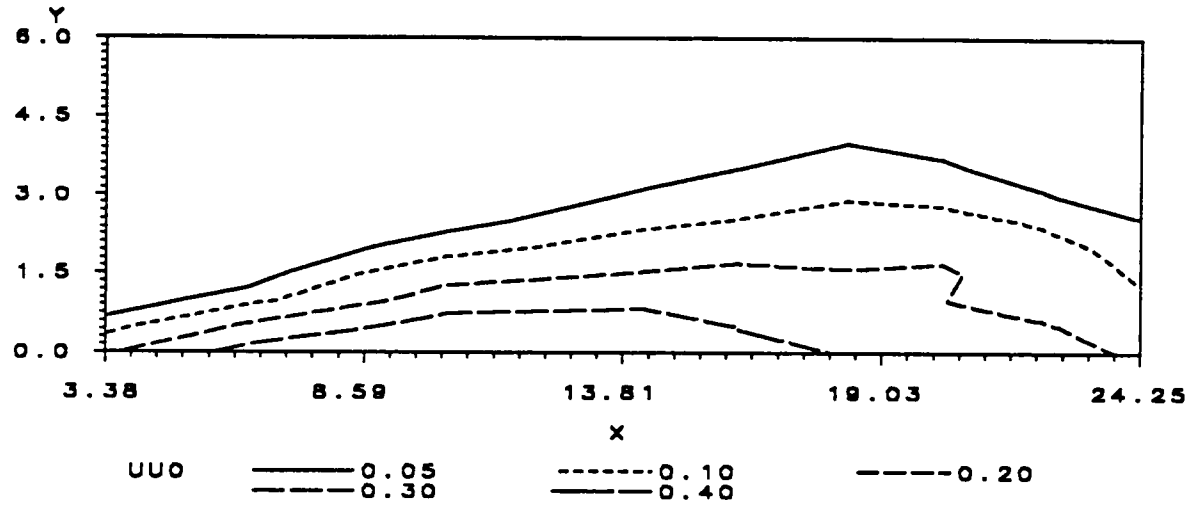

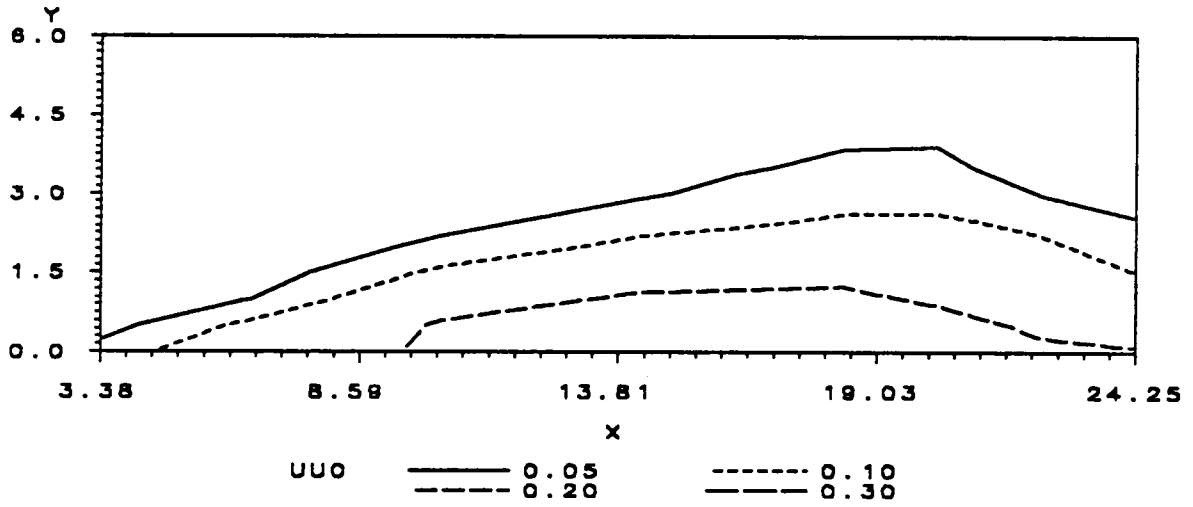

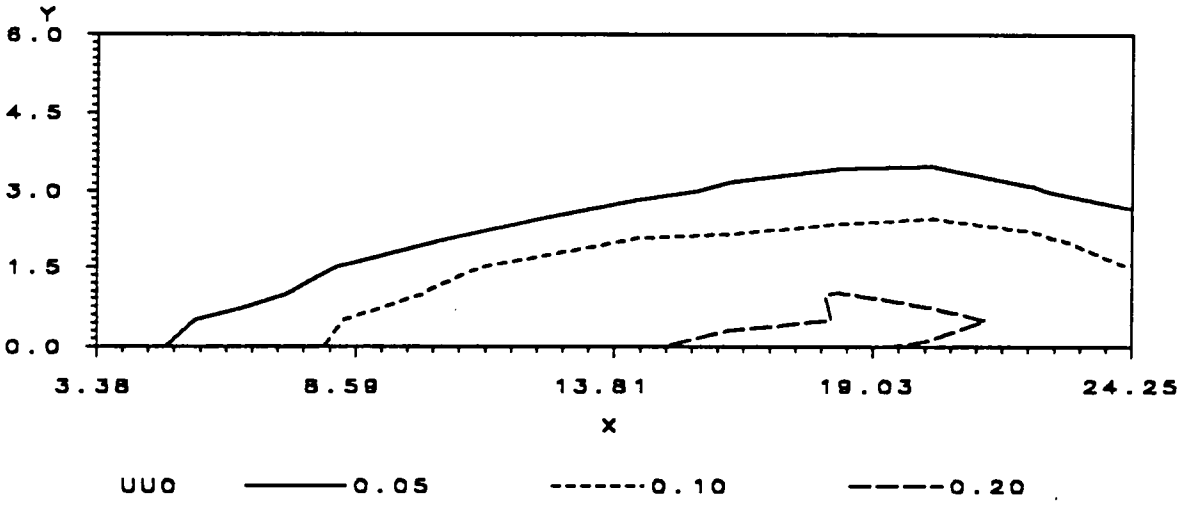

Figure 24. Mean velocity contour plots for 4 Hz - 4 psig for straight tube inlet configuration. Top - t/T = 0.125, center - t/T = 0.167, bottom - t/T = 0.2083.

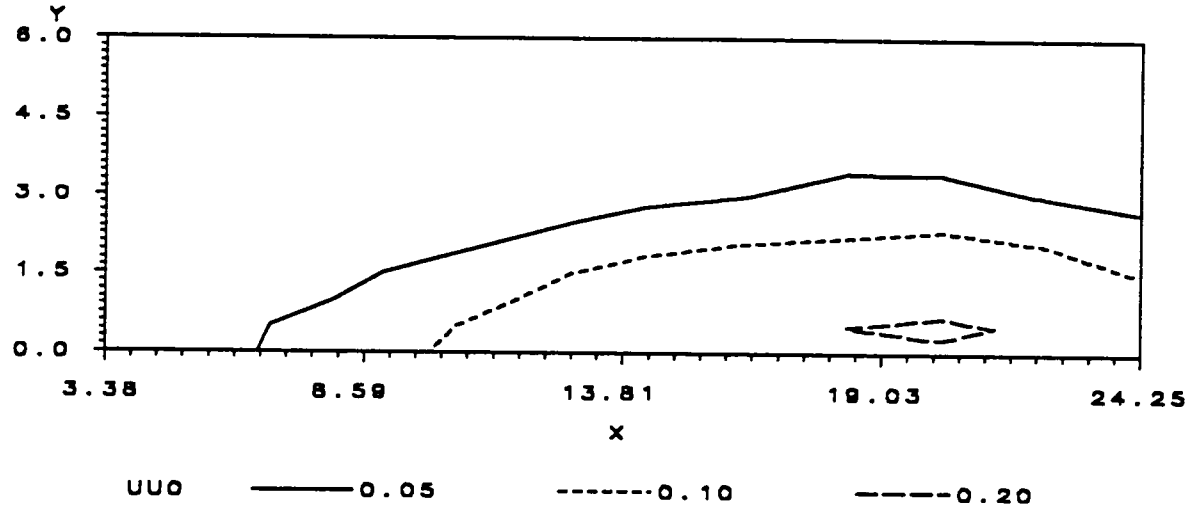

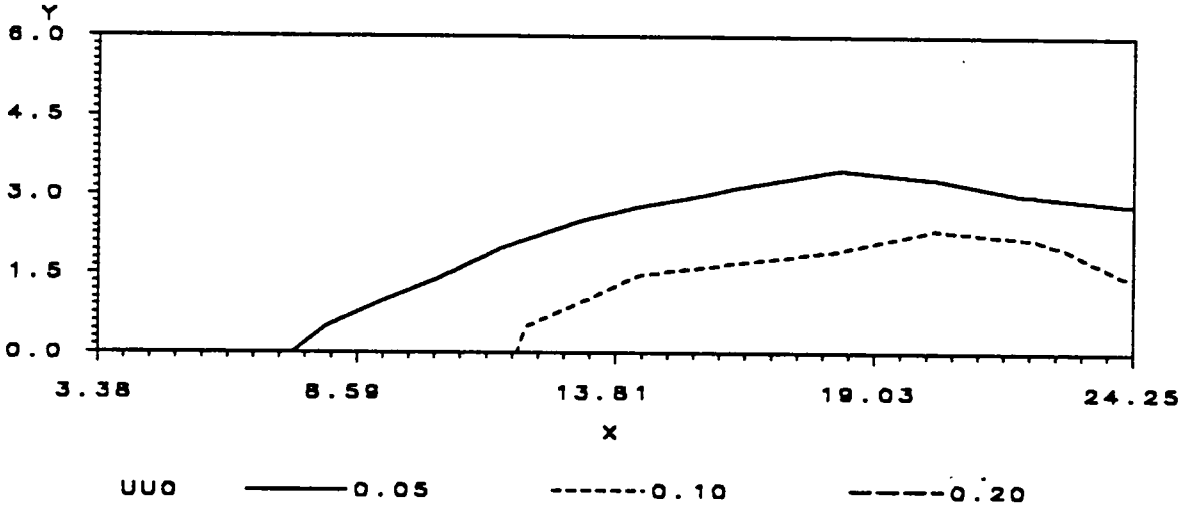

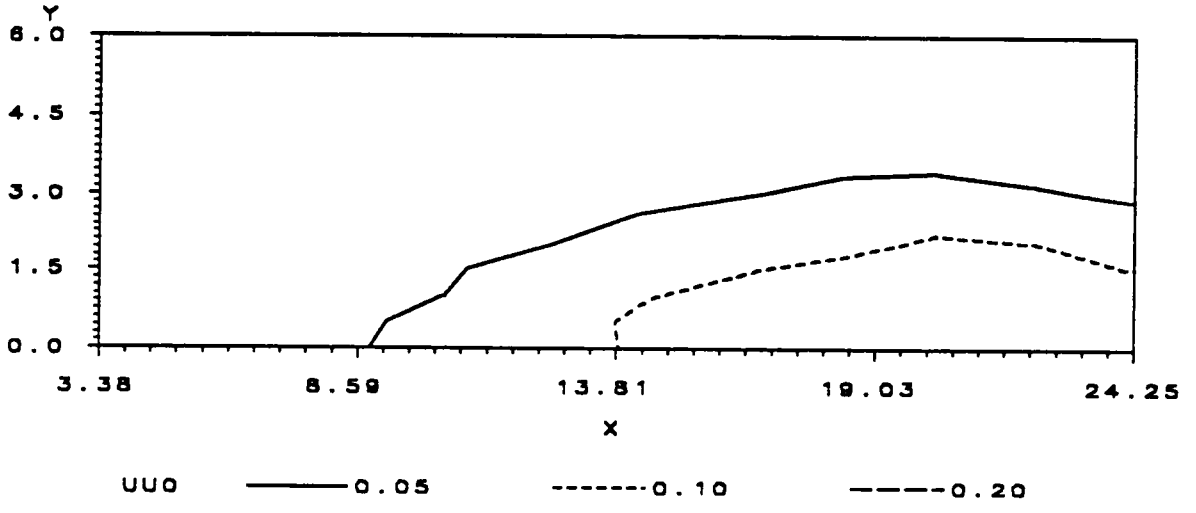

Figure 25. Mean velocity contour plots for 4 Hz - 4 psig for straight tube inlet configuration. Top - t/T = 0.2500, center - t/T = 0.2917, bottom - t/T = 0.3333.

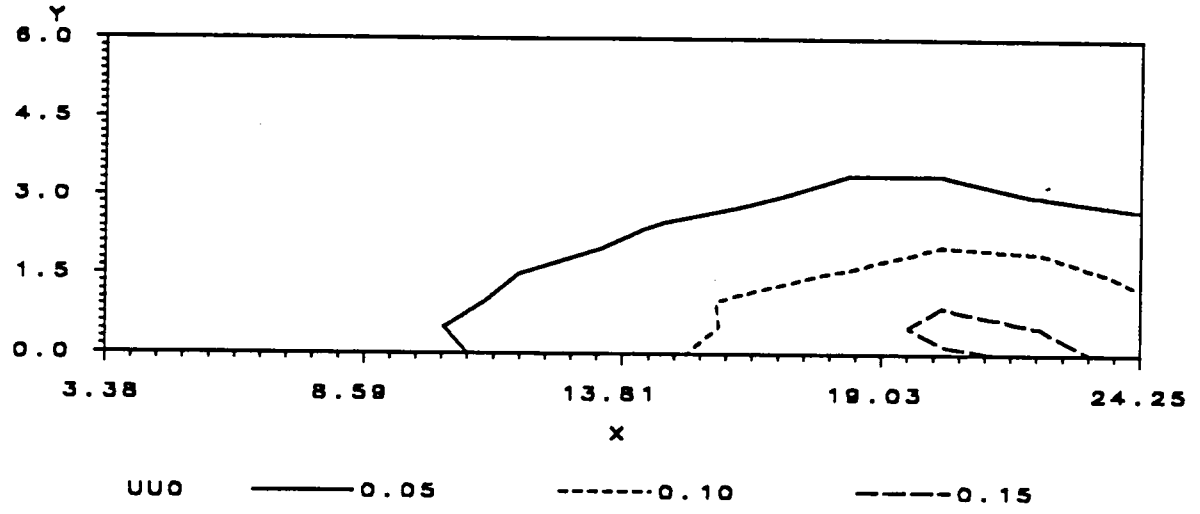

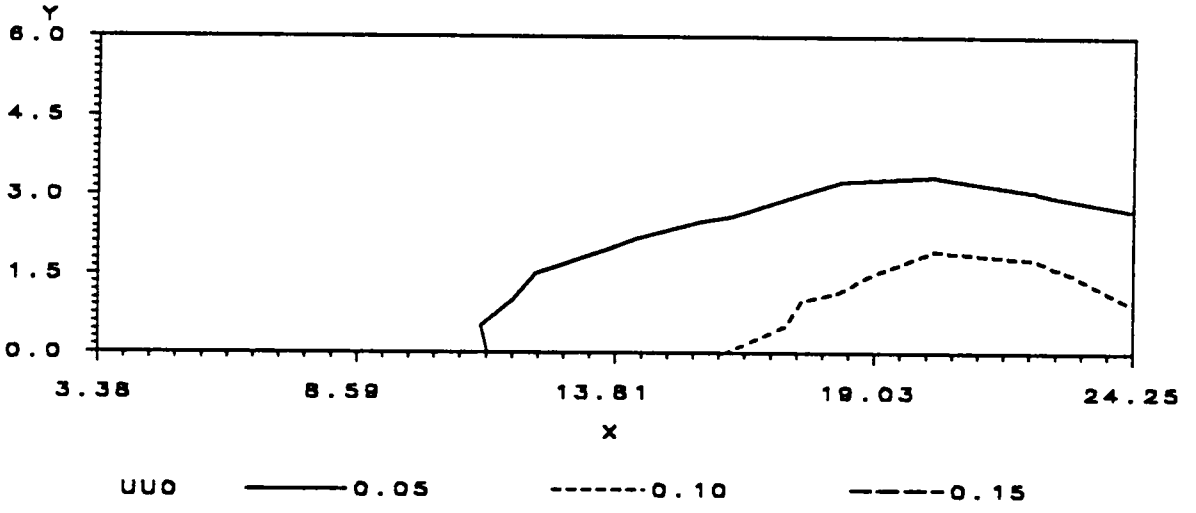

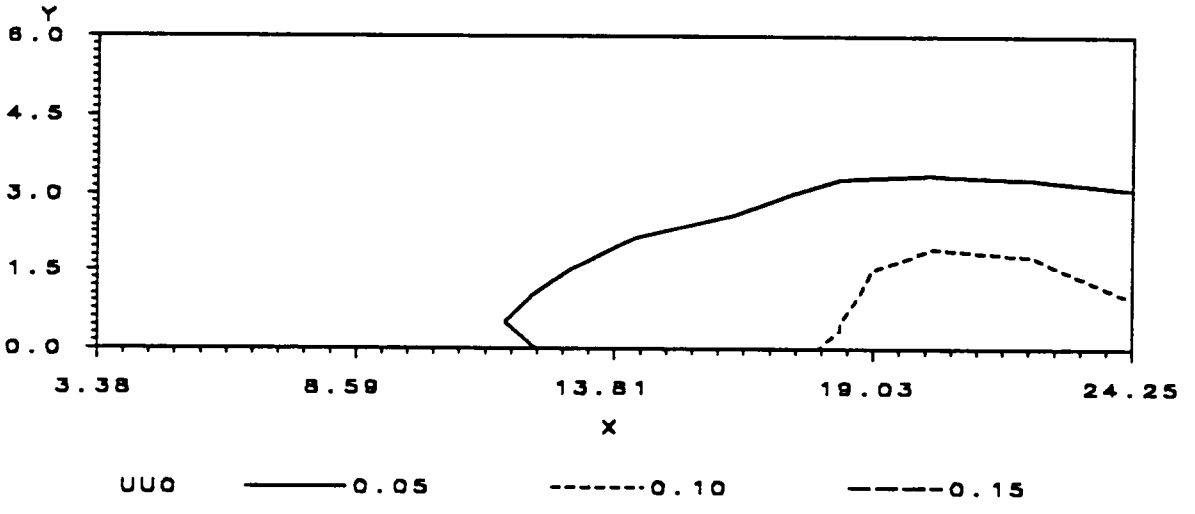

Figure 26. Mean velocity contour plots for 4 Hz - 4 psig for straight tube inlet configuration. Top - t/T = 0.3750, center - t/T = 0.4167, bottom - t/T = 0.4583.

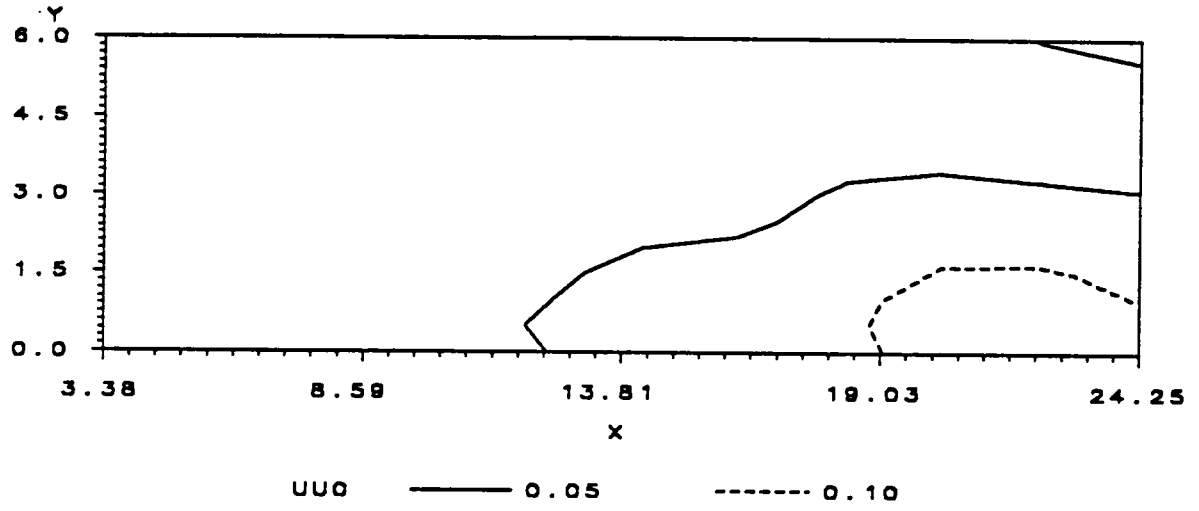

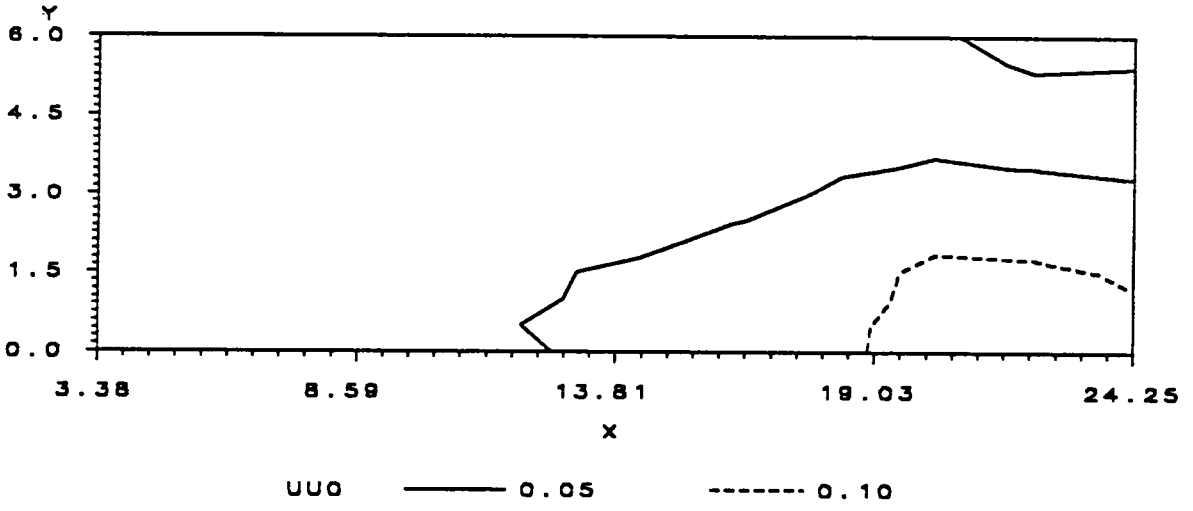

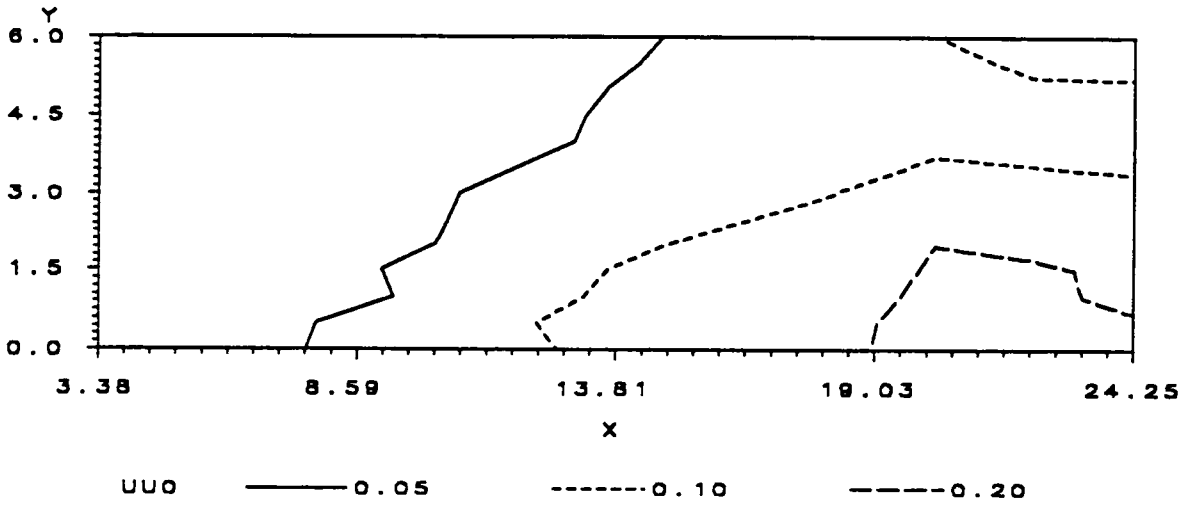

Figure 27. Mean velocity contour plots for 4 Hz - 4 psig for straight tube inlet configuration. Top - t/T = 0.500, center - t/T = 0.5417, bottom - t/T = 0.5833.

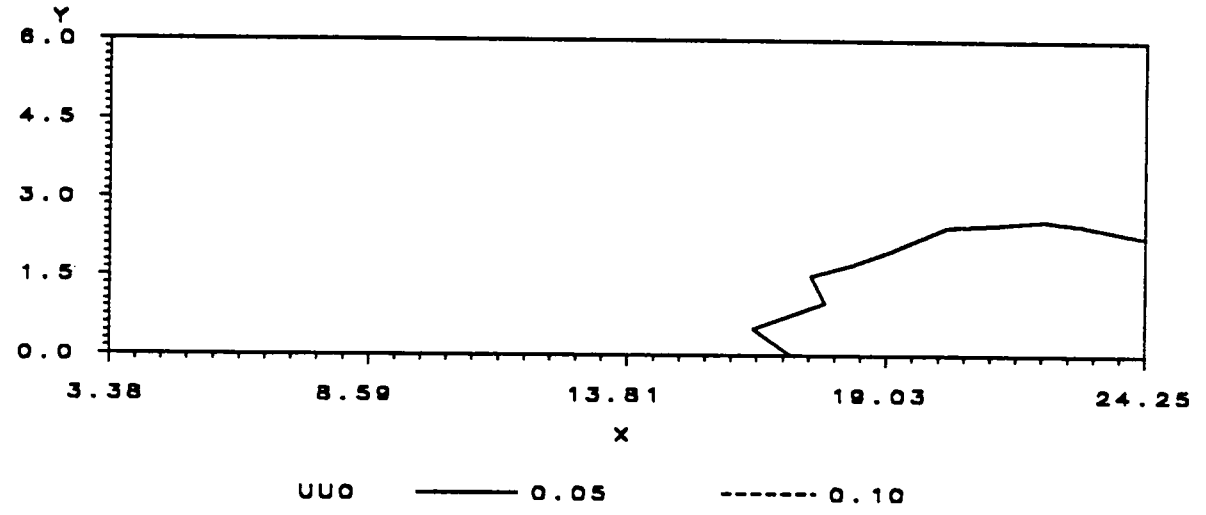

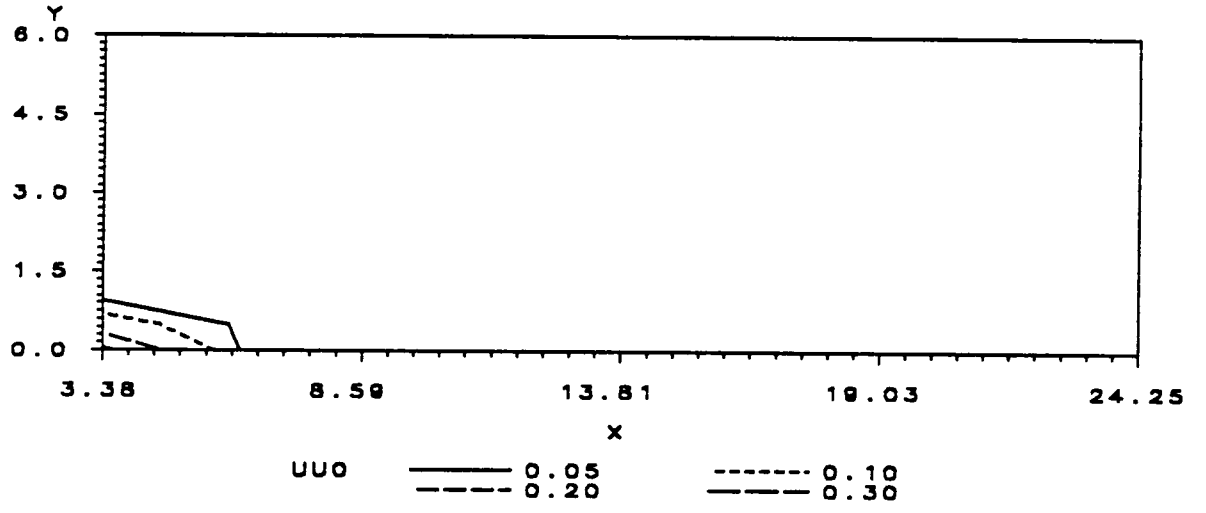

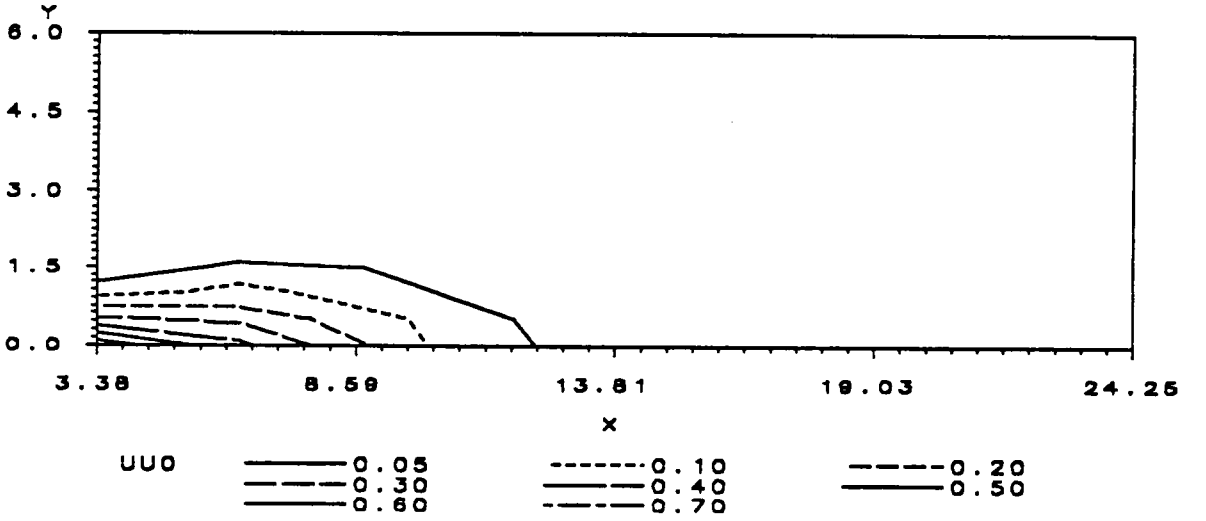

Figure 28. Mean velocity contour plots for 4 Hz - 4 psig for straight tube inlet configuration. Top - t/T = 0.6250, center - t/T = 0.6667, bottom - t/T = 0.7083.

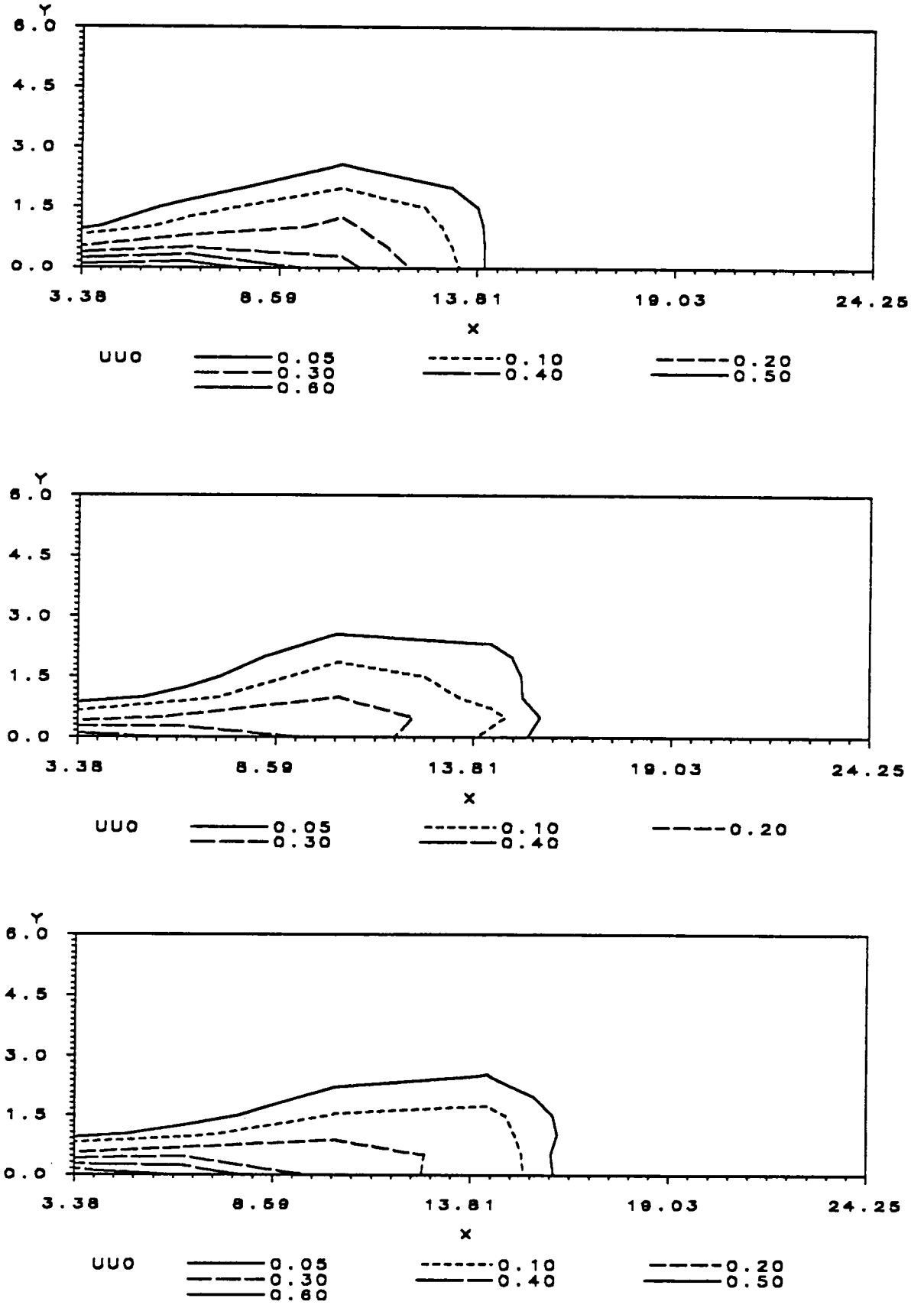

Figure 29. Mean velocity contour plots for 4 Hz - 4 psig for straight tube inlet configuration. Top - t/T = 0.750, center - t/T = 0.7917, bottom - t/T = 0.8333.

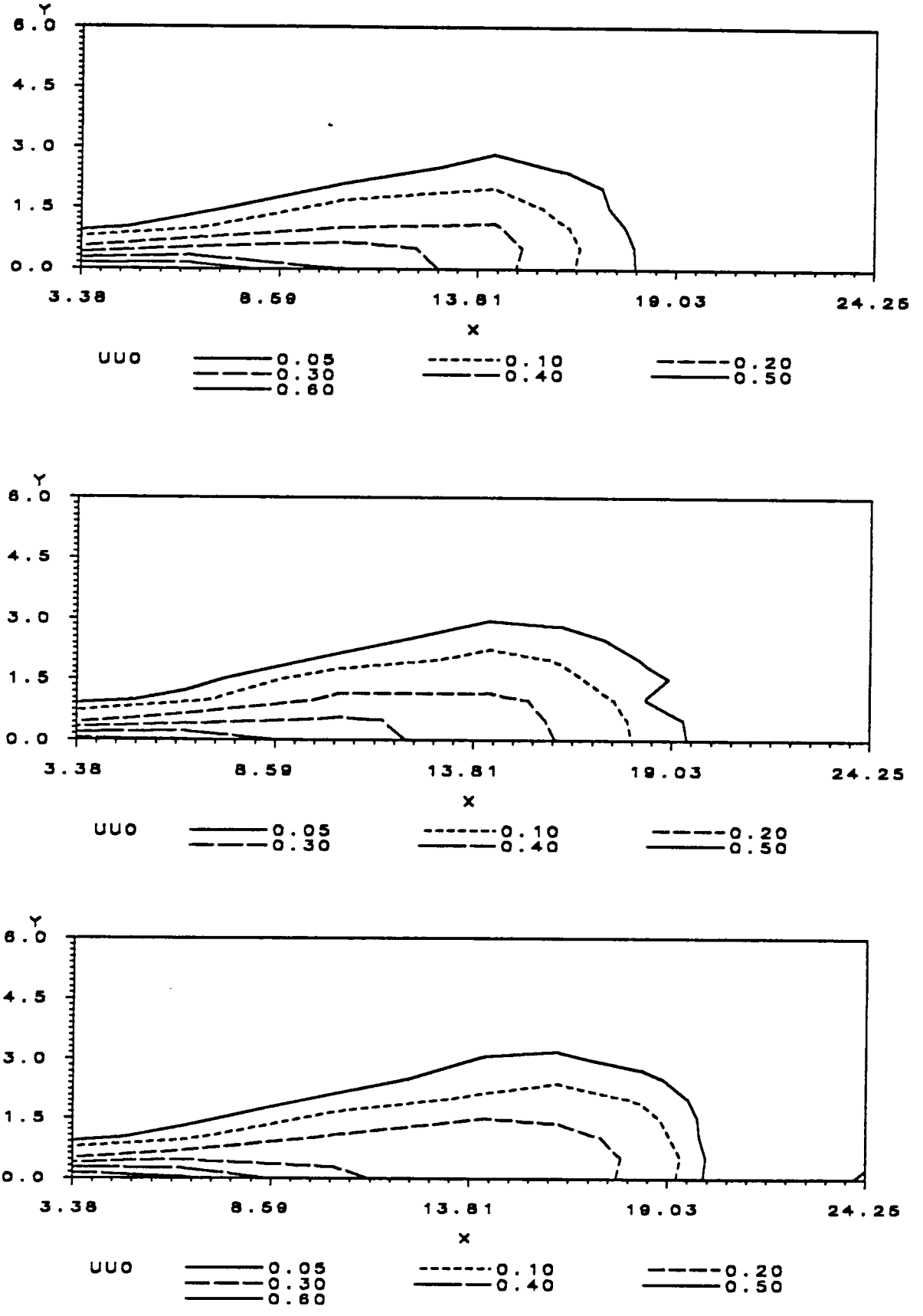

Figure 30. Mean velocity contour plots for 4 Hz - 4 psig for straight tube inlet configuration. Top - t/T = 0.8750, center - t/T = 0.9167, bottom - t/T = 0.9583.

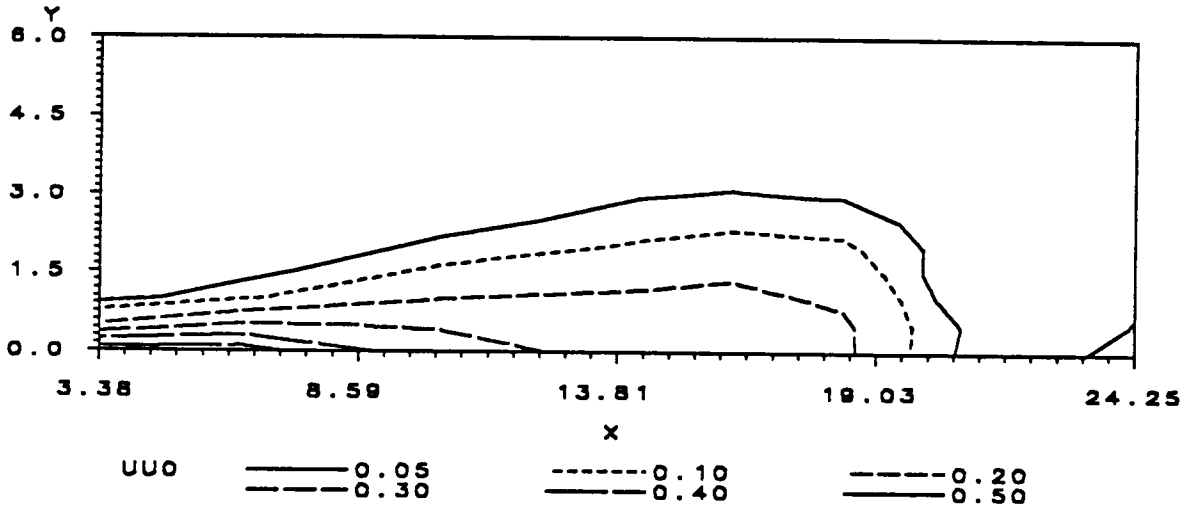

Figure 31. Mean velocity contour plots for 4 Hz - 4 psig for straight tube inlet configuration. Top - t/T = 1.000.

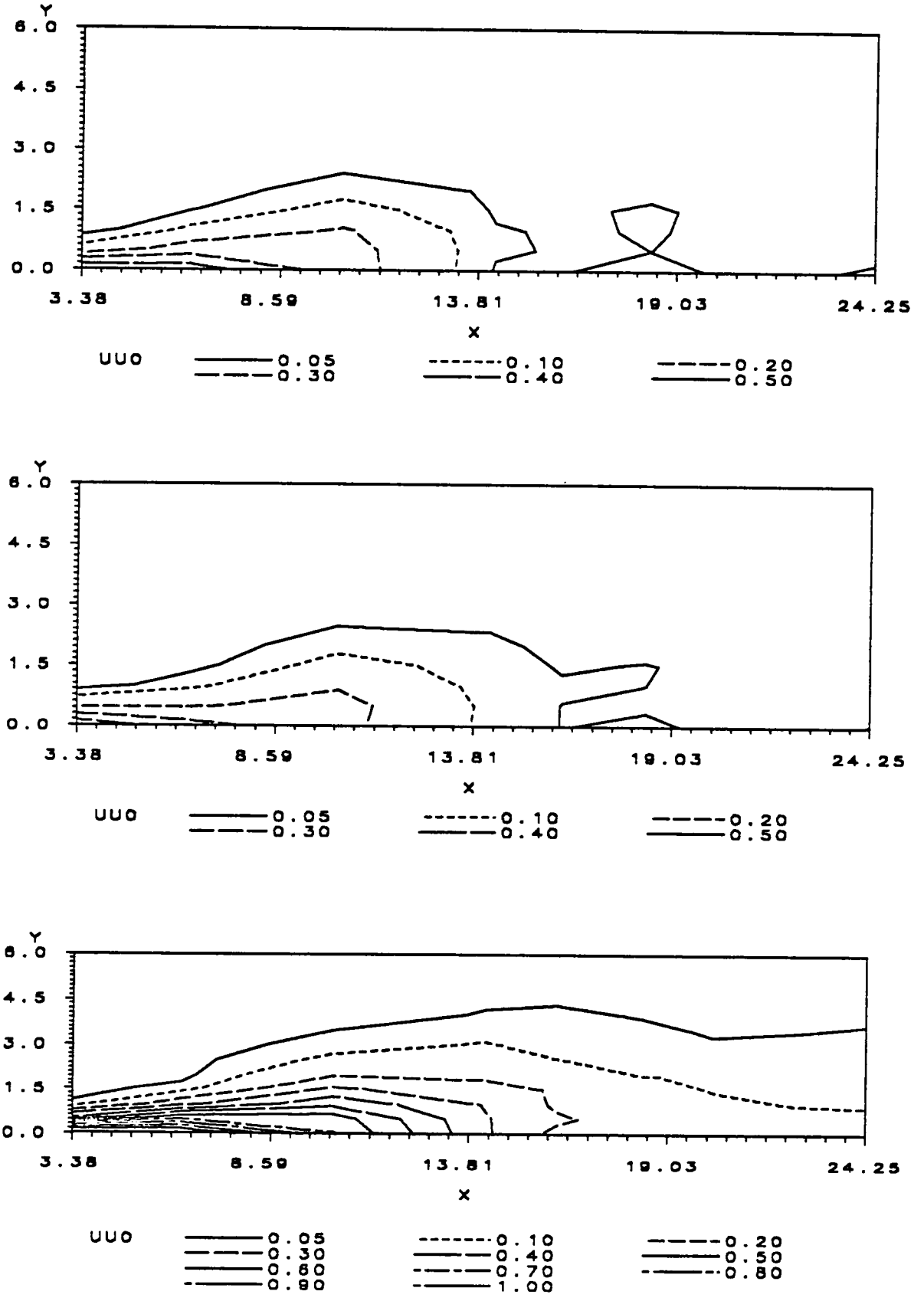

Figure 32. Mean velocity contour plots for 8 Hz - 4 psig for straight tube inlet configuration. Top - t/T = 0.000, center - t/T = 0.091, bottom - t/T = 0.182.

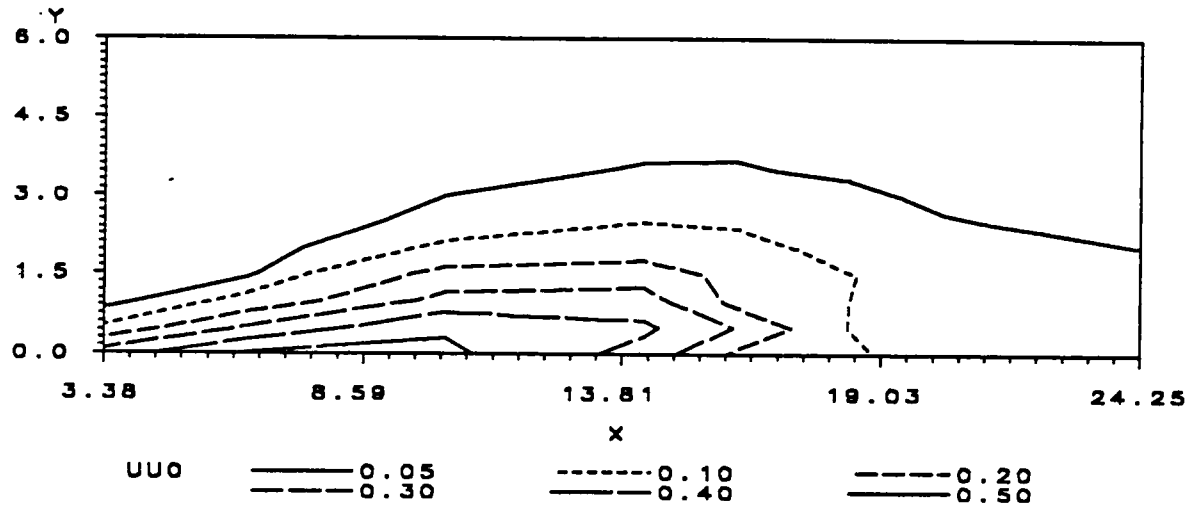

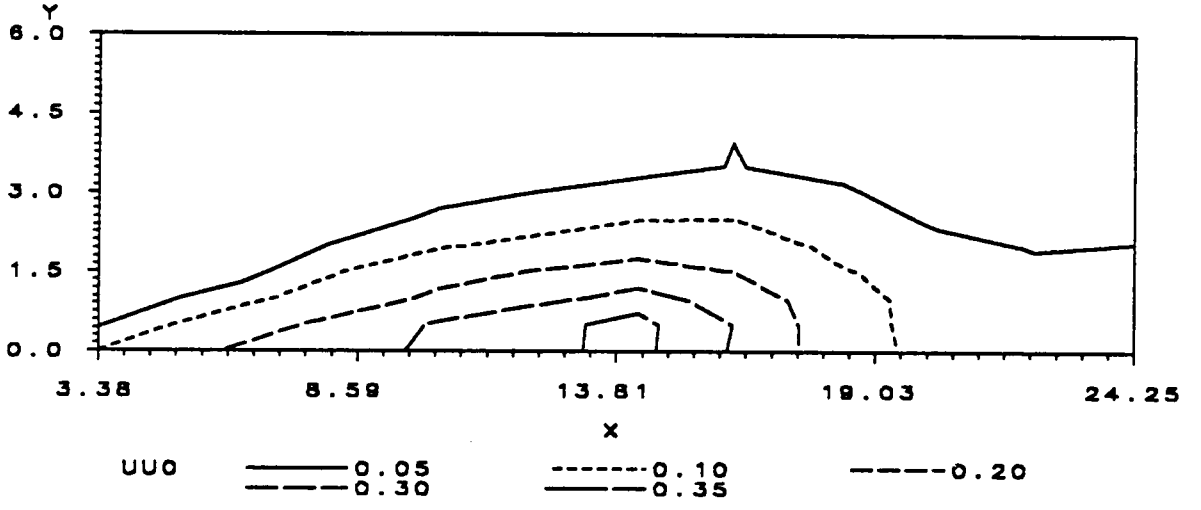

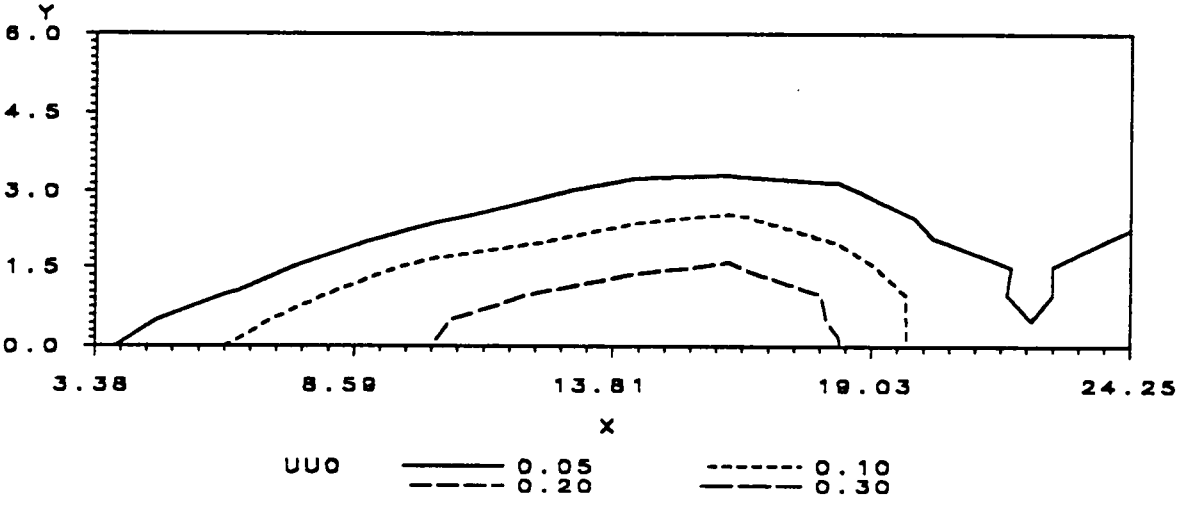

Figure 33. Mean velocity contour plots for 8 Hz - 4 psig for straight tube inlet configuration. Top - t/T = 0.273, center - t/T = 0.364, bottom - t/T = 0.4545.

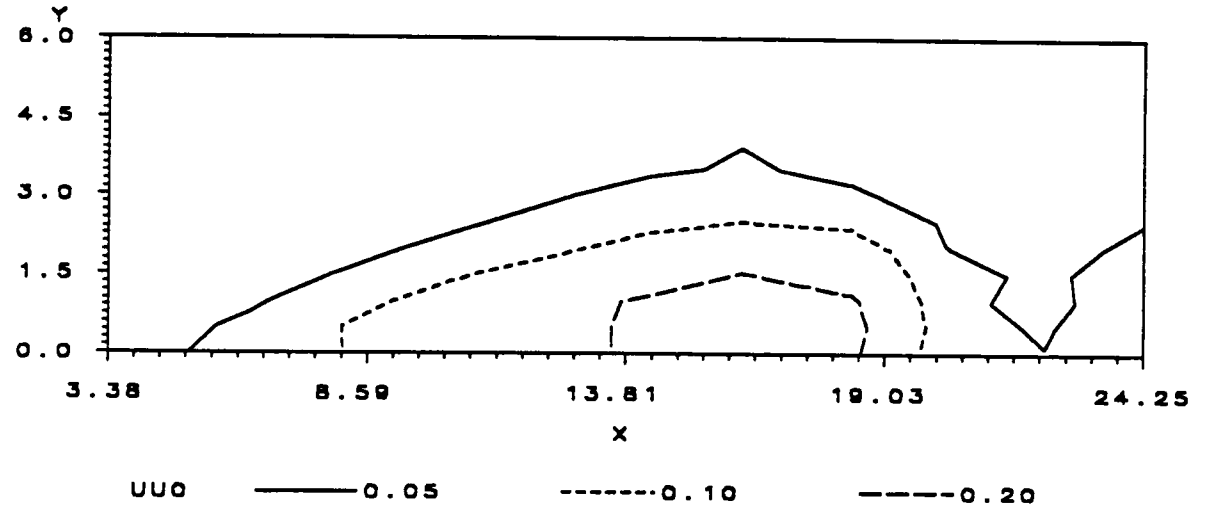

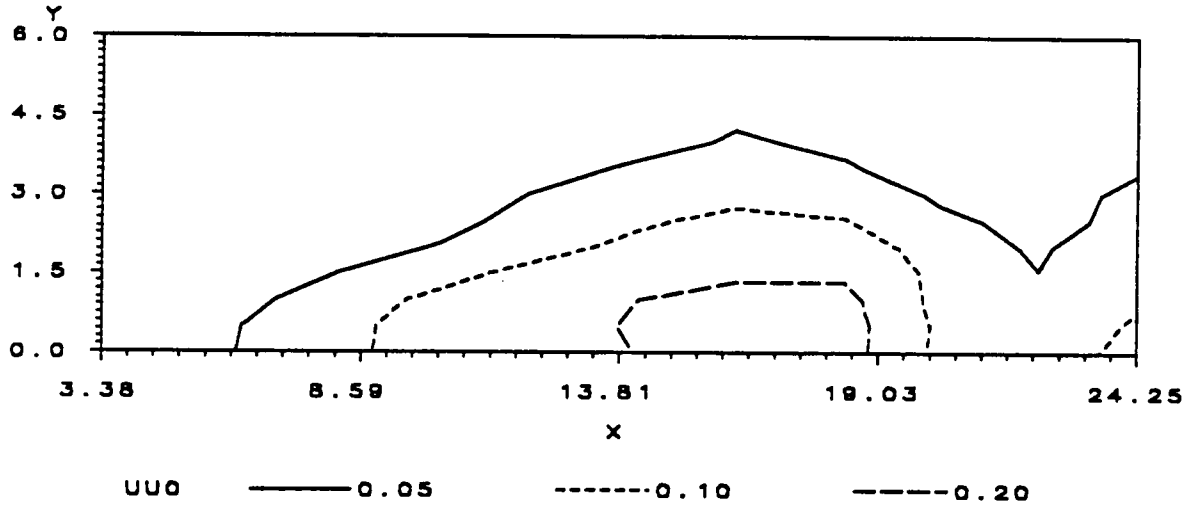

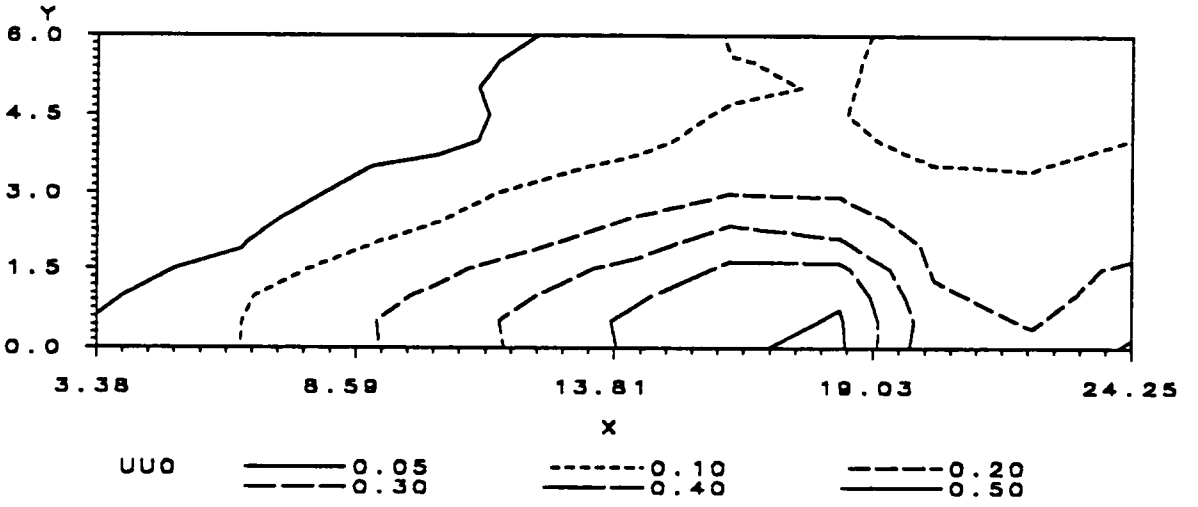

Figure 34. Mean velocity contour plots for 8 Hz - 4 psig for straight tube inlet configuration. Top - t/T = 0.5454, center - t/T = 0.6364, bottom - t/T = 0.7273.

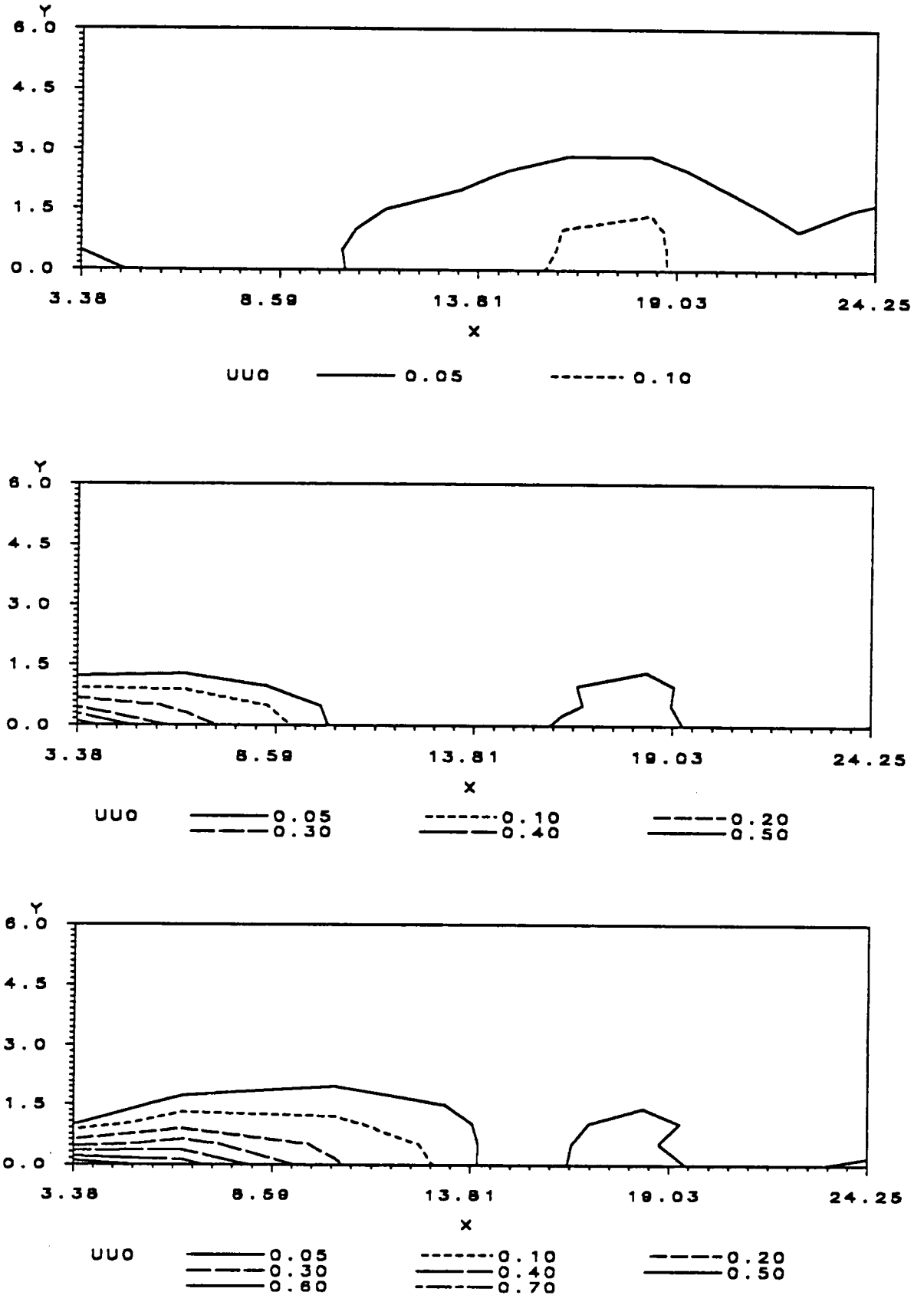

Figure 35. Mean velocity contour plots for 8 Hz - 4 psig for straight tube inlet configuration. Top - t/T = 0.8182, center - t/T = 0.9091, bottom - t/T = 1.000.

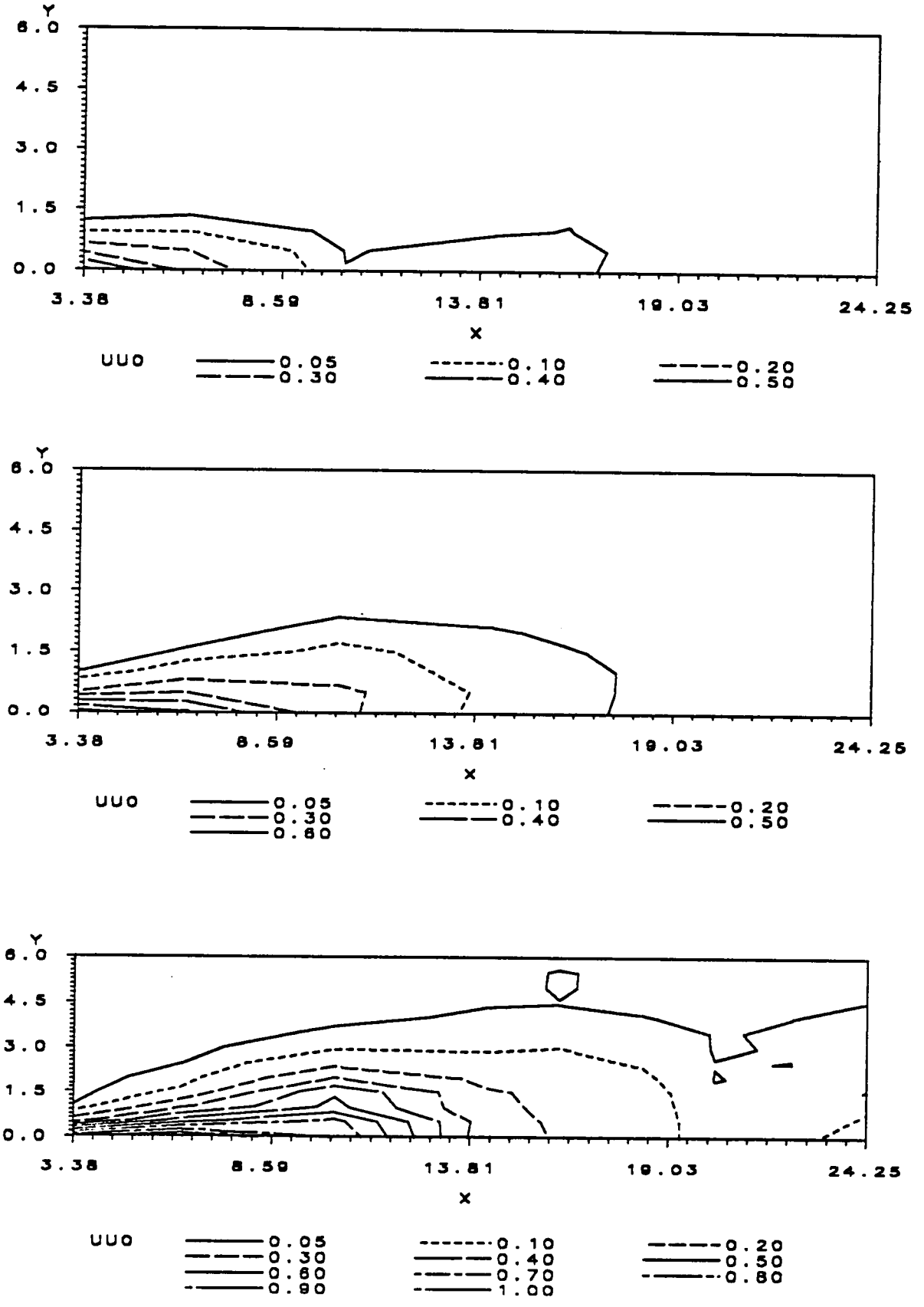

Figure 36. Mean velocity contour plots for 12 Hz - 4 psig for straight tube inlet configuration. Top - t/T = 0.000, center - t/T = 0.143, bottom - t/T = 0.286.

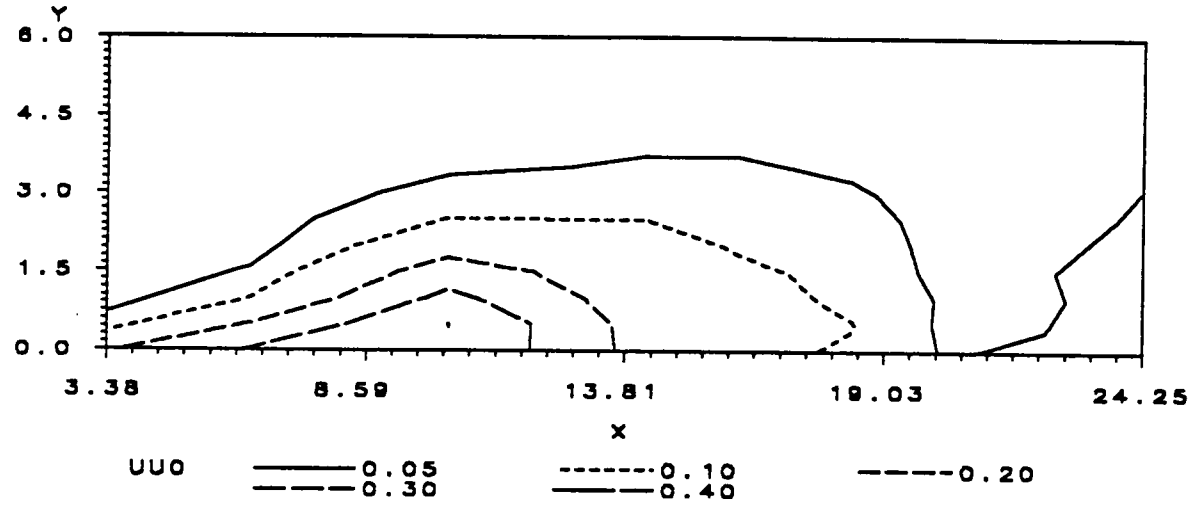

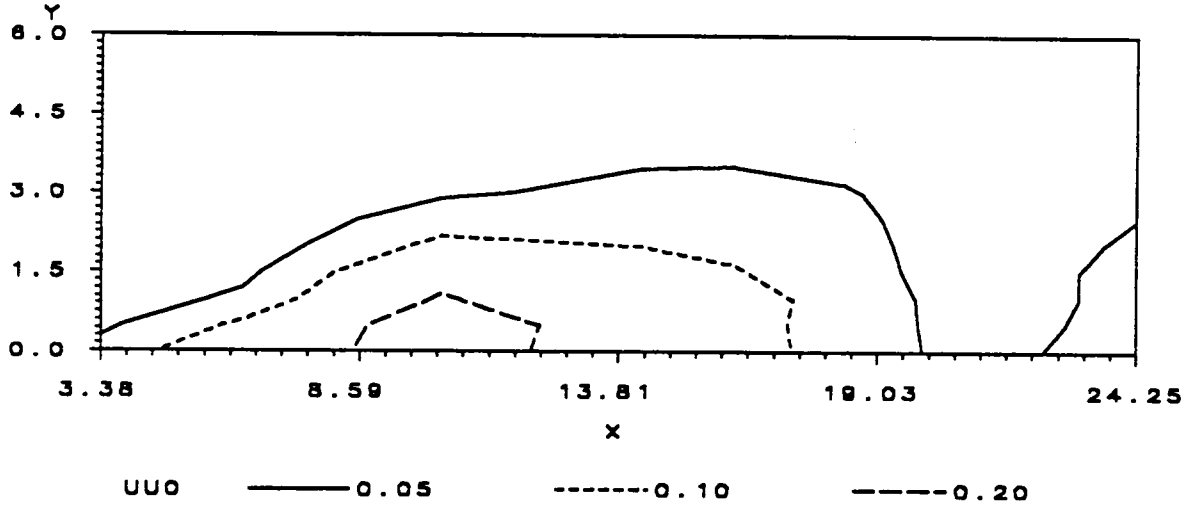

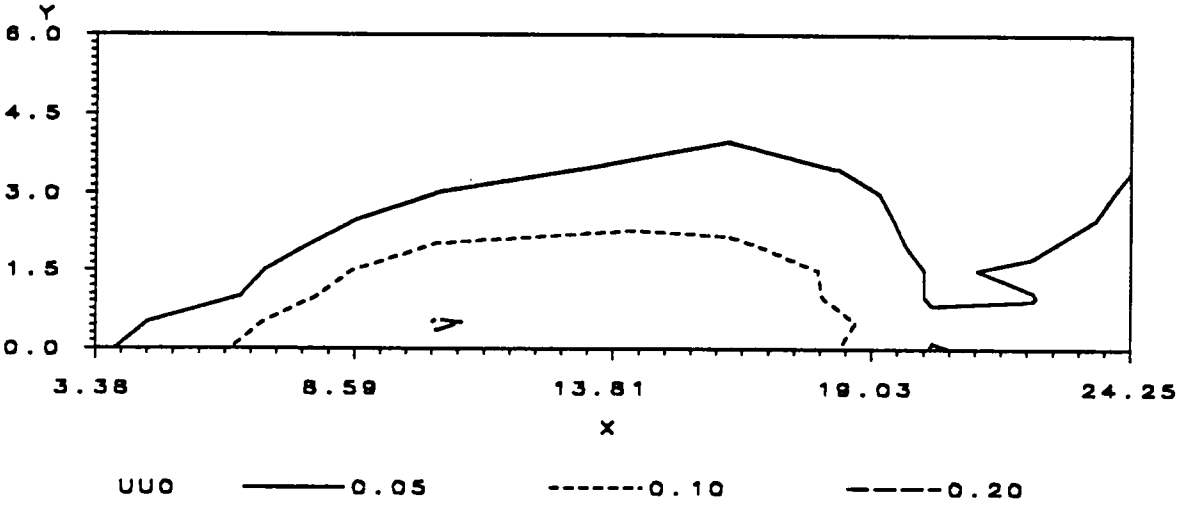

Figure 37. Mean velocity contour plots for 12 Hz - 4 psig for straight tube inlet configuration. Top - t/T = 0.429, center - t/T = 0.571, bottom - t/T = 0.7143.

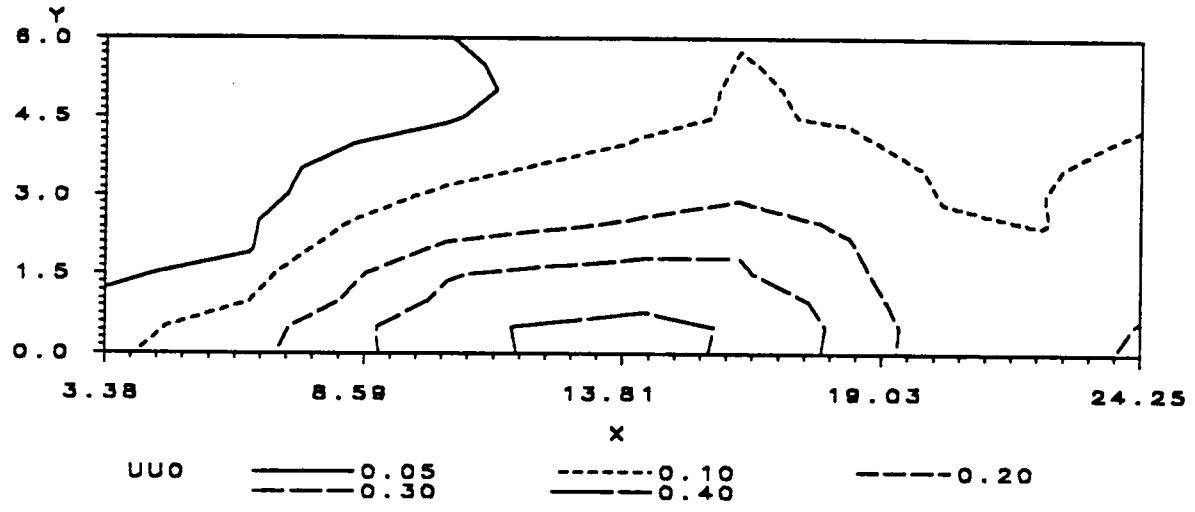

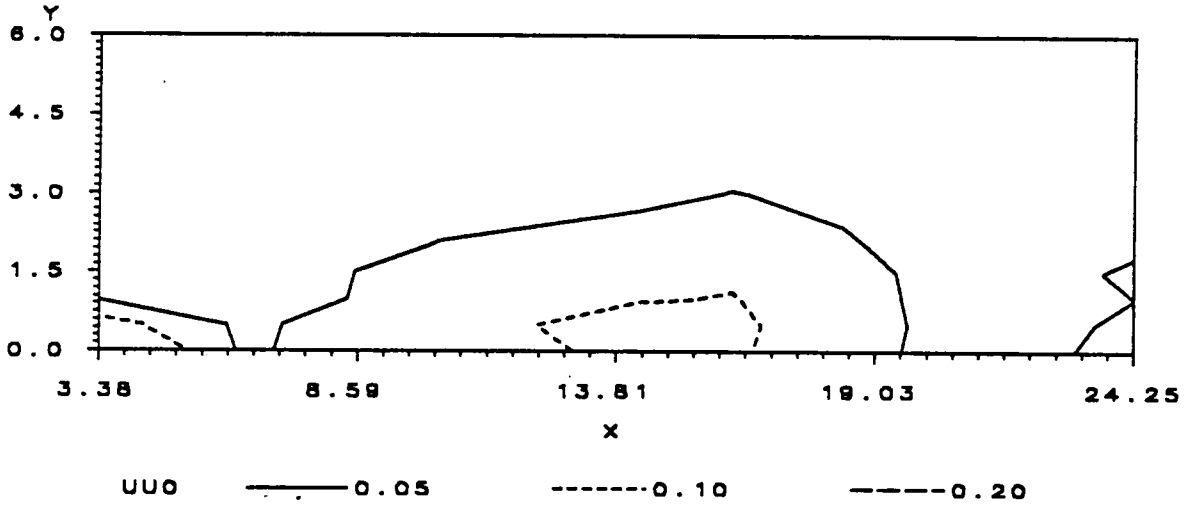

Figure 38. Mean velocity contour plots for 12 Hz - 4 psig for straight tube inlet configuration. Top - t/T = 0.857, center - t/T = 1.000.

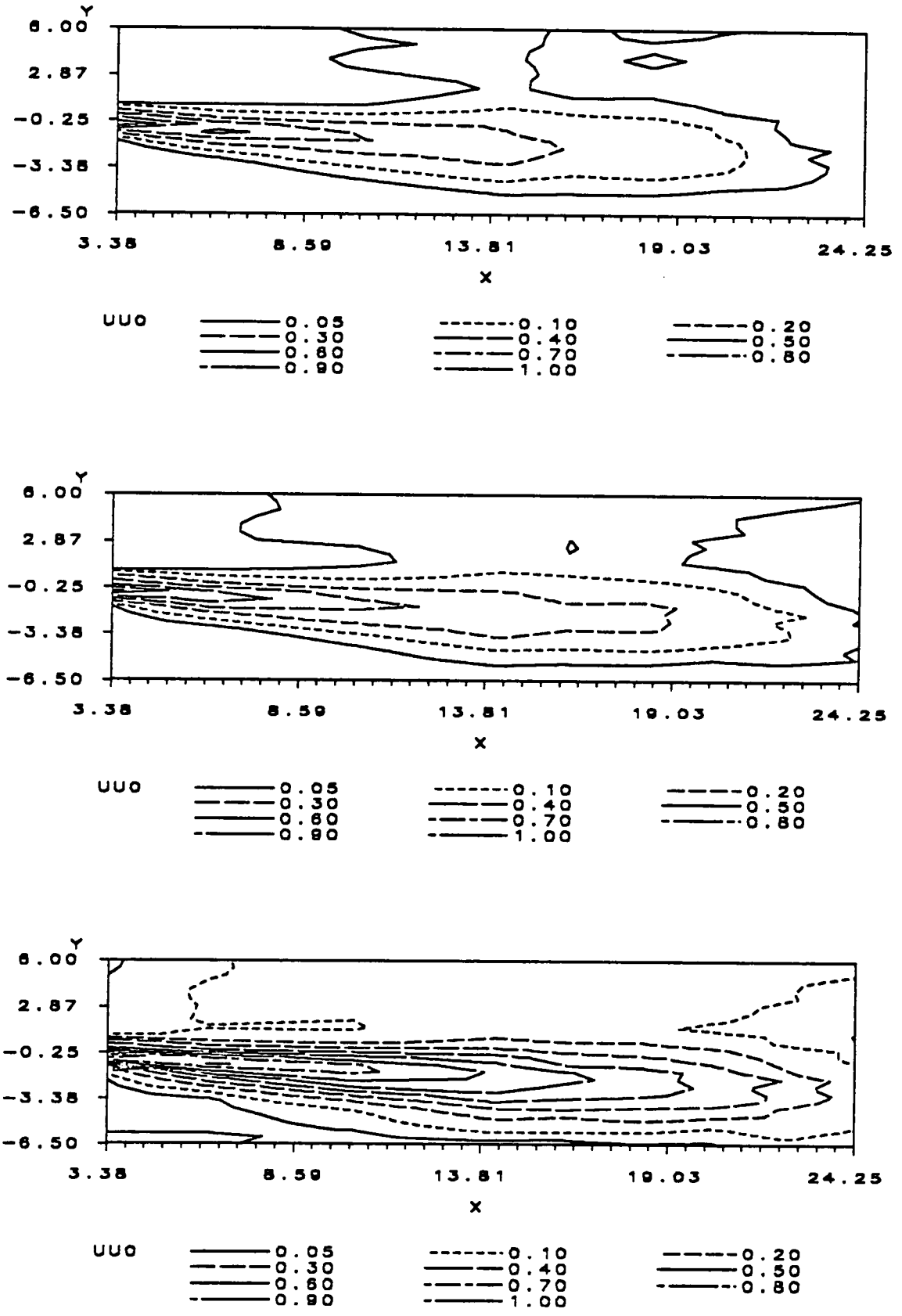

Figure 39. Mean velocity contour plots for 4 Hz - 4 psig for bent tube inlet configuration. Top - t/T = 0.000, center - t/T = 0.042, bottom - t/T = 0.083.

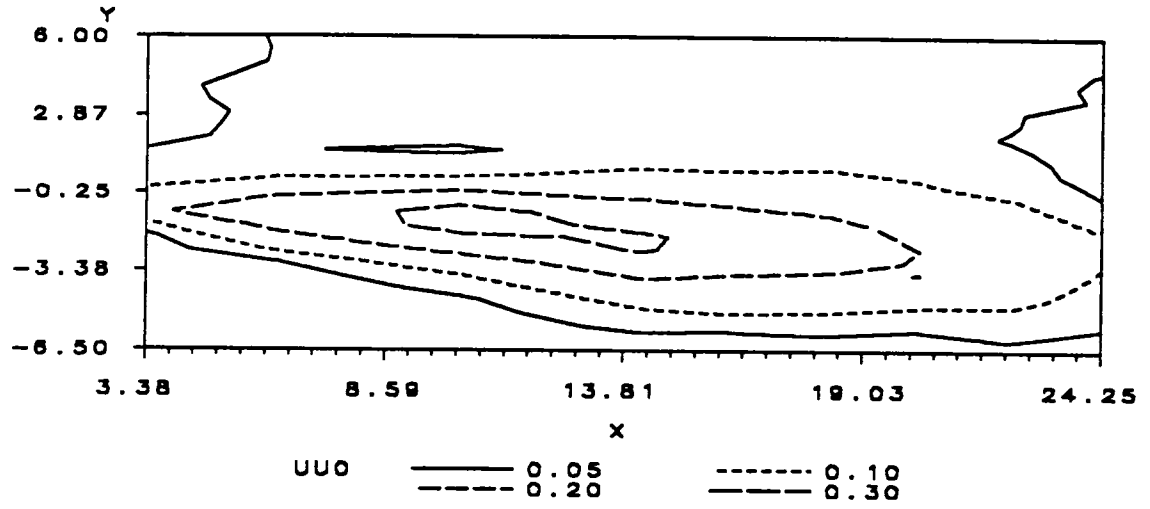

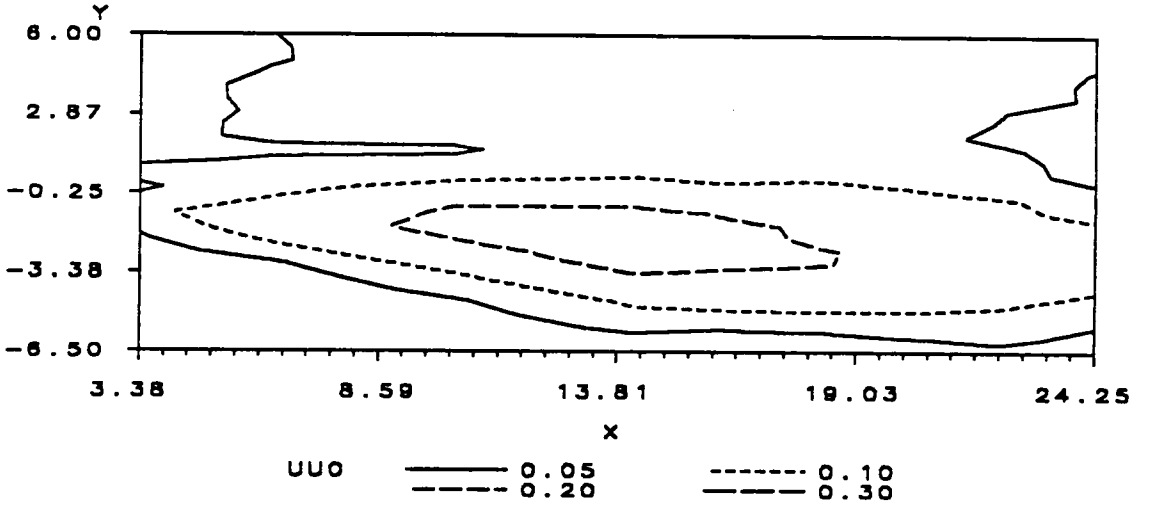

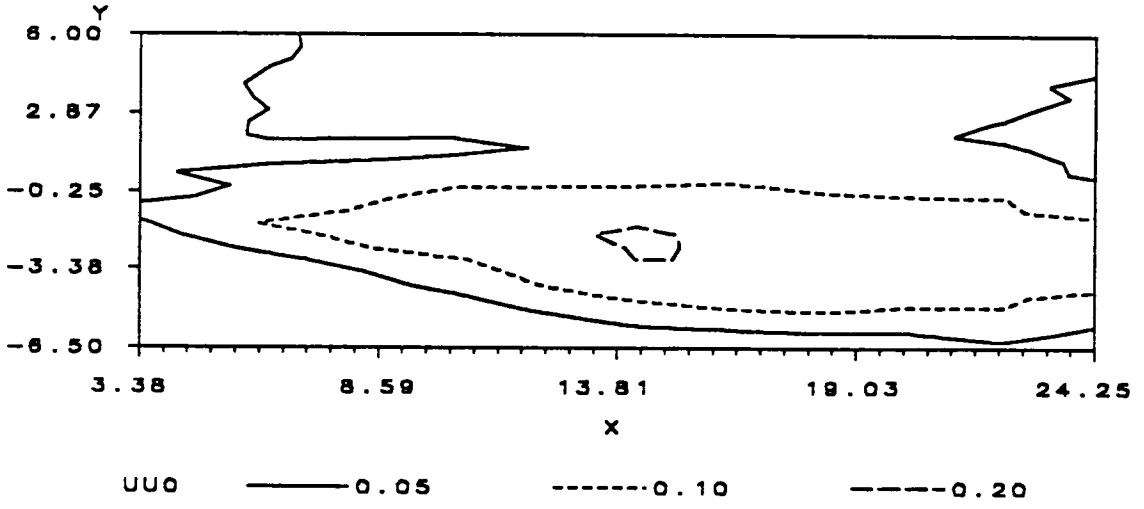

Figure 40. Mean velocity contour plots for 4 Hz - 4 psig for bent tube inlet configuration. Top - t/T = 0.125, center - t/T = 0.167, bottom - t/T = 0.2083.

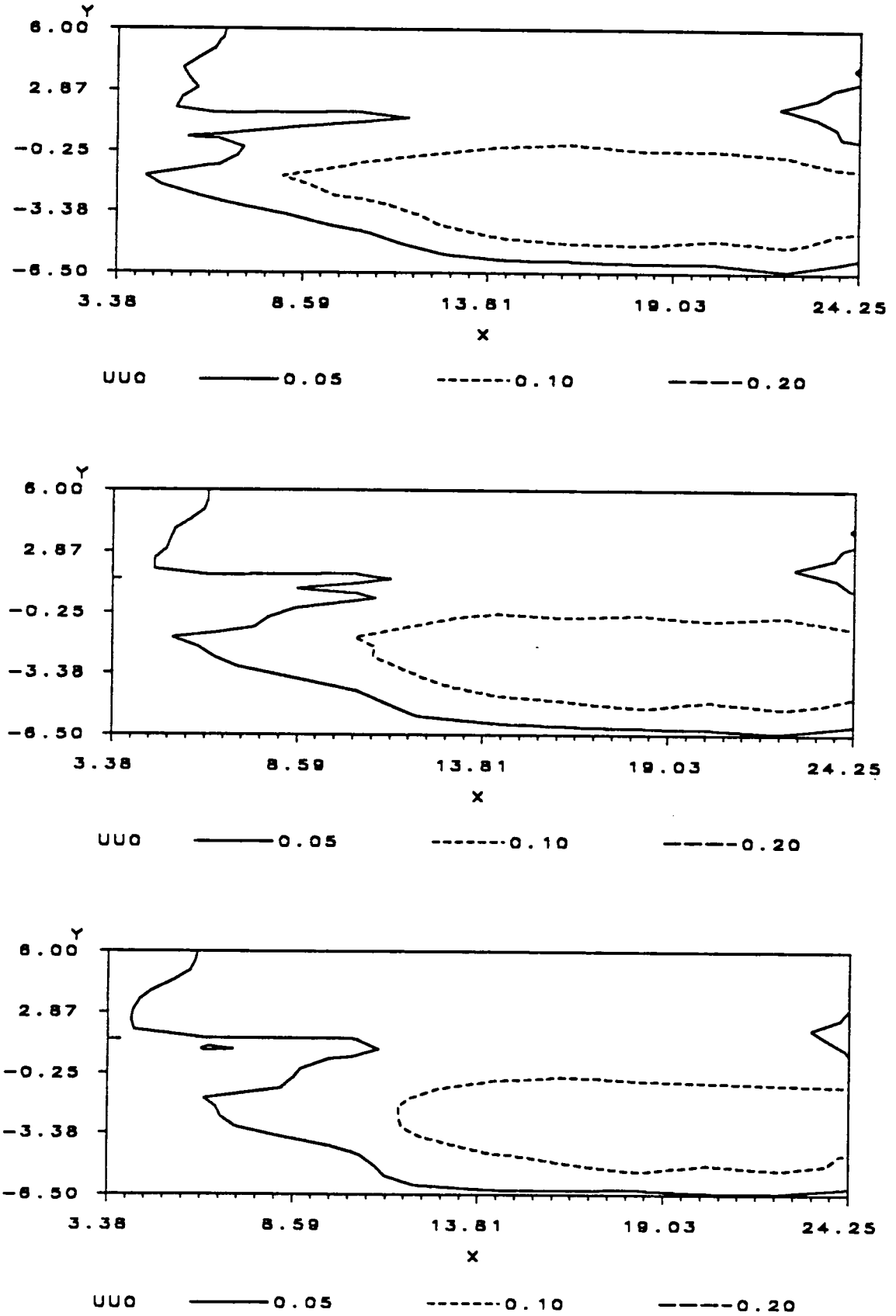

Figure 41. Mean velocity contour plots for 4 Hz - 4 psig for bent tube inlet configuration. Top - t/T = 0.2500, center - t/T = 0.2917, bottom - t/T = 0.3333.

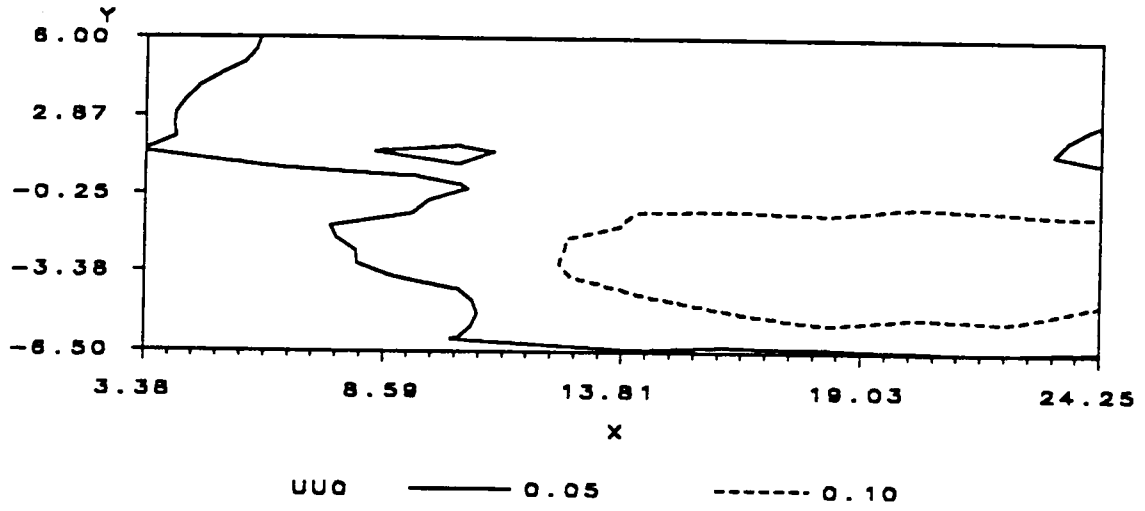

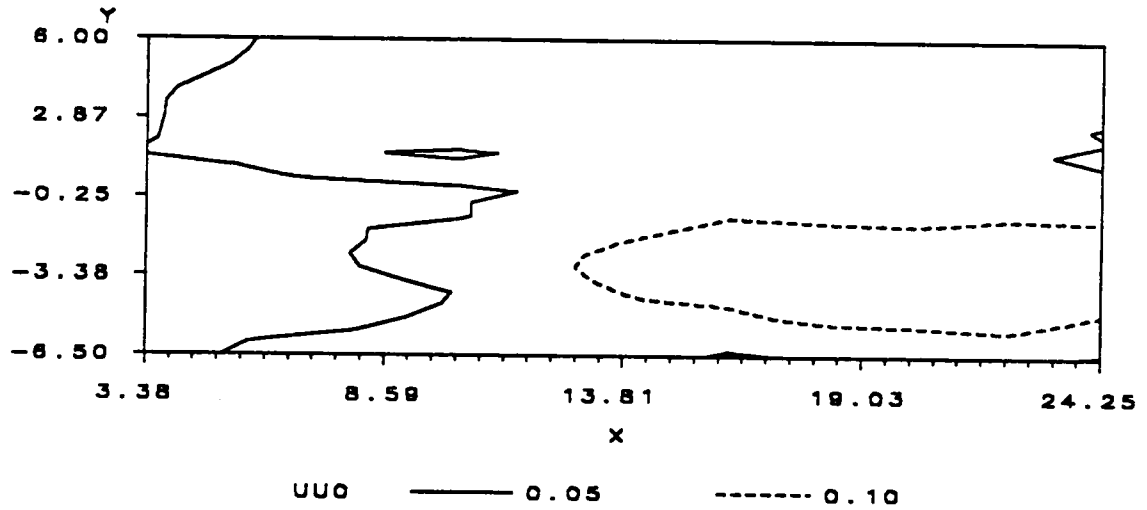

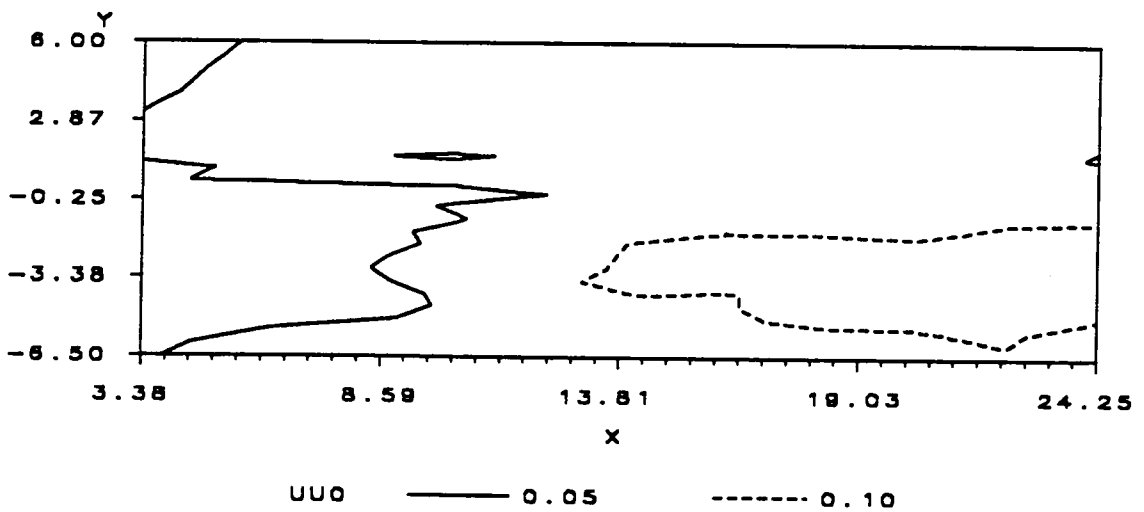

Figure 42. Mean velocity contour plots for 4 Hz - 4 psig for bent tube inlet configuration. Top - t/T = 0.3750, center - t/T = 0.4167, bottom - t/T = 0.4583.

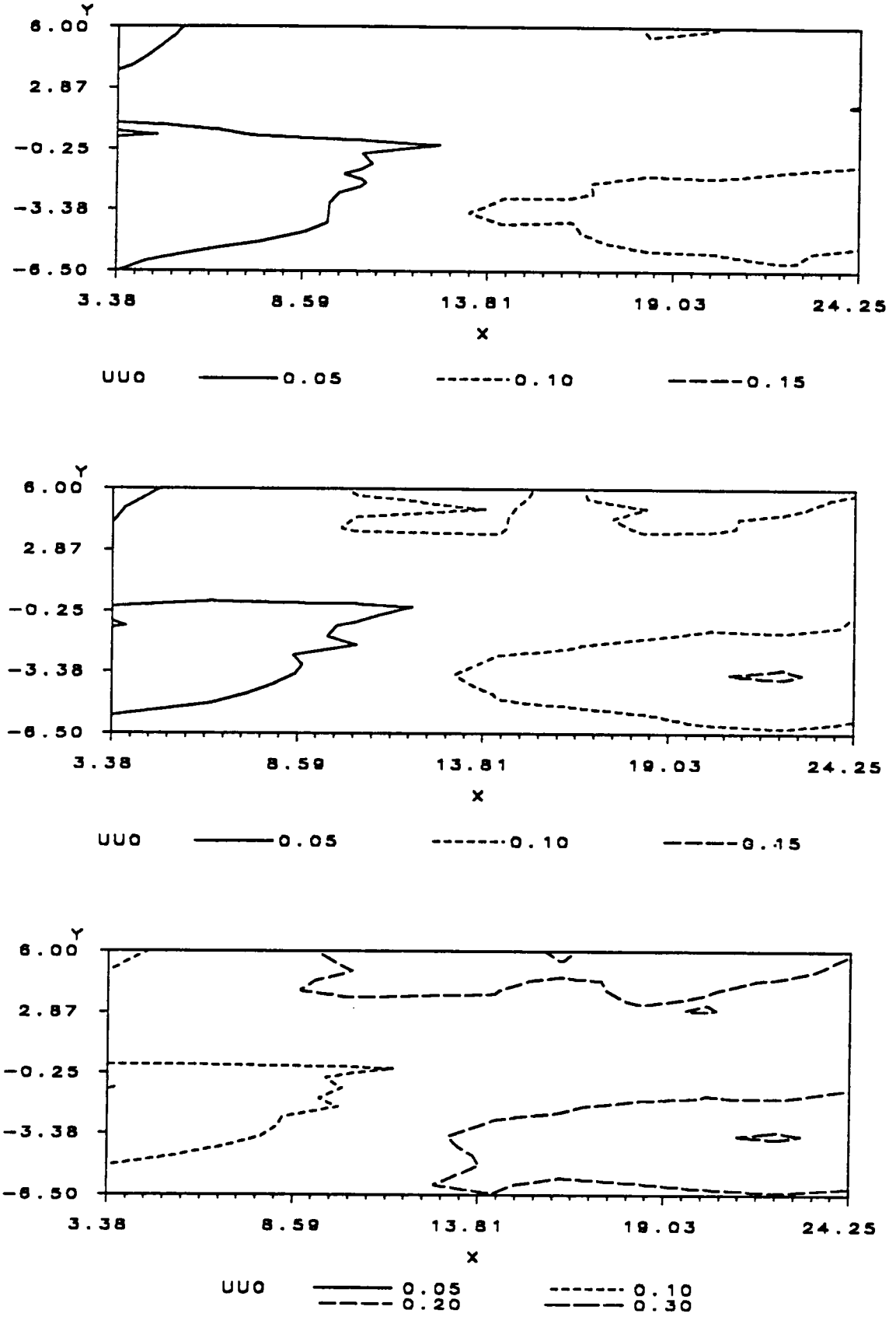

Figure 43. Mean velocity contour plots for 4 Hz - 4 psig for bent tube inlet configuration. Top - t/T = 0.500, center - t/T = 0.5417, bottom - t/T = 0.5833.

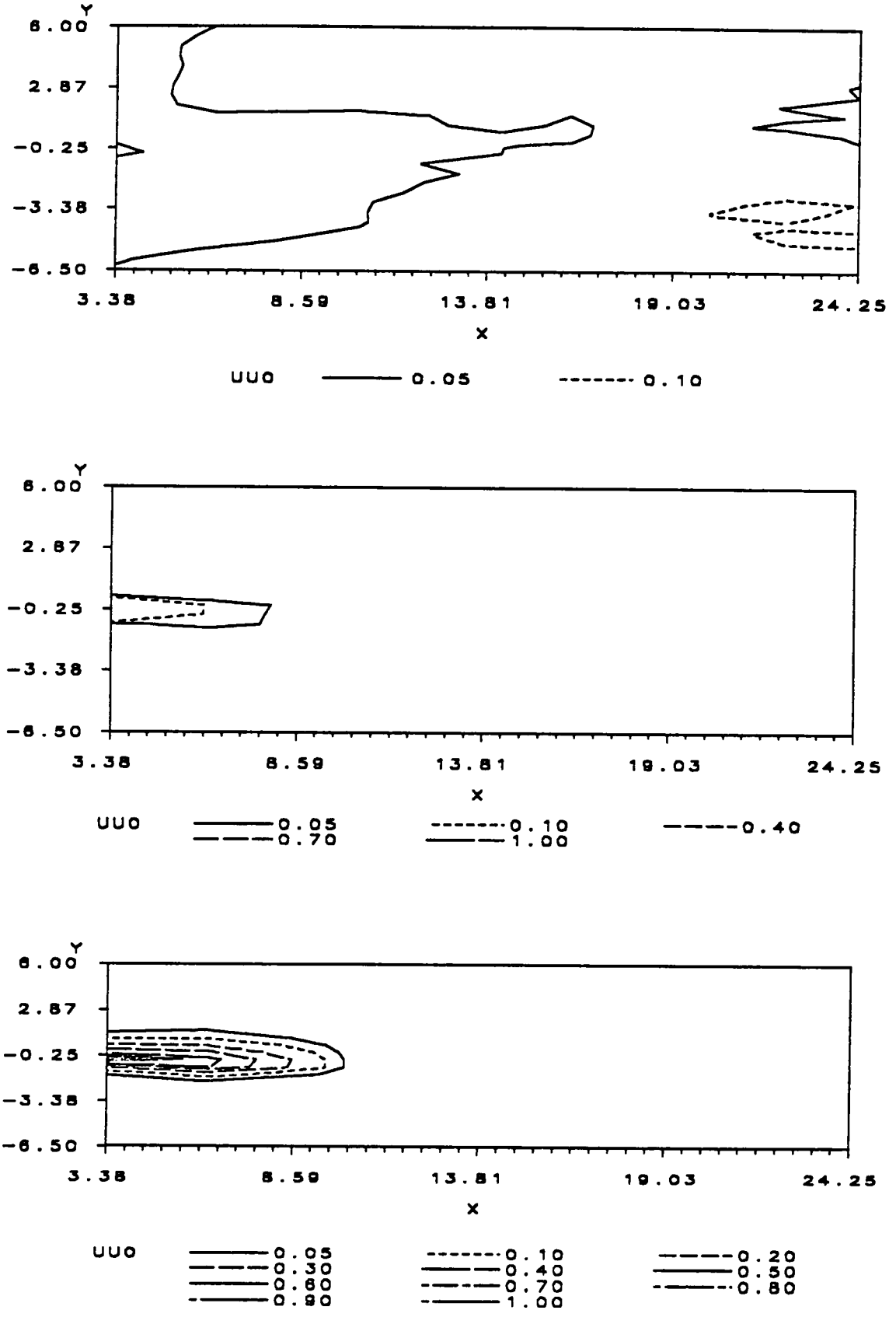

Figure 44. Mean velocity contour plots for 4 Hz - 4 psig for bent tube inlet configuration. Top - t/T = 0.6250, center - t/T = 0.6667, bottom - t/T = 0.7083.

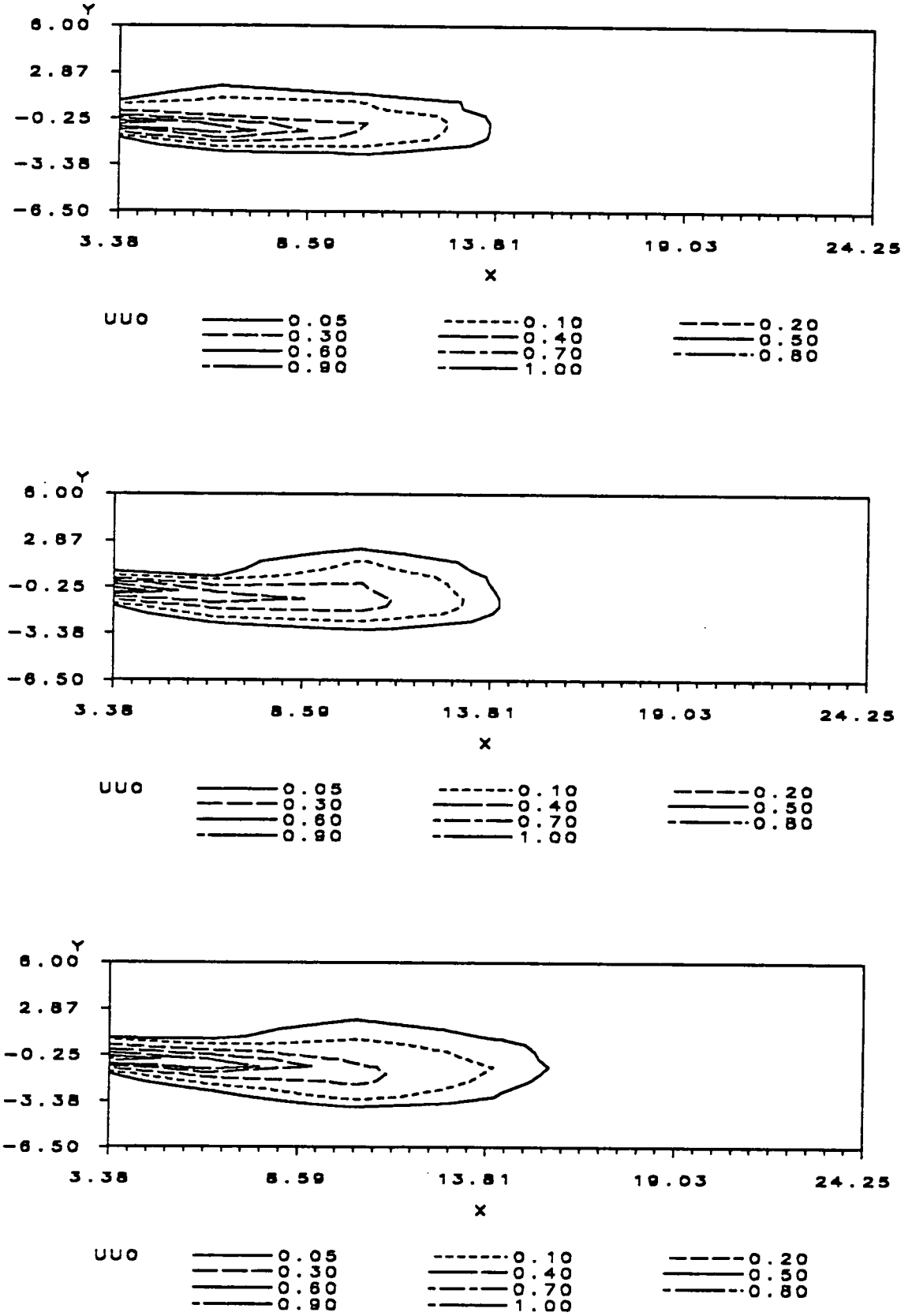

Figure 45. Mean velocity contour plots for 4 Hz - 4 psig for bent tube inlet configuration. Top - t/T = 0.750, center - t/T = 0.7917, bottom - t/T = 0.8333.

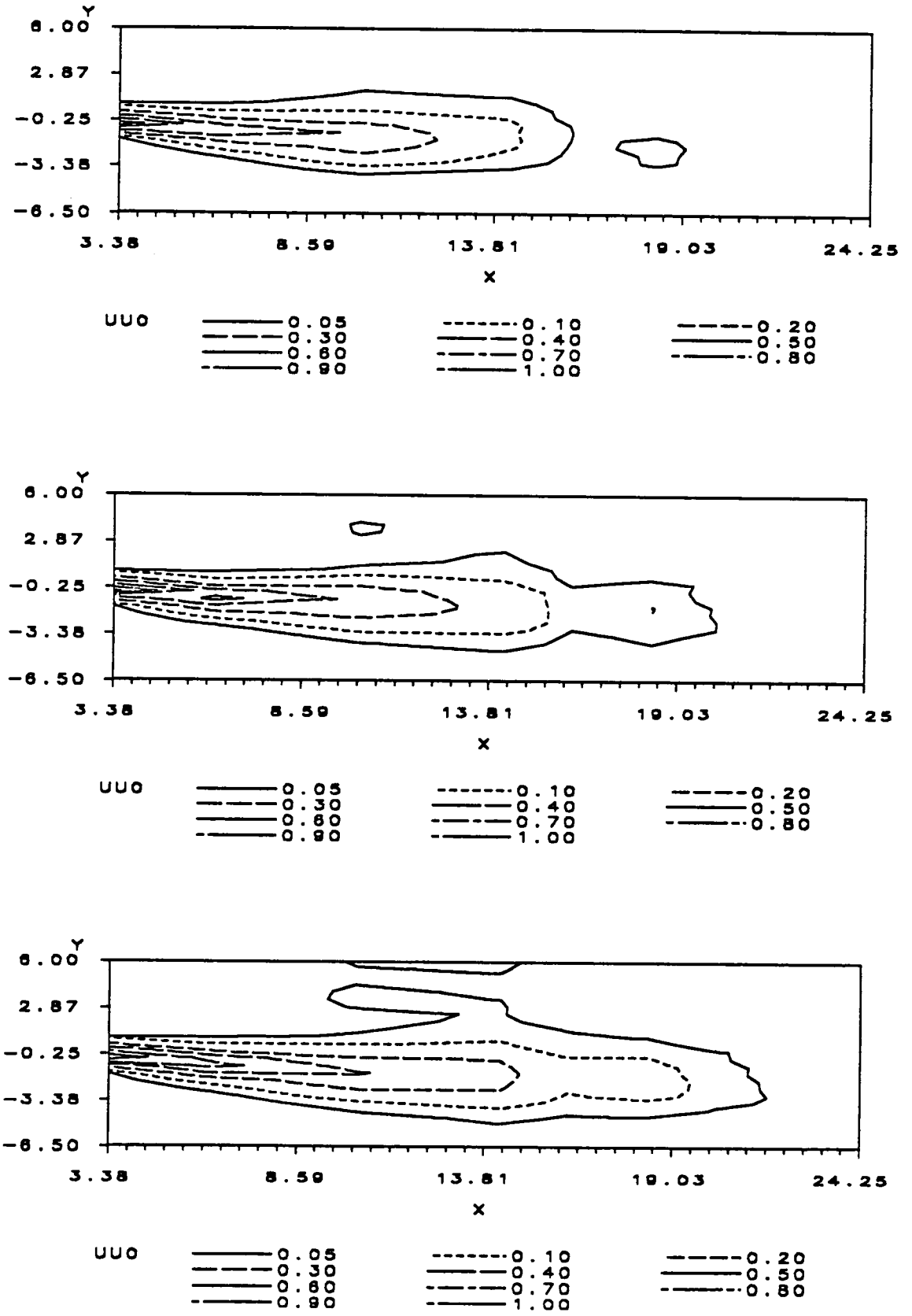

Figure 46. Mean velocity contour plots for 4 Hz - 4 psig for bent tube inlet configuration. Top - t/T = 0.8750, center - t/T = 0.9167, bottom - t/T = 0.9583.

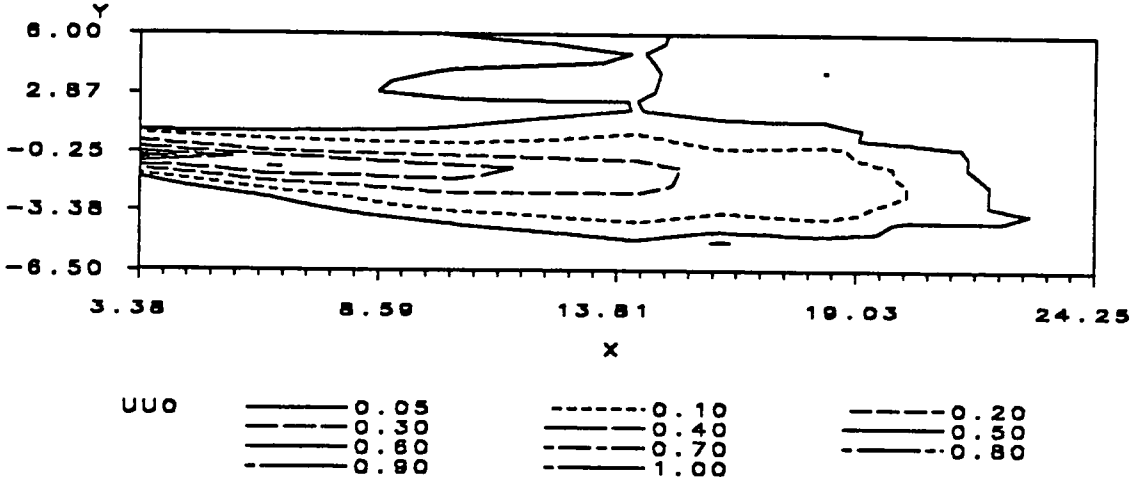

Figure 47. Mean velocity contour plots for 4 Hz - 4 psig for bent tube inlet configuration. Top - t/T = 1.000.

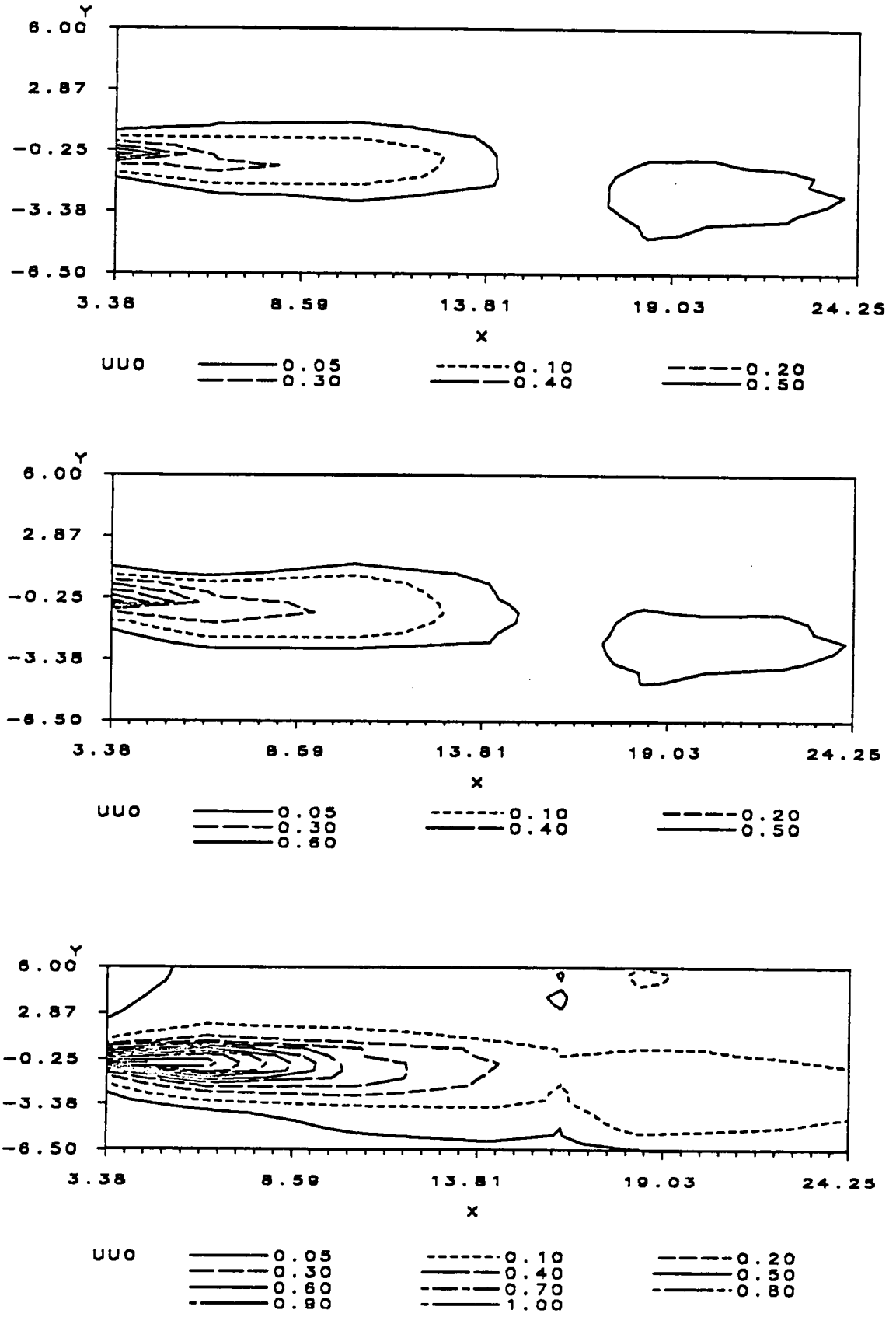

Figure 48. Mean velocity contour plots for 8 Hz - 4 psig for bent tube inlet configuration. Top - t/T = 0.000, center - t/T = 0.091, bottom - t/T = 0.182.

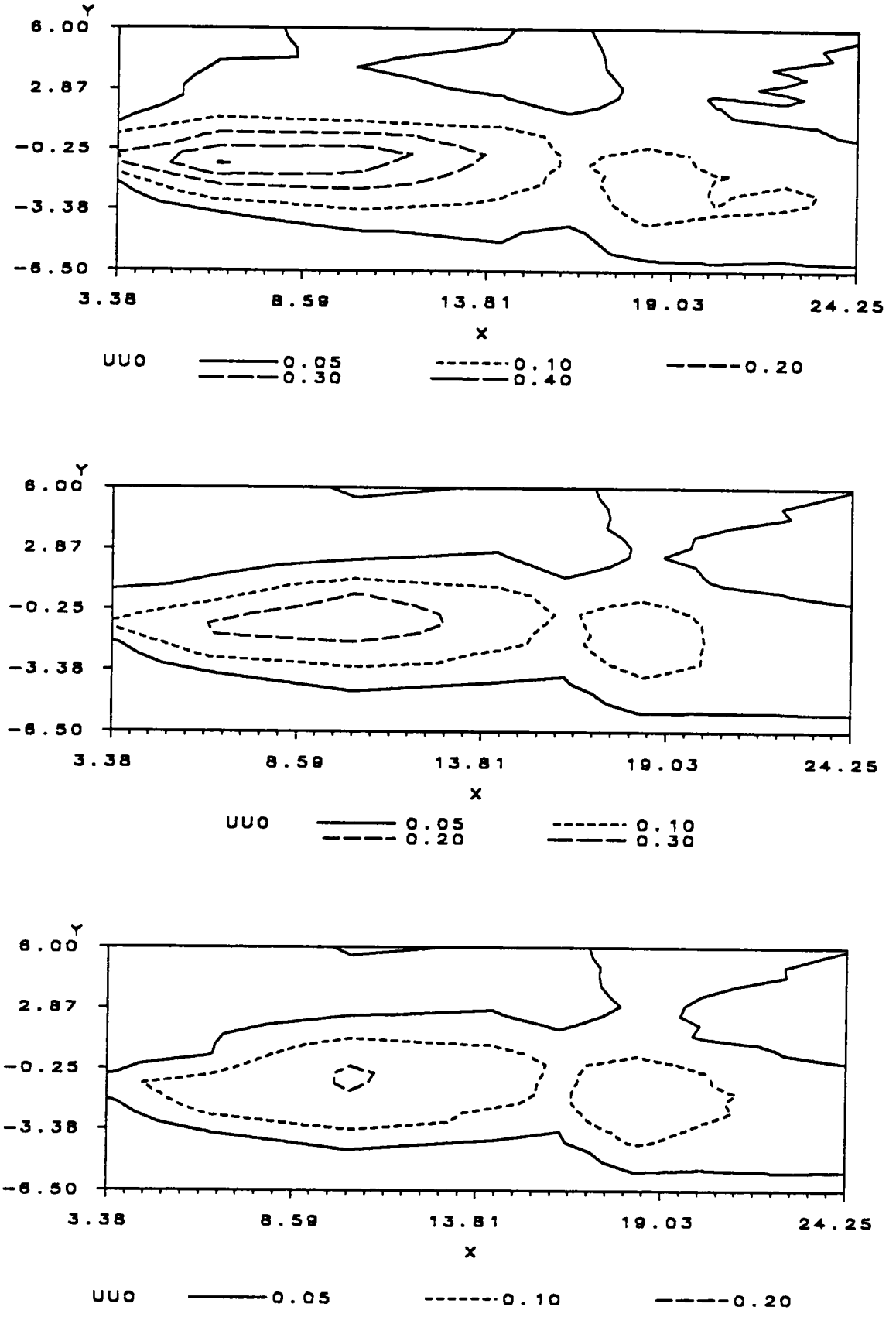

Figure 49. Mean velocity contour plots for 8 Hz - 4 psig for bent tube inlet configuration. Top - t/T = 0.273, center - t/T = 0.364, bottom - t/T = 0.4545.

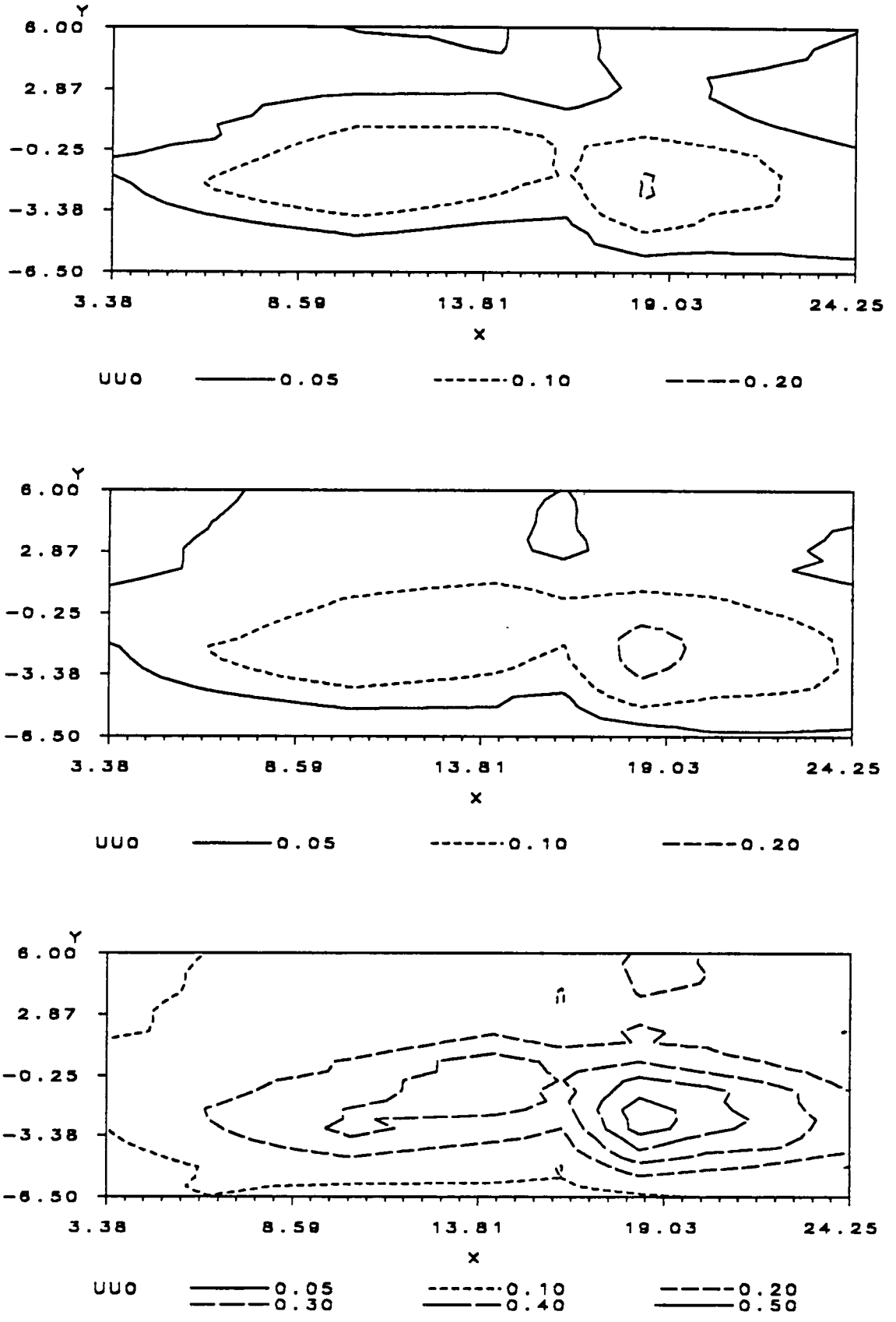

Figure 50. Mean velocity contour plots for 8 Hz - 4 psig for bent tube inlet configuration. Top - t/T = 0.5454, center - t/T = 0.6364, bottom - t/T = 0.7273.

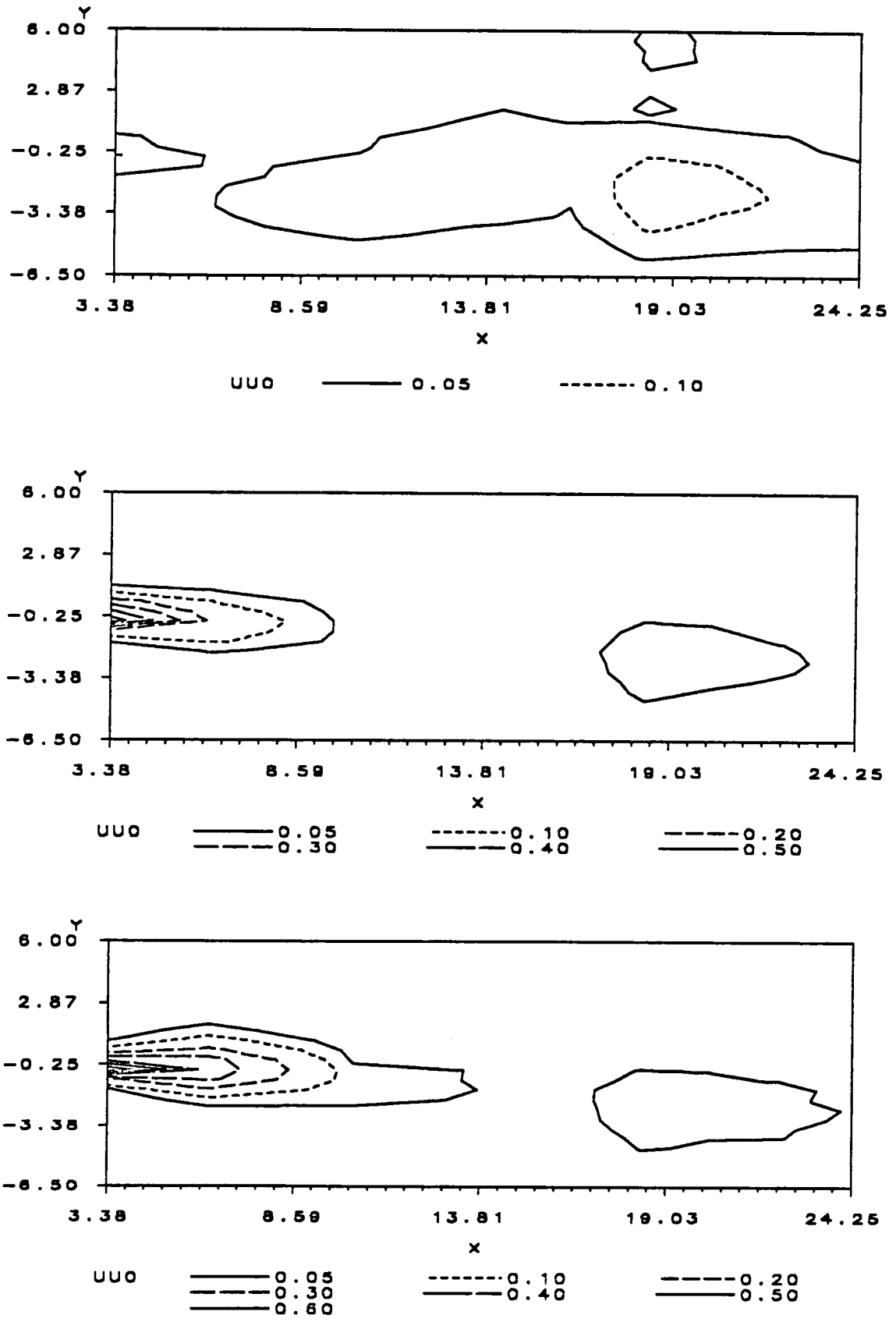

Figure 51. Mean velocity contour plots for 8 Hz - 4 psig for bent tube inlet configuration. Top - t/T = 0.8182, center - t/T = 0.9091, bottom - t/T = 1.000.

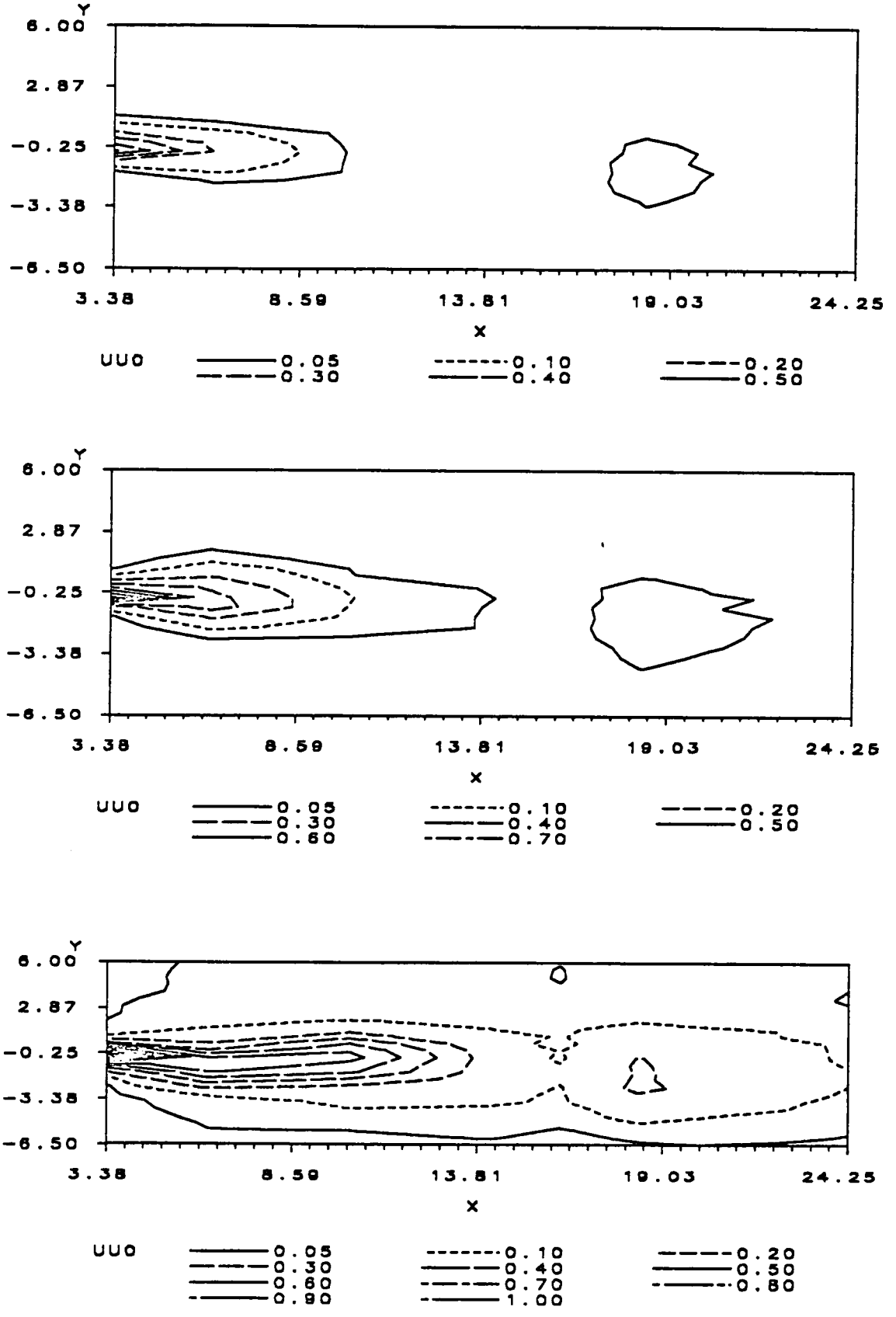

Figure 52. Mean velocity contour plots for 12 Hz - 4 psig for bent tube inlet configuration. Top - t/T = 0.000, center - t/T = 0.143, bottom - t/T = 0.286.

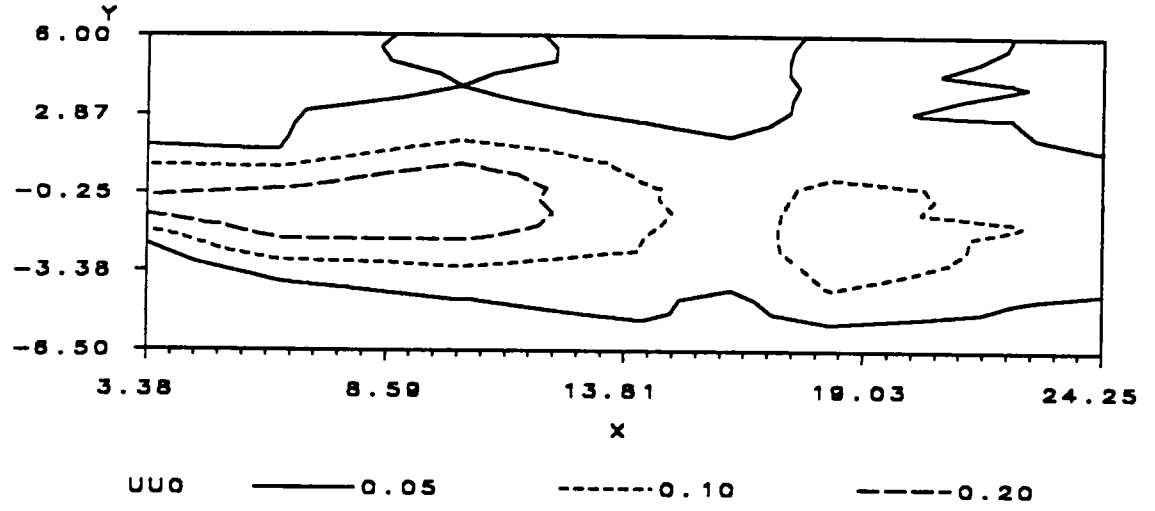

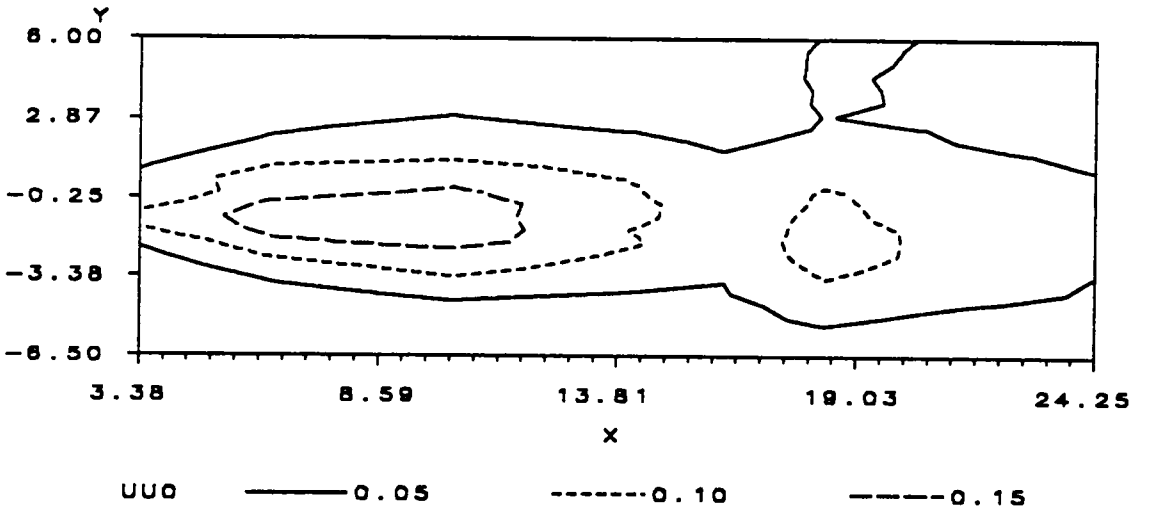

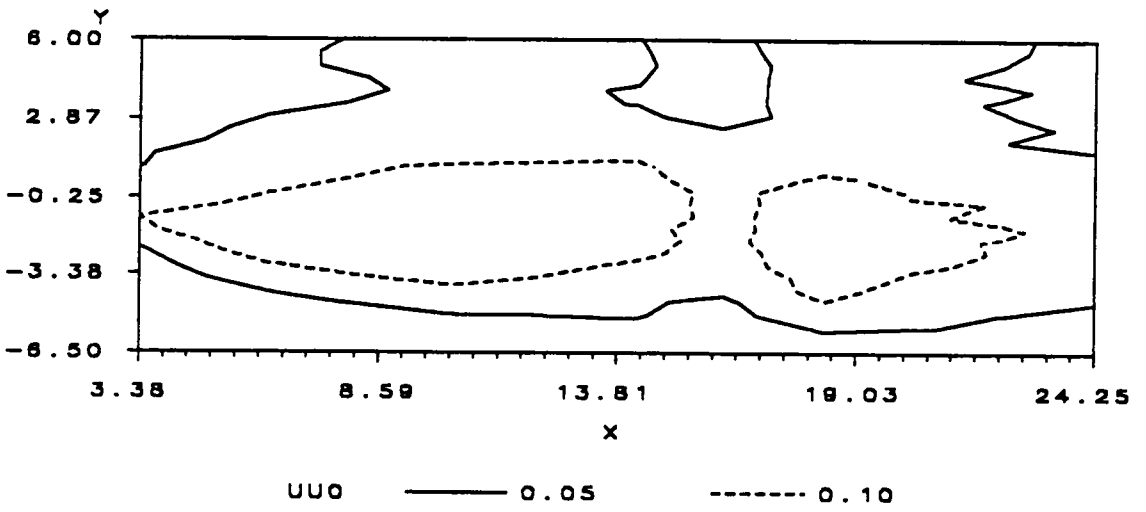

Figure 53. Mean velocity contour plots for 12 Hz - 4 psig for bent tube inlet configuration. Top - t/T = 0.429, center - t/T = 0.571, bottom - t/T = 0.7143.

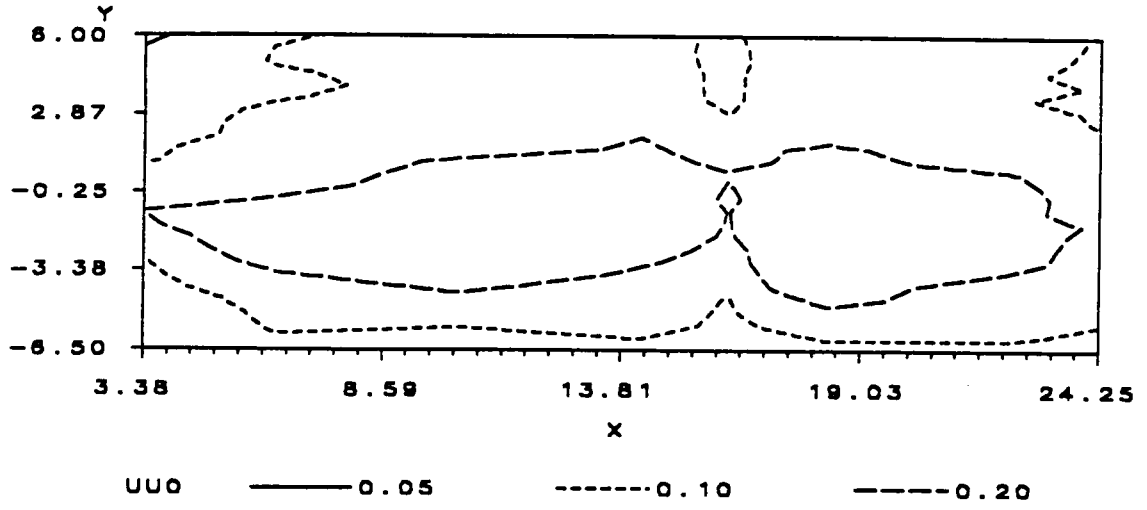

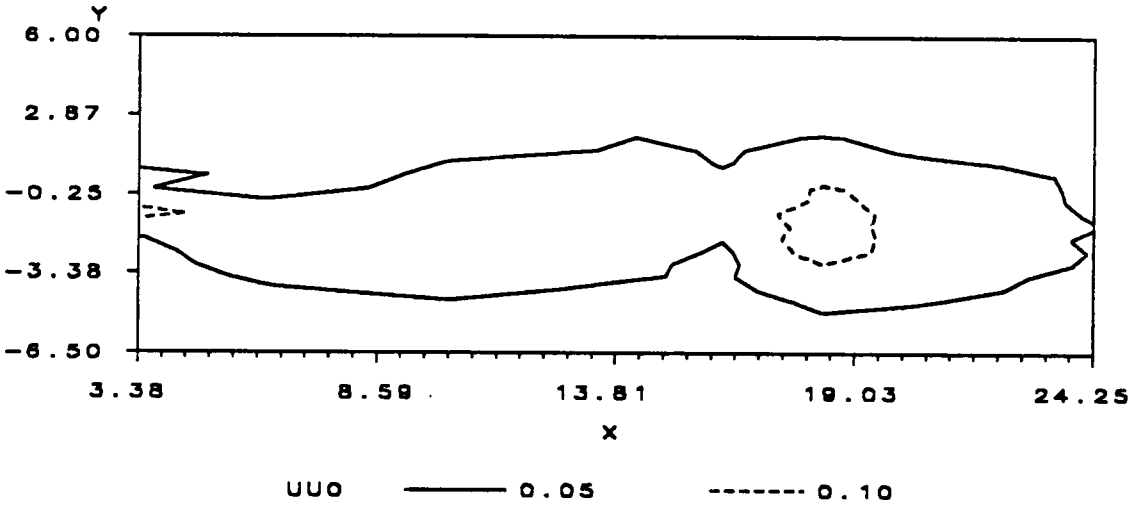

Figure 54. Mean velocity contour plots for 12 Hz - 4 psig for bent tube inlet configuration. Top - t/T = 0.857, center - t/T = 1.000.

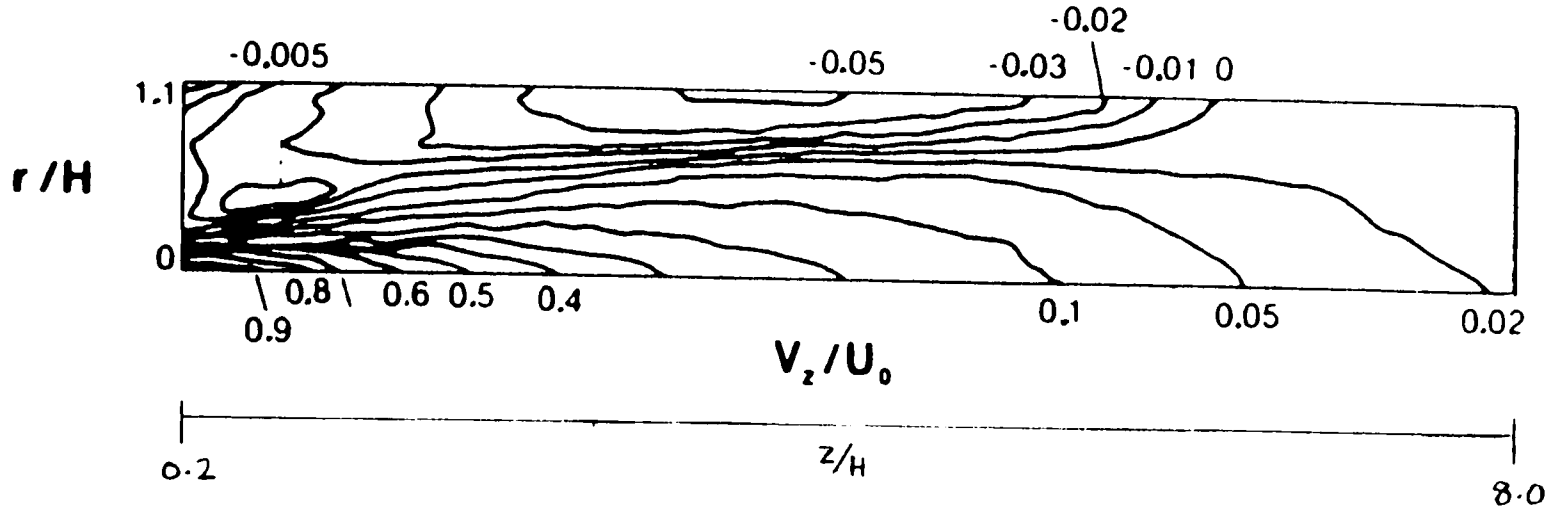

r - radial co-ordinate
z - axial co-ordinate
H - step height
V_Z - Mean Axial Velocity
U_o - Jet Inlet Velocity

Figure 55. Contours of mean axial velocity (Morrison et al (1988)).

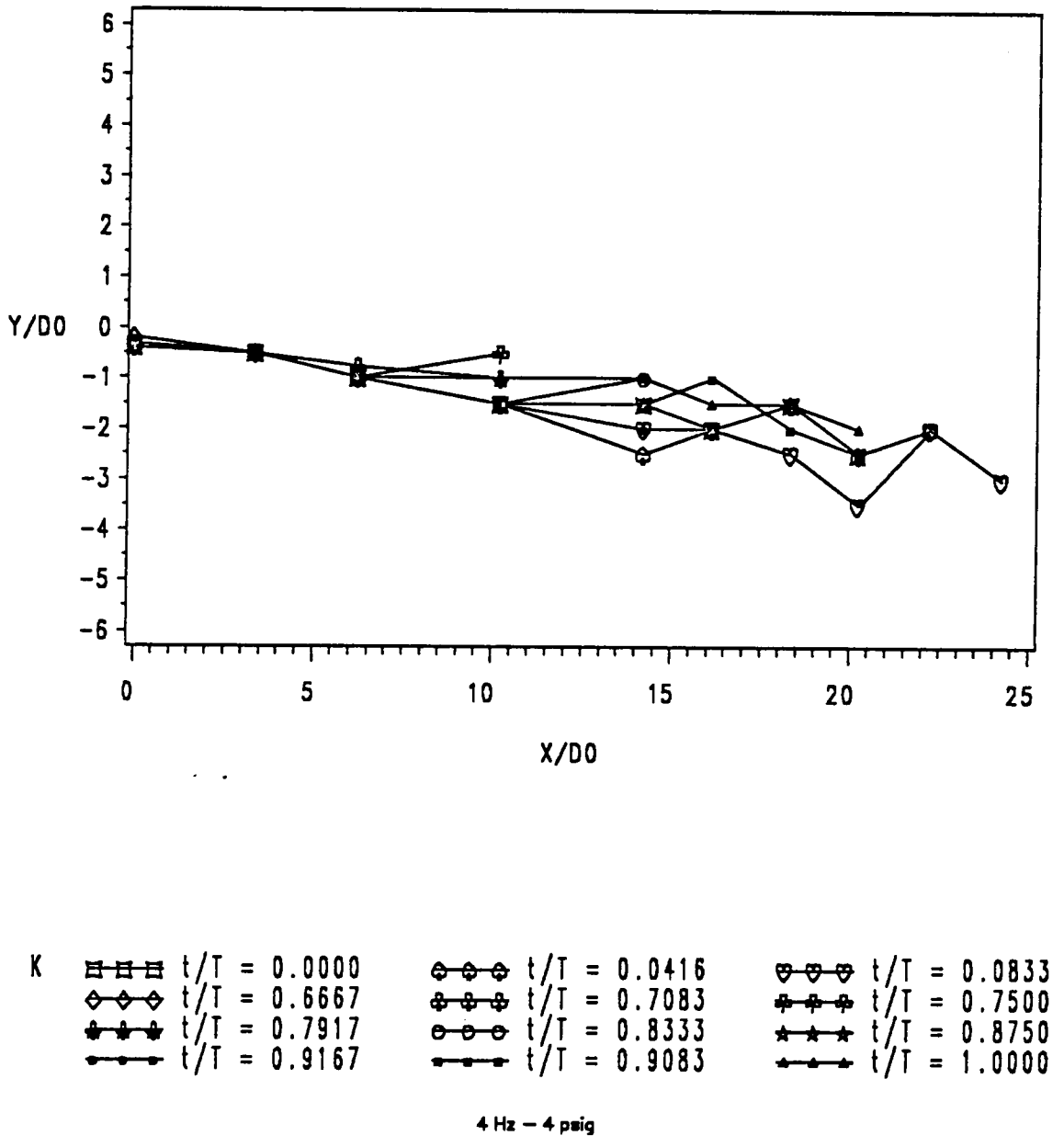

Figure 56. Deviation from centerline of the point of maximum velocity in the plane.: For the case of 4 Hz.

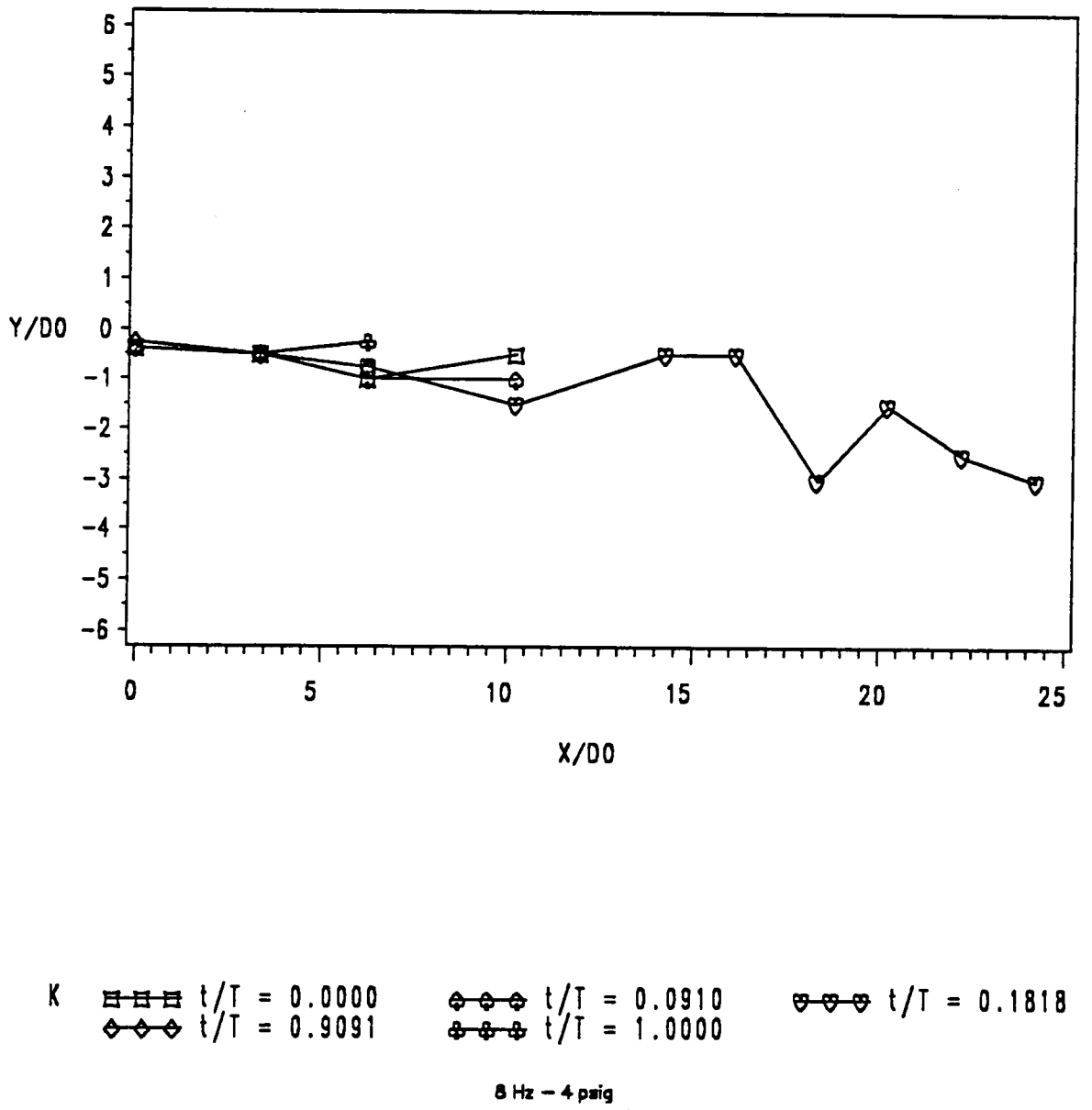

Figure 57. Deviation from centerline of the point of maximum velocity in the plane.: For the case of 8 Hz.

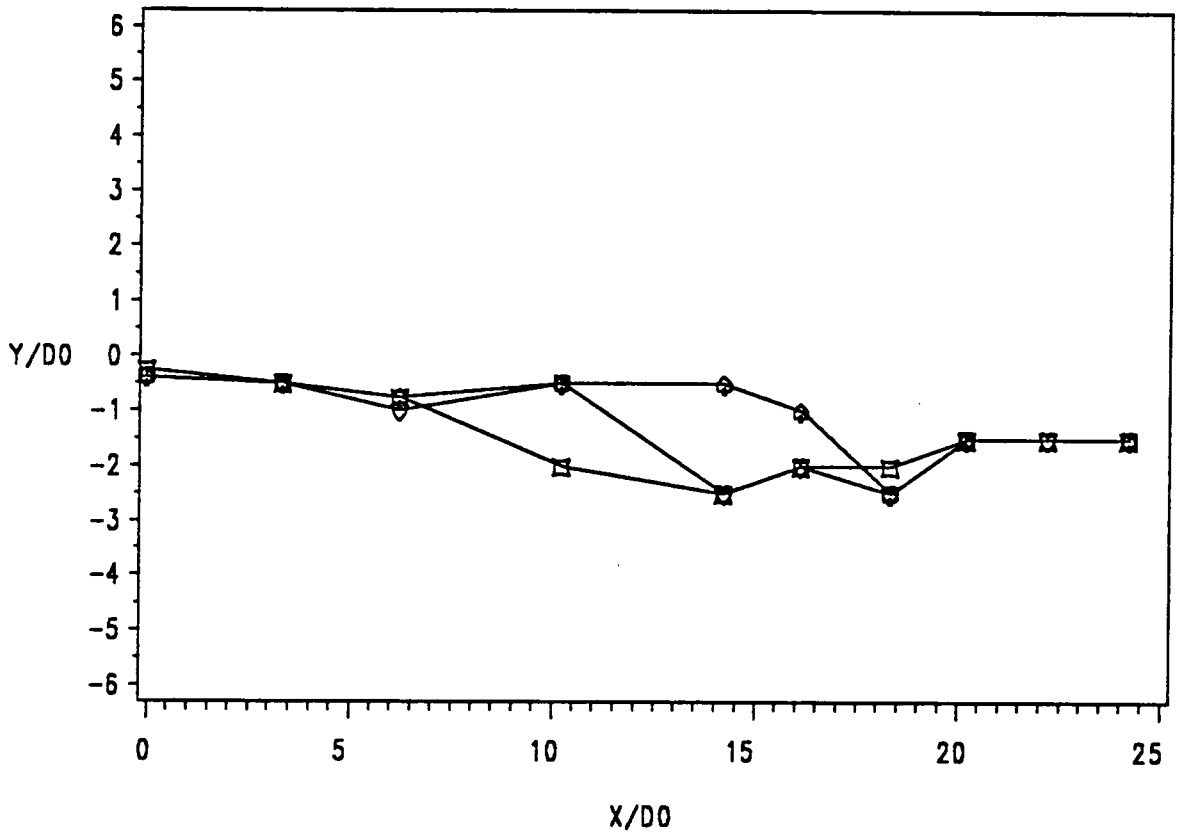

Figure 58. Deviation from centerline of the point of maximum velocity in the plane.: For the case of 12 Hz.

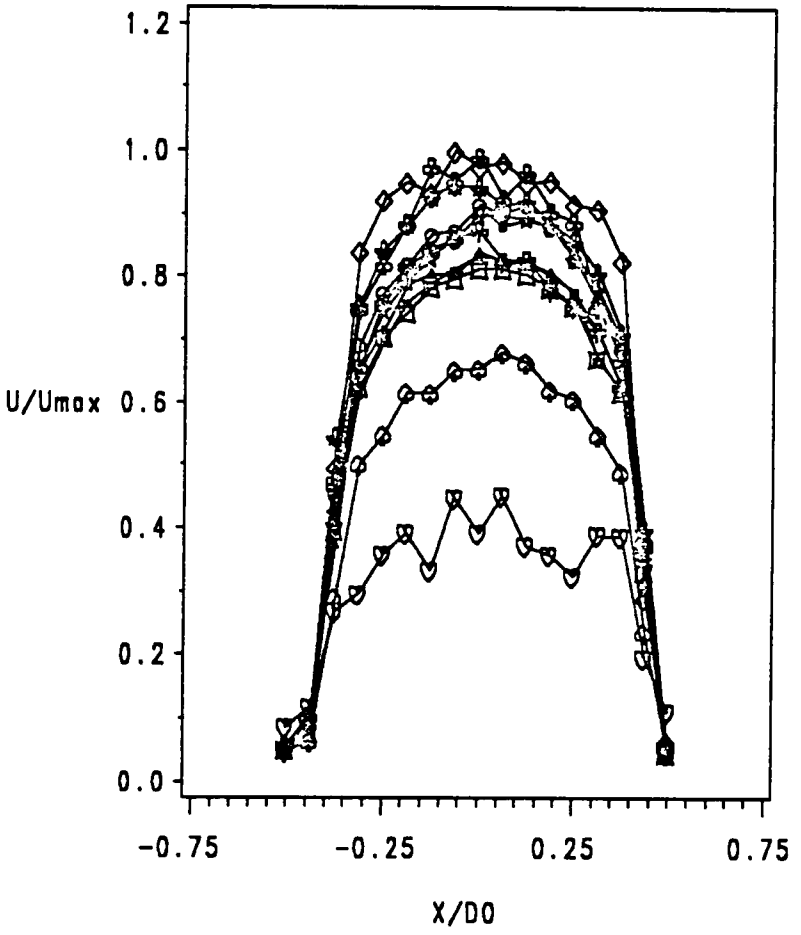

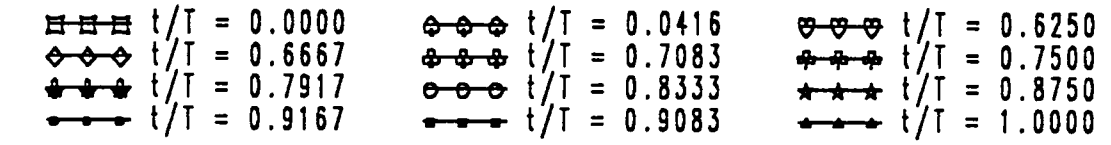

Figure 59. Gas generator model entrance velocity profiles for charging phases.: For straight tube inlet configuration at 4 Hz - 4 psig.

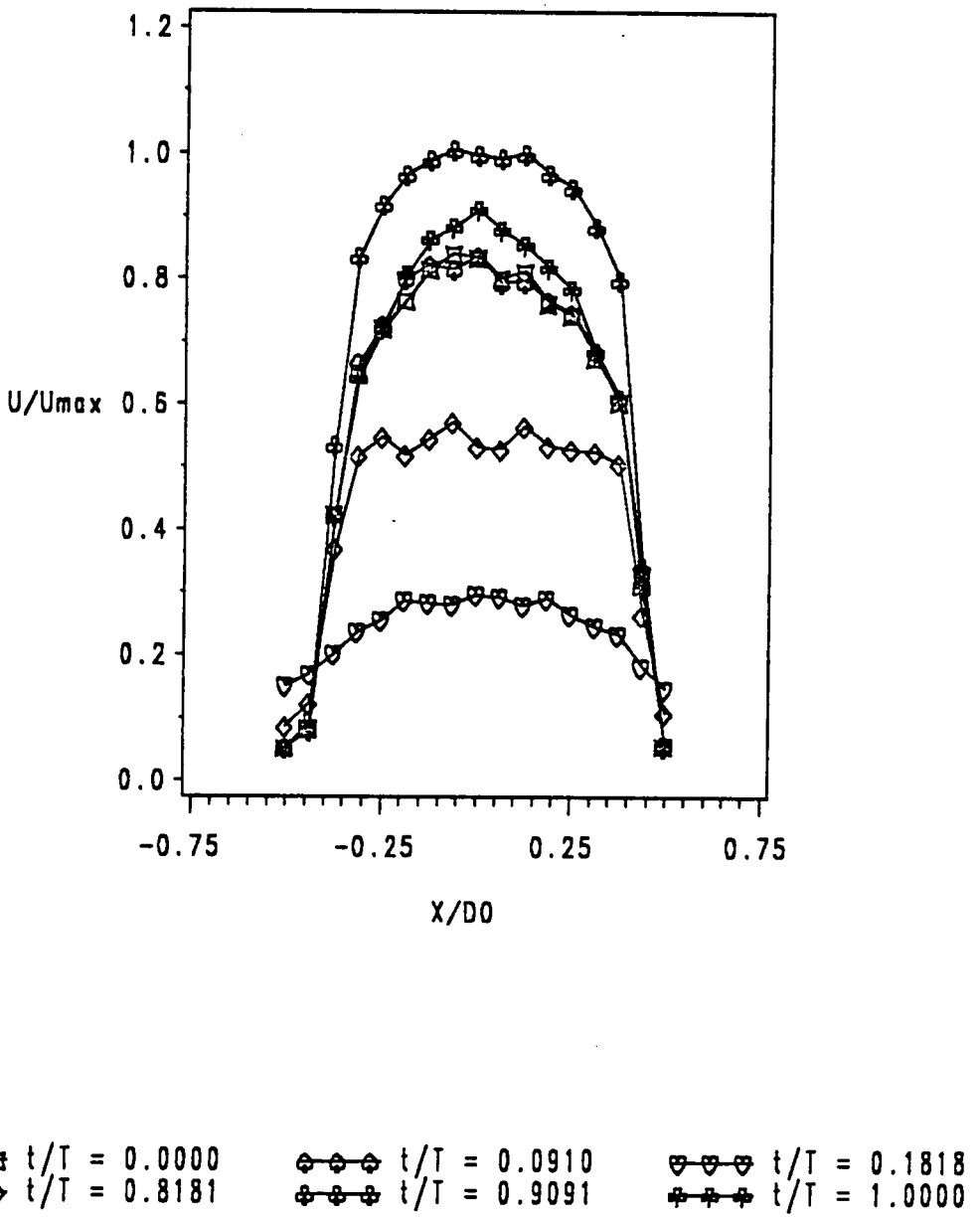

Figure 60. Gas generator model entrance velocity profiles for charging phases.: For straight tube inlet configuration at 8 Hz - 4 psig.

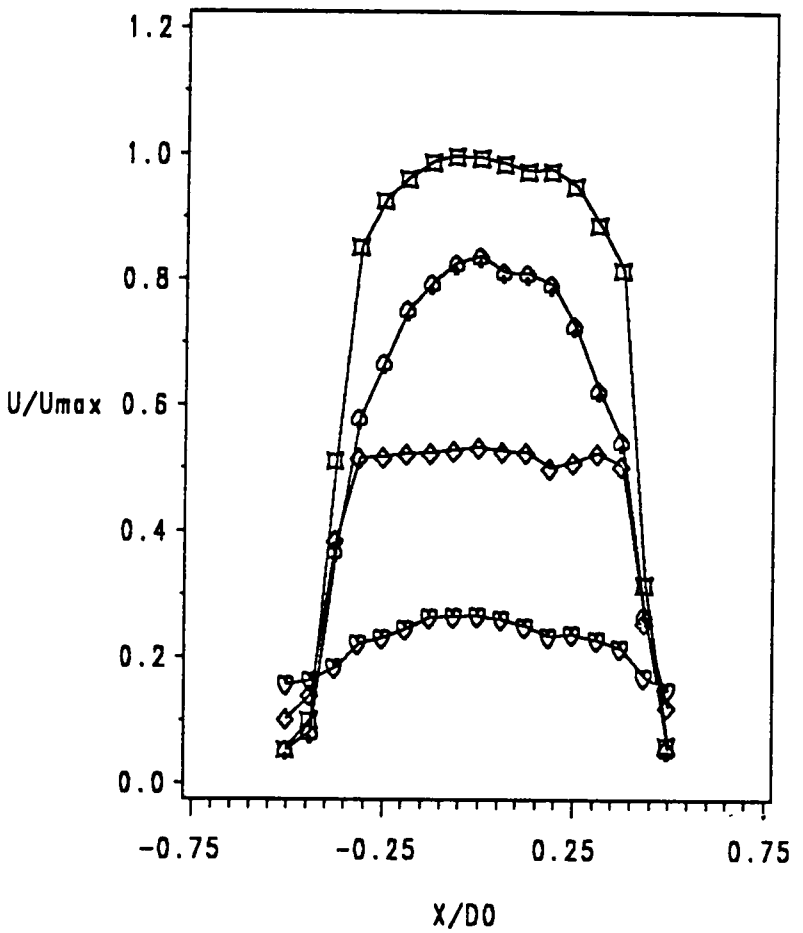

Figure 61. Gas generator model entrance velocity profiles for charging phases.: For straight tube inlet configuration at 12 Hz - 4 psig.

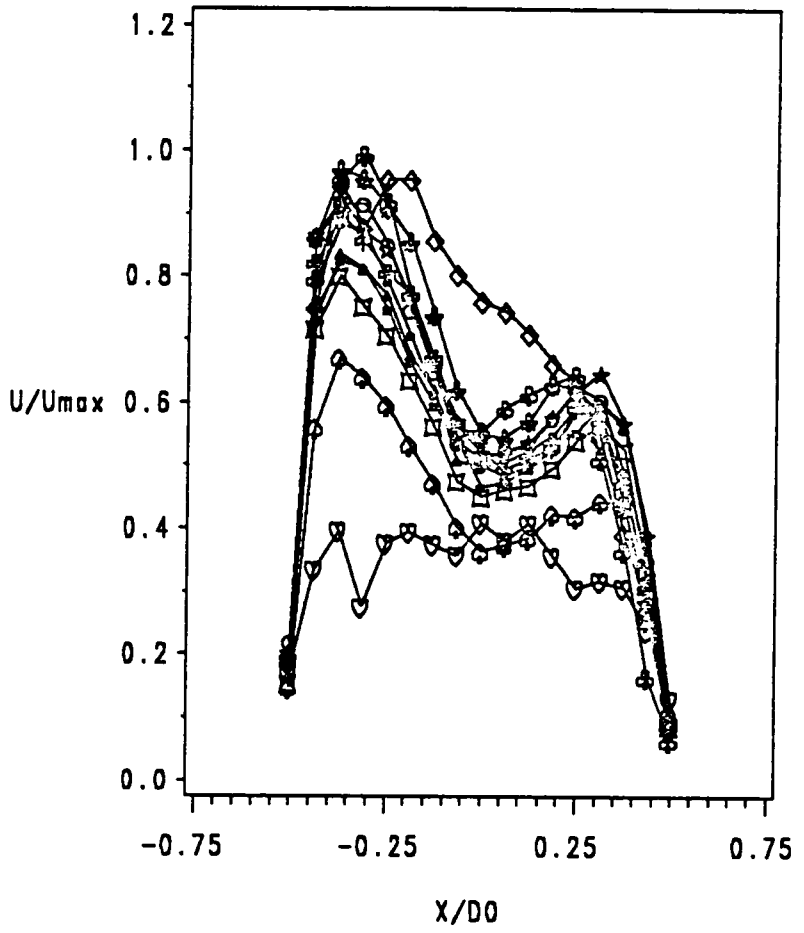

Figure 62. Gas generator model entrance velocity profiles for charging phases.: For bent tube inlet configuration at 4 Hz - 4 psig.

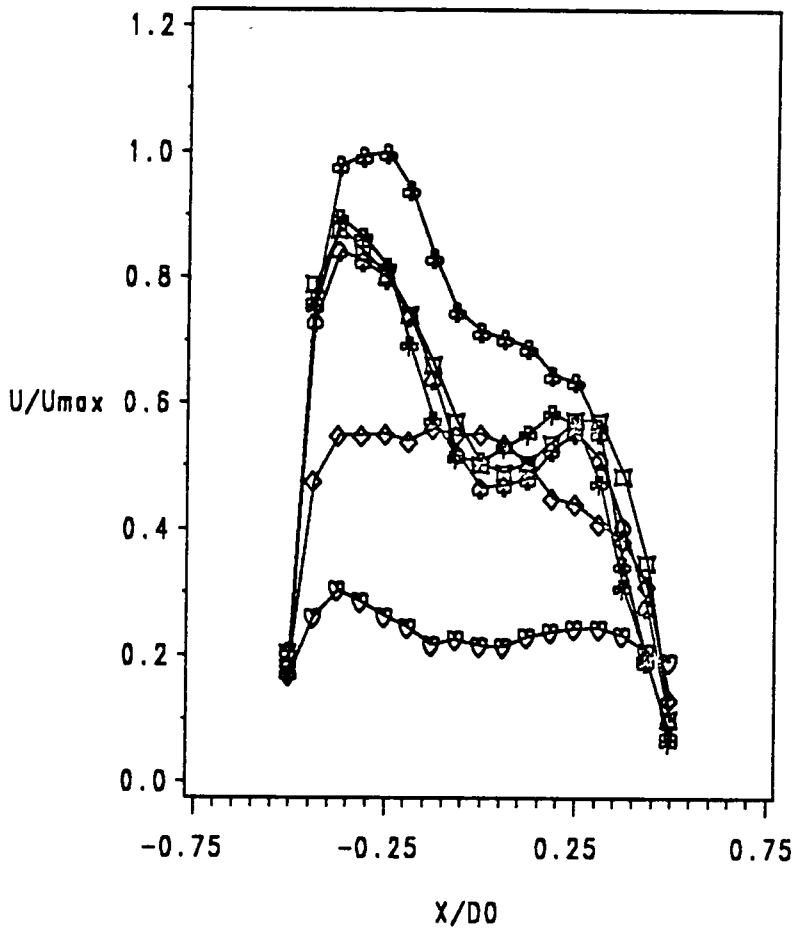

Figure 63. Gas generator model entrance velocity profiles for charging phases.: For bent tube inlet configuration at 8 Hz - 4 psig.

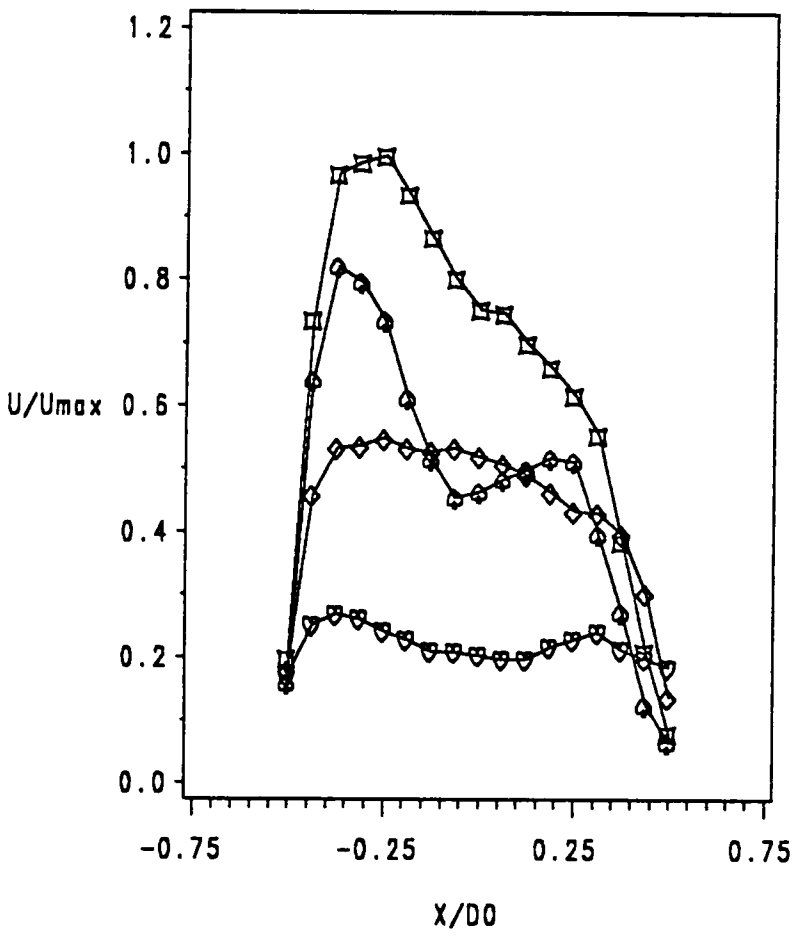

Figure 64. Gas generator model entrance velocity profiles for charging phases.: For bent tube inlet configuration at 12 Hz - 4 psig.

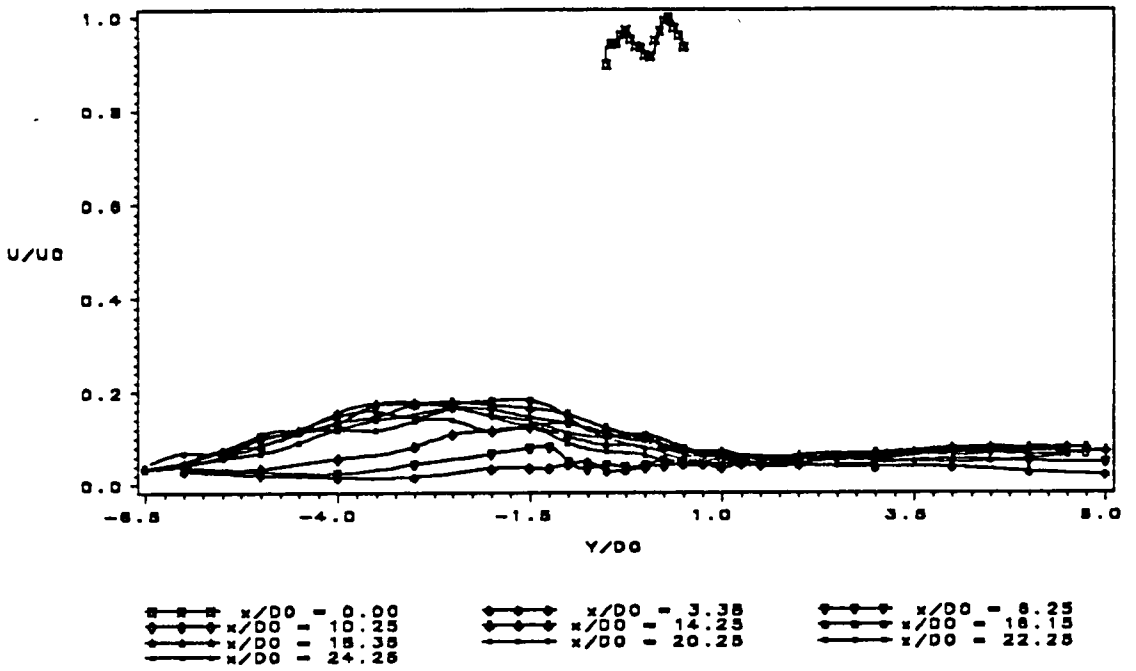

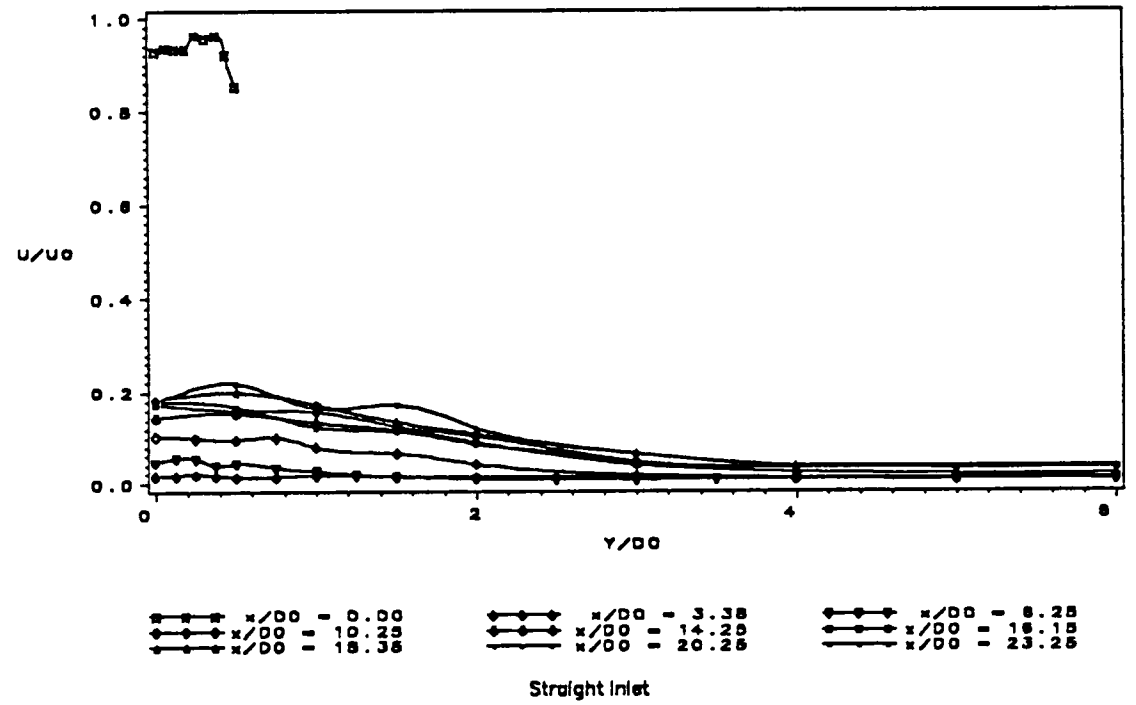

Figure 65. Gas generator model velocity profiles for a venting phase. For bent tube and straight tube inlet configurations at 4 Hz - 4 psig - t/T = 0.250.

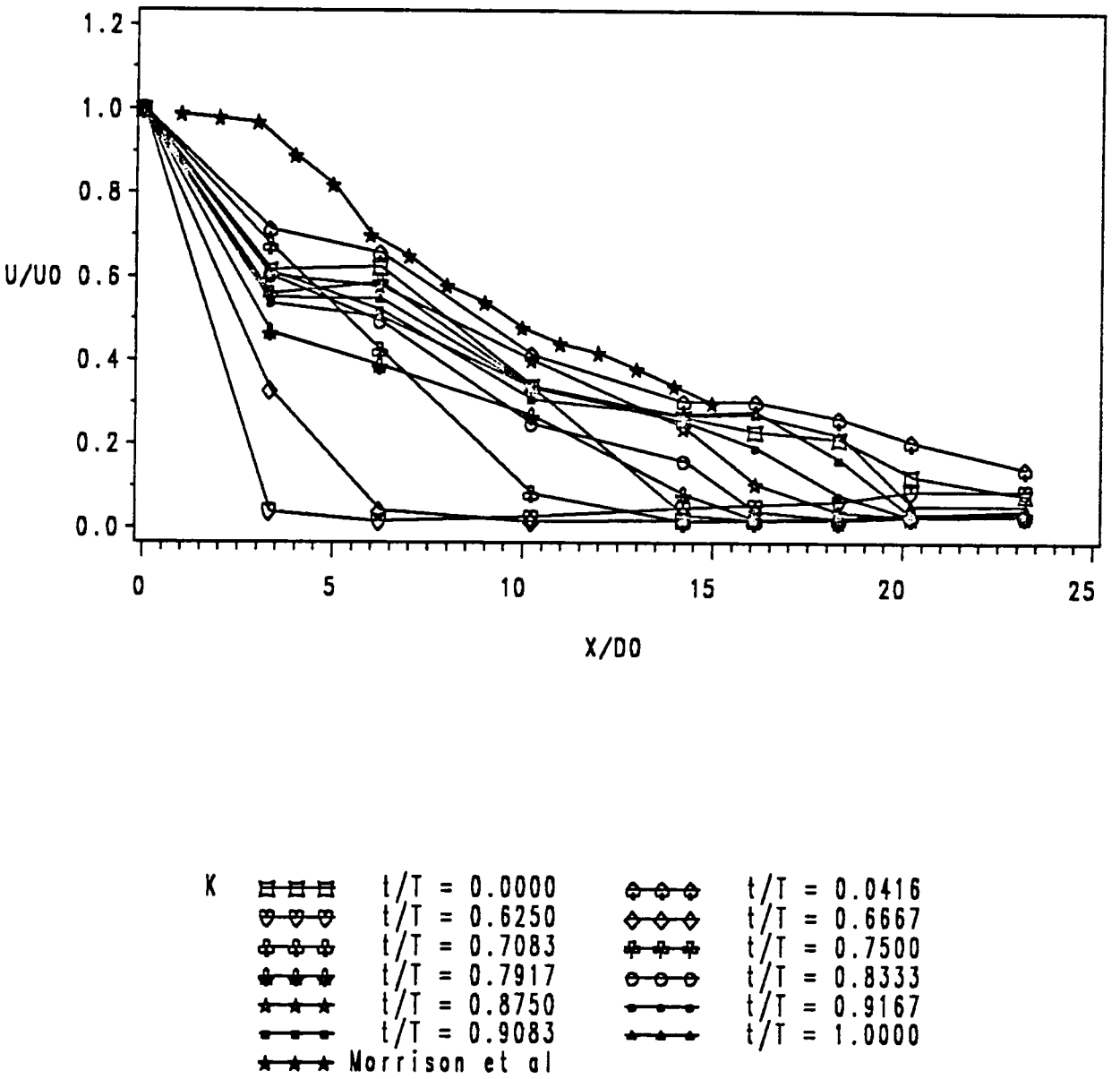

Figure 66. Centerline velocity decay for charging phases in the straight tube configuration.: At 4 Hz - 4 spig.

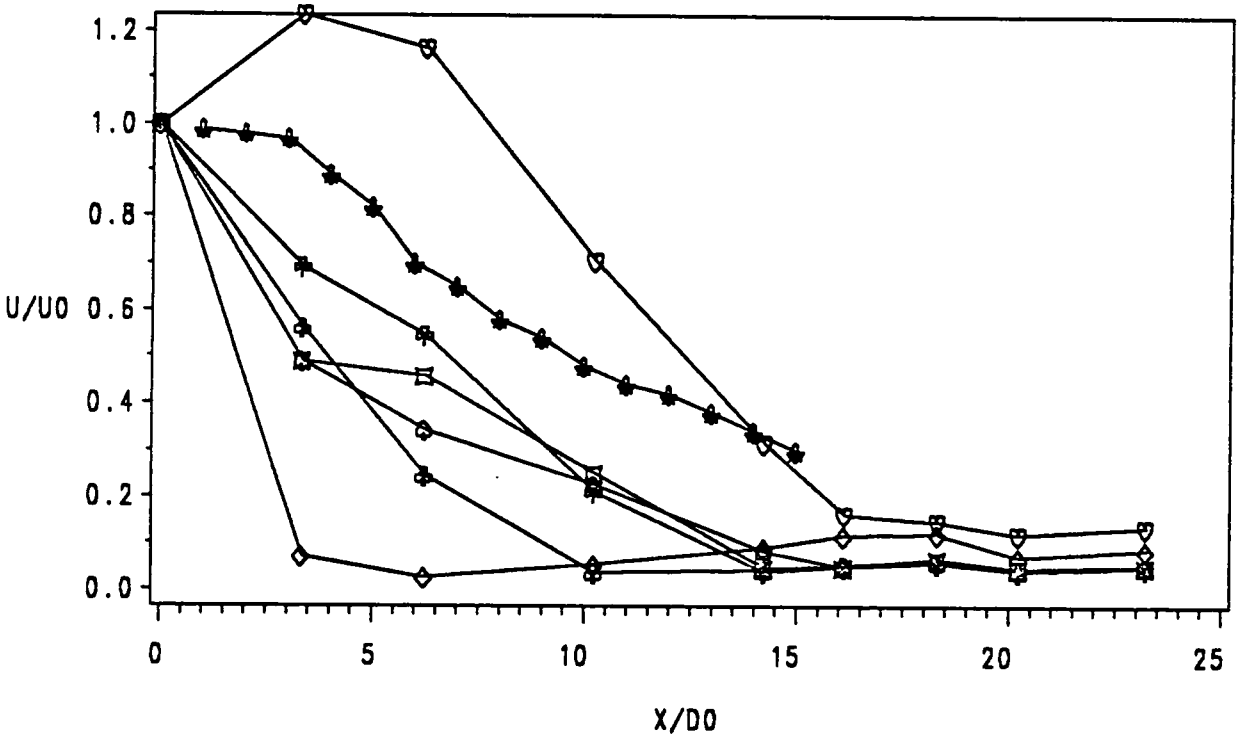

Figure 67. Centerline velocity decay for charging phases in the straight tube configuration.: At 8 Hz - 4 spig.

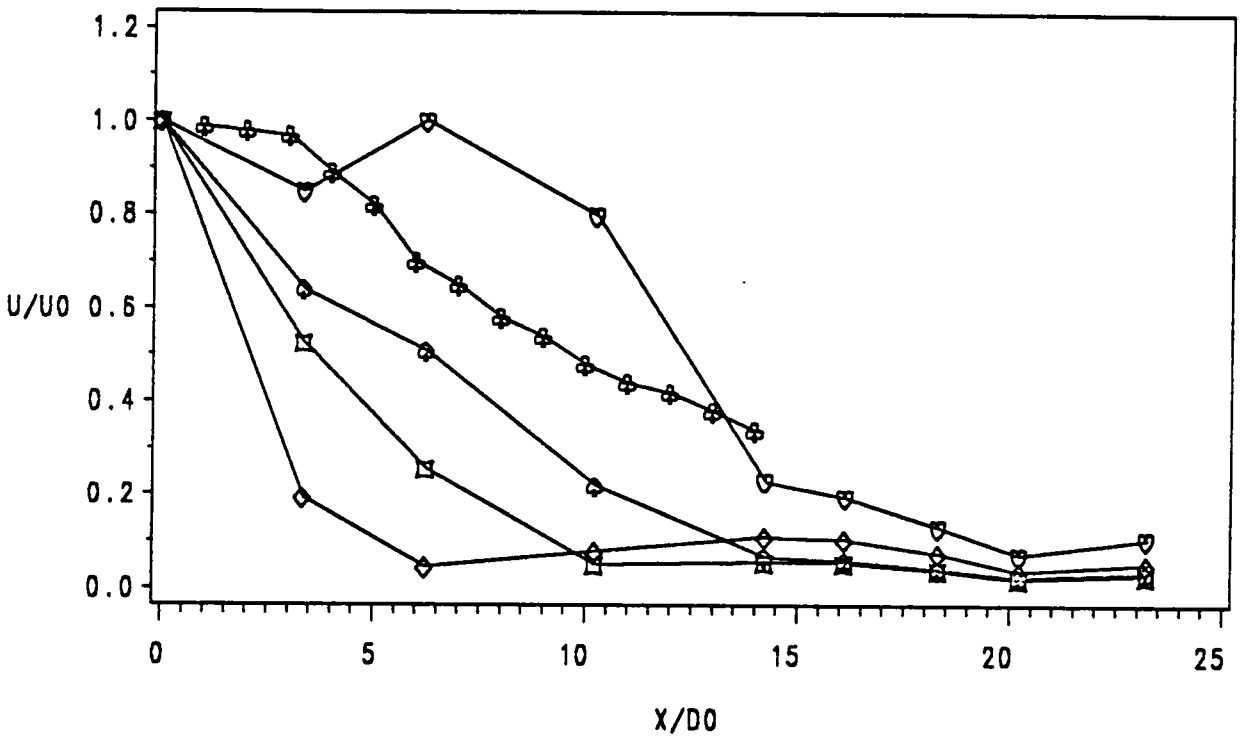

Figure 68. Centerline velocity decay for charging phases in the straight tube configuration.: At 12 Hz - 4 spig.

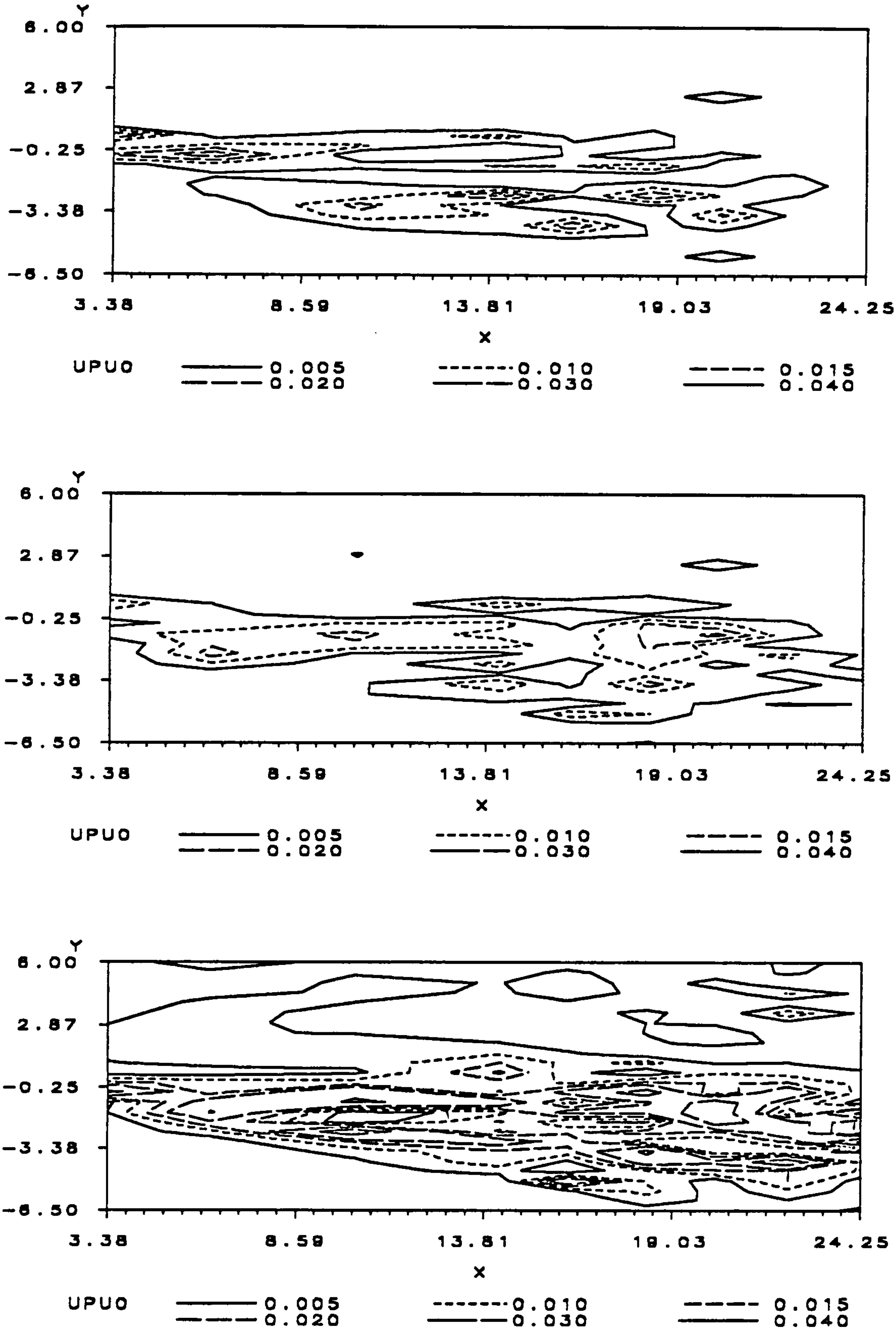

Figure 69. Axial turbulence contour plots for 4 Hz - 4 psig for bent tube inlet configuration. Top - t/T = 0.000, center - t/T = 0.042, bottom - t/T = 0.083.

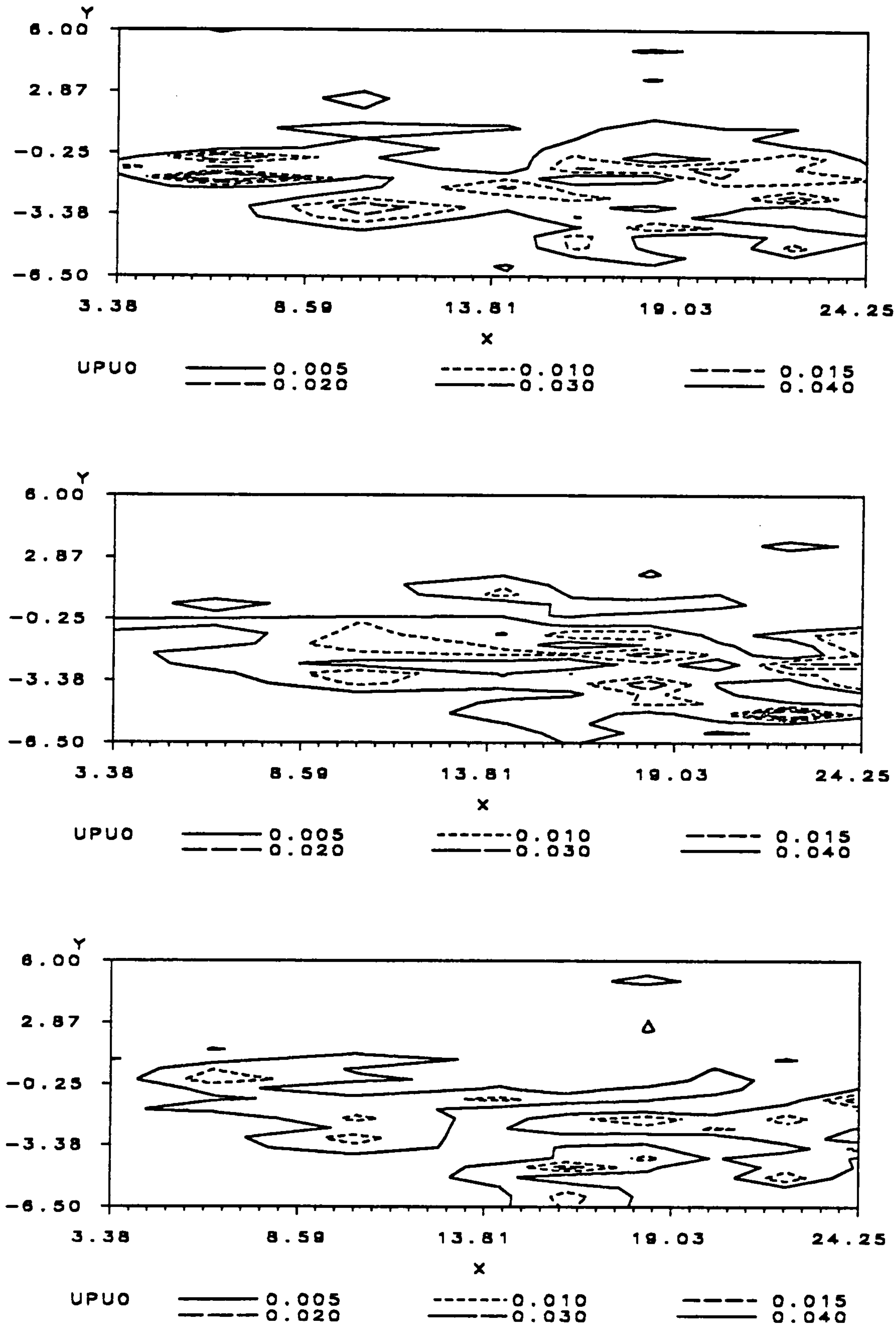

Figure 70. Axial turbulence contour plots for 4 Hz - 4 psig for bent tube inlet configuration. Top - t/T = 0.125, center - t/T = 0.167, bottom - t/T = 0.2083.

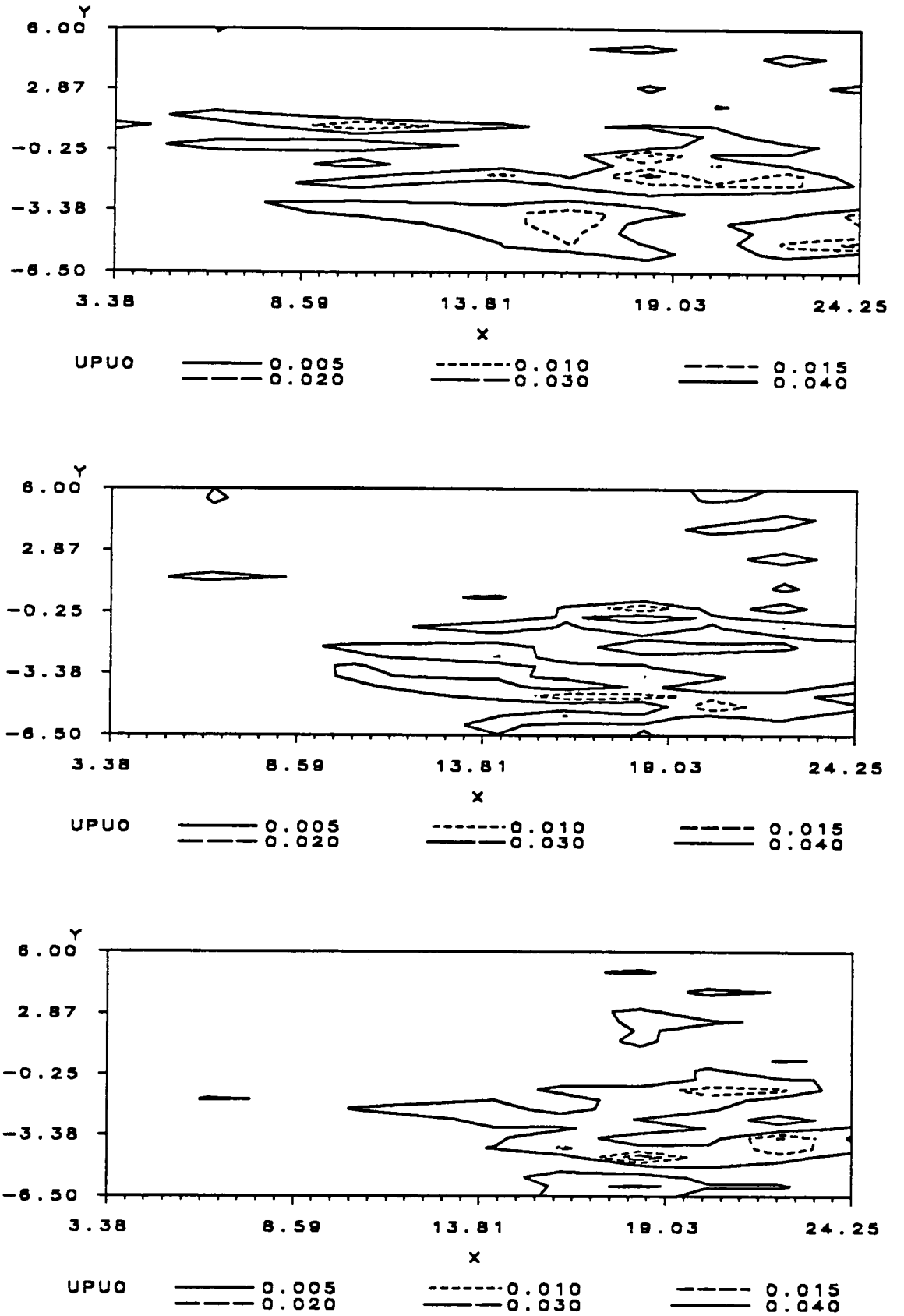

Figure 71. Axial turbulence contour plots for 4 Hz - 4 psig for bent tube inlet configuration. Top - t/T = 0.2500, center - t/T = 0.2917, bottom - t/T = 0.3333.

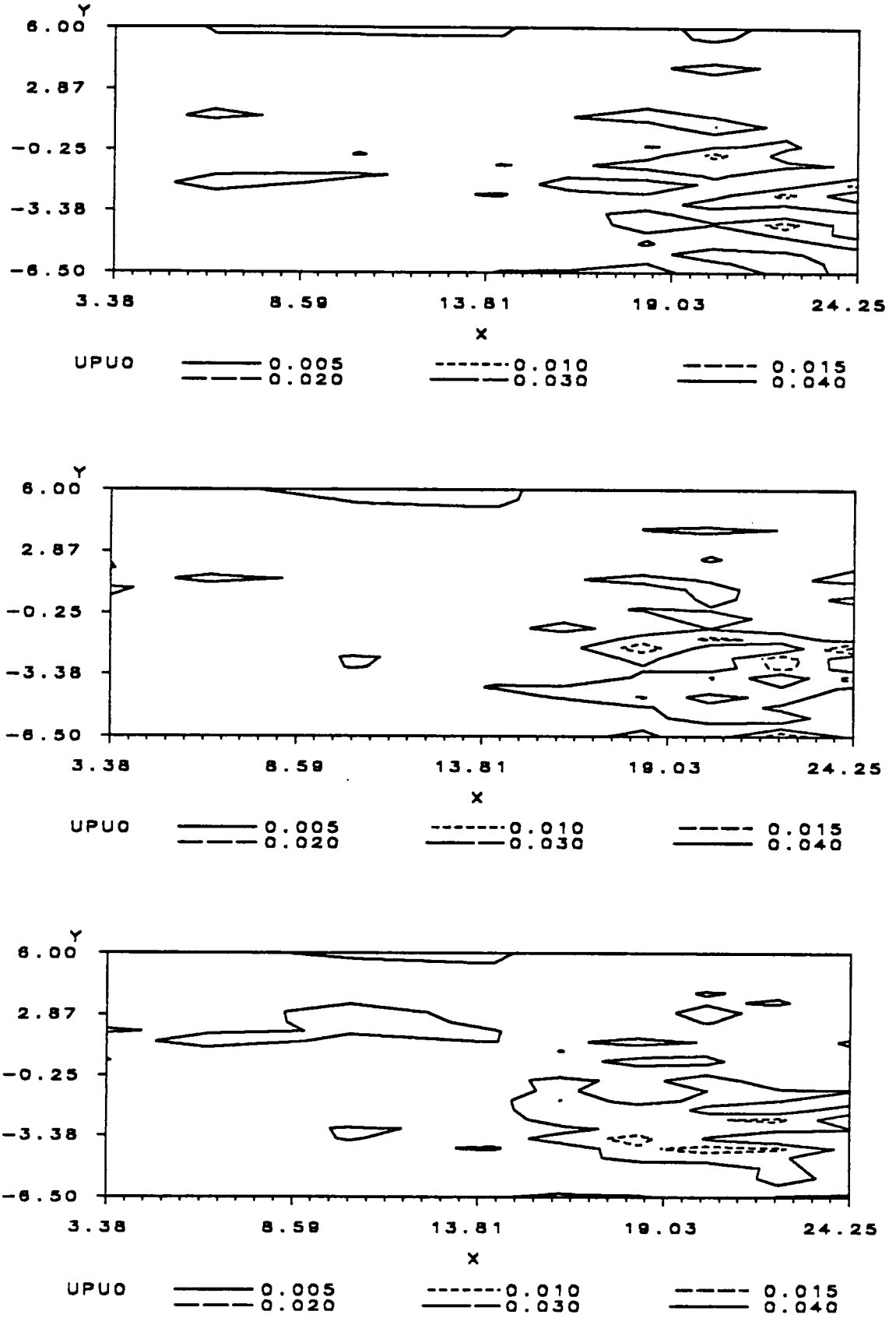

Figure 72. Axial turbulence contour plots for 4 Hz - 4 psig for bent tube inlet configuration. Top - t/T = 0.3750, center - t/T = 0.4167, bottom - t/T = 0.4583.

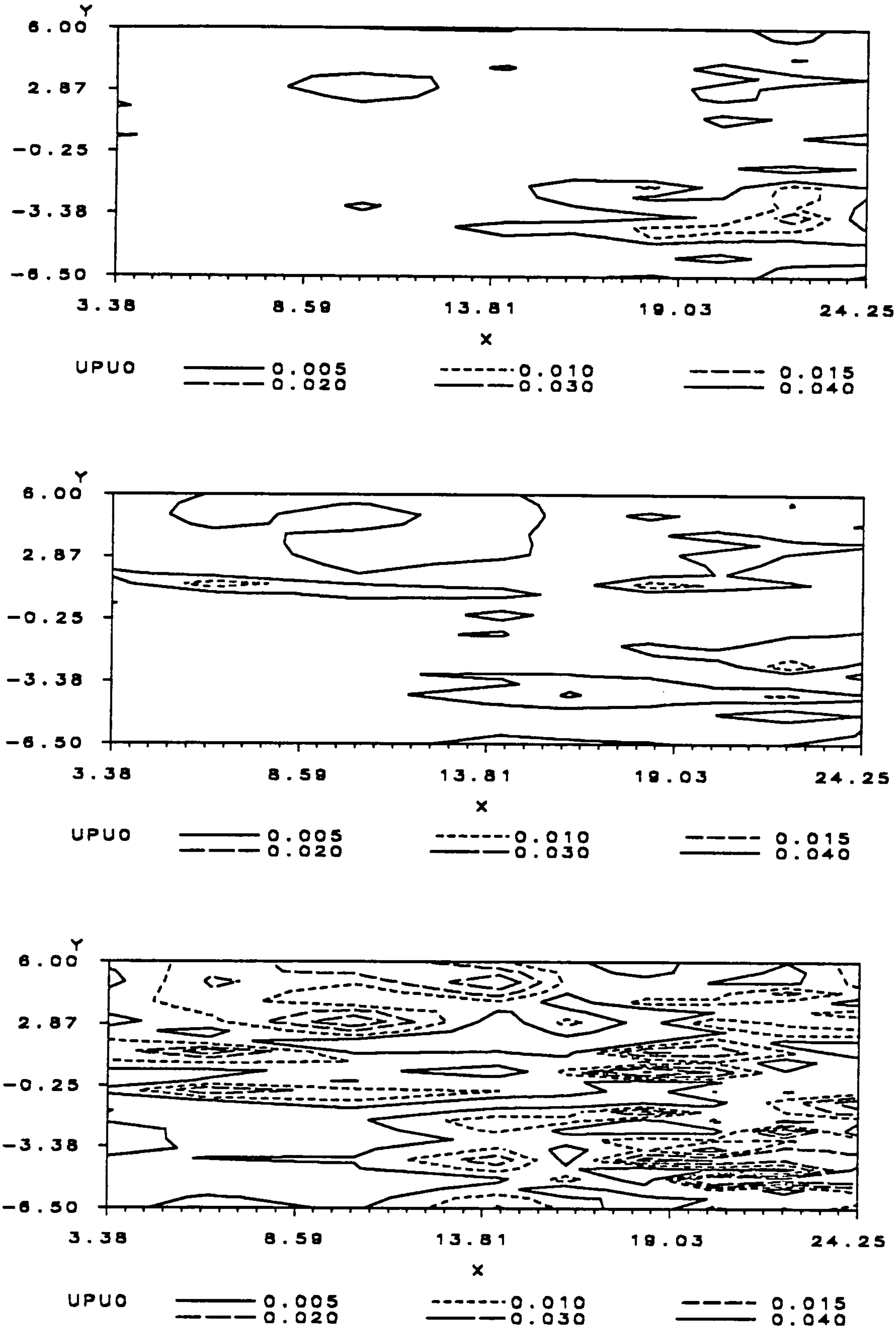

Figure 73. Axial turbulence contour plots for 4 Hz - 4 psig for bent tube inlet configuration. Top - t/T = 0.500, center - t/T = 0.5417, bottom - t/T = 0.5833.

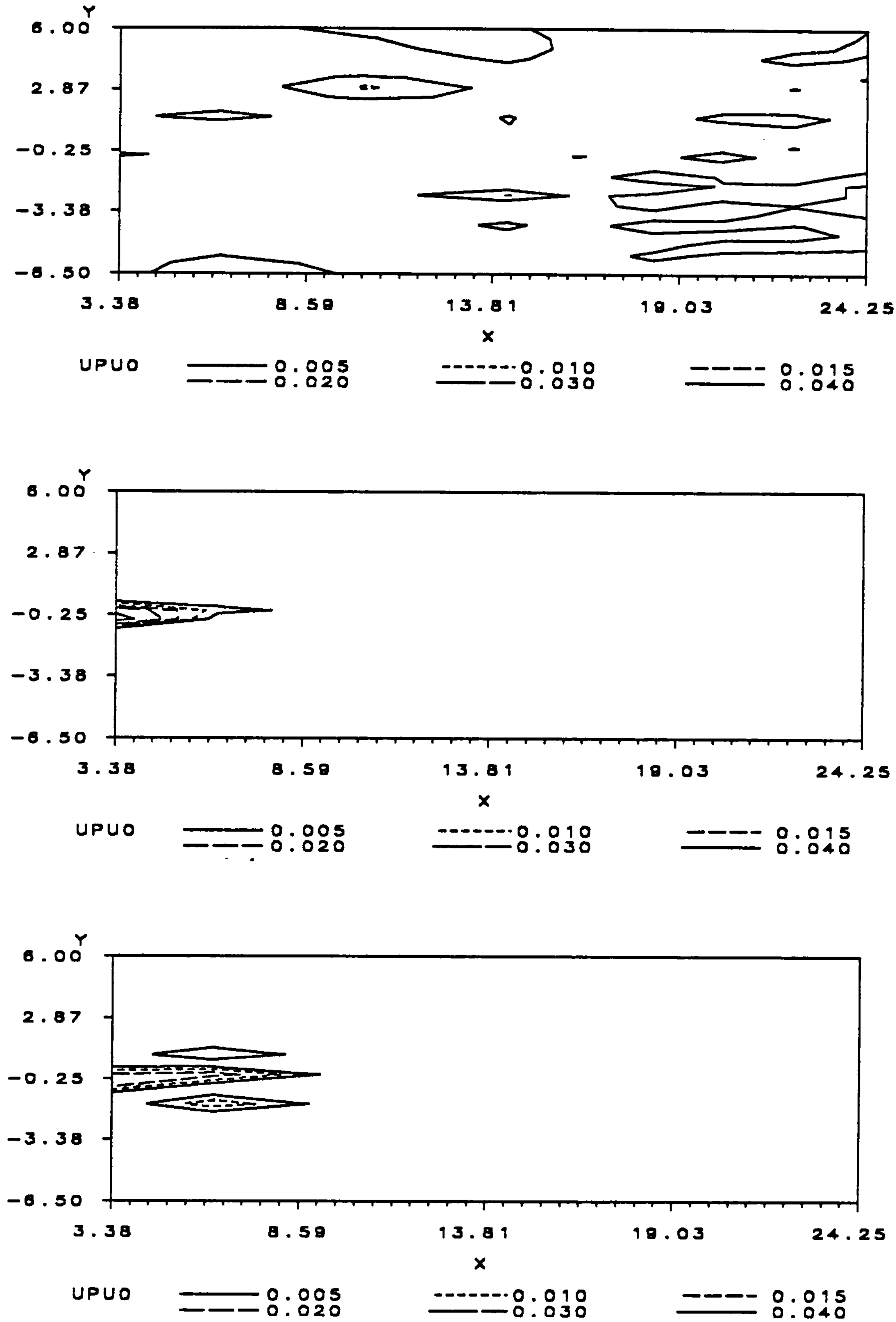

Figure 74. Axial turbulence contour plots for 4 Hz - 4 psig for bent tube inlet configuration. Top - t/T = 0.6250, center - t/T = 0.6667, bottom - t/T = 0.7083.

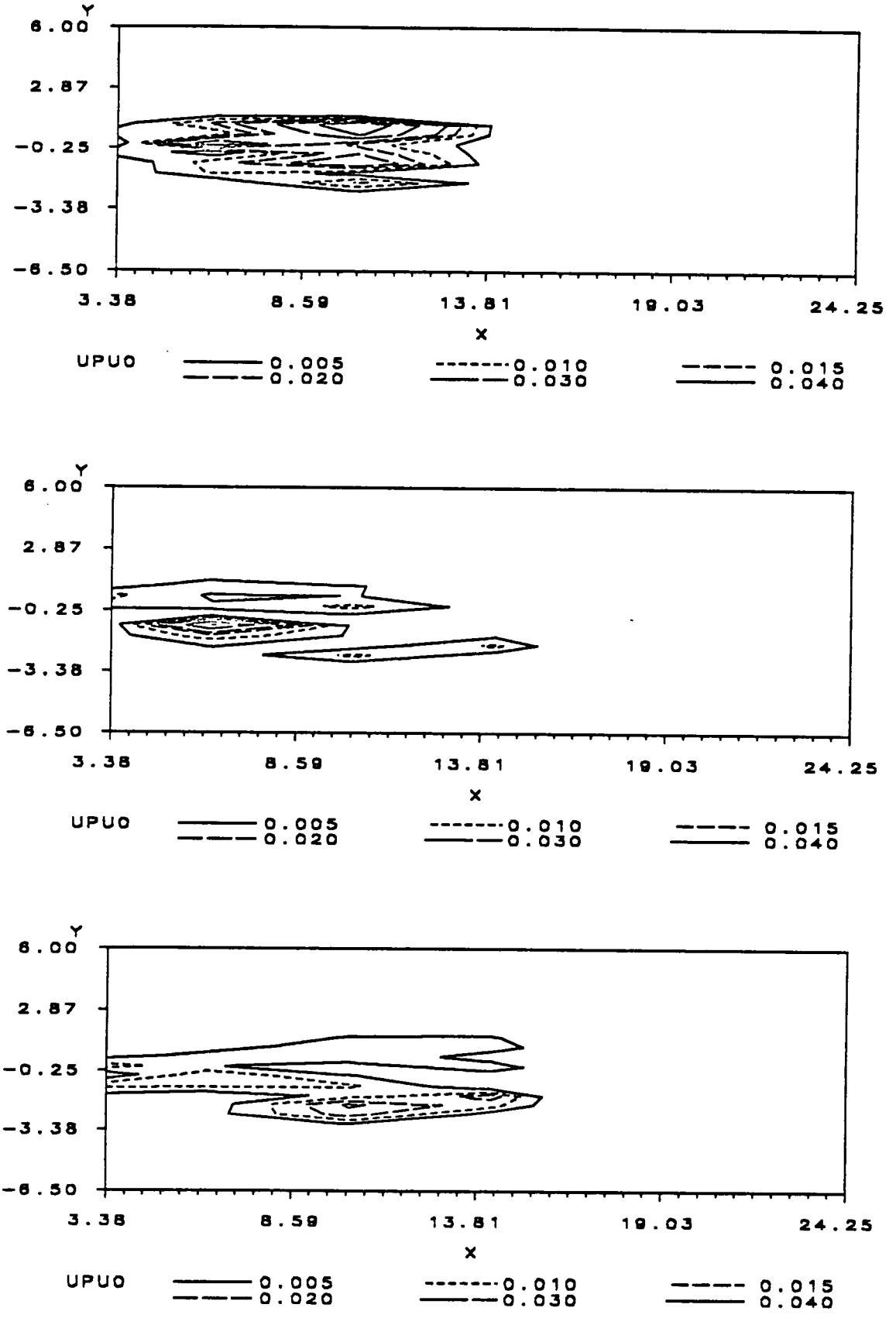

Figure 75. Axial turbulence contour plots for 4 Hz - 4 psig for bent tube inlet configuration. Top - t/T = 0.750, center - t/T = 0.7917, bottom - t/T = 0.8333.

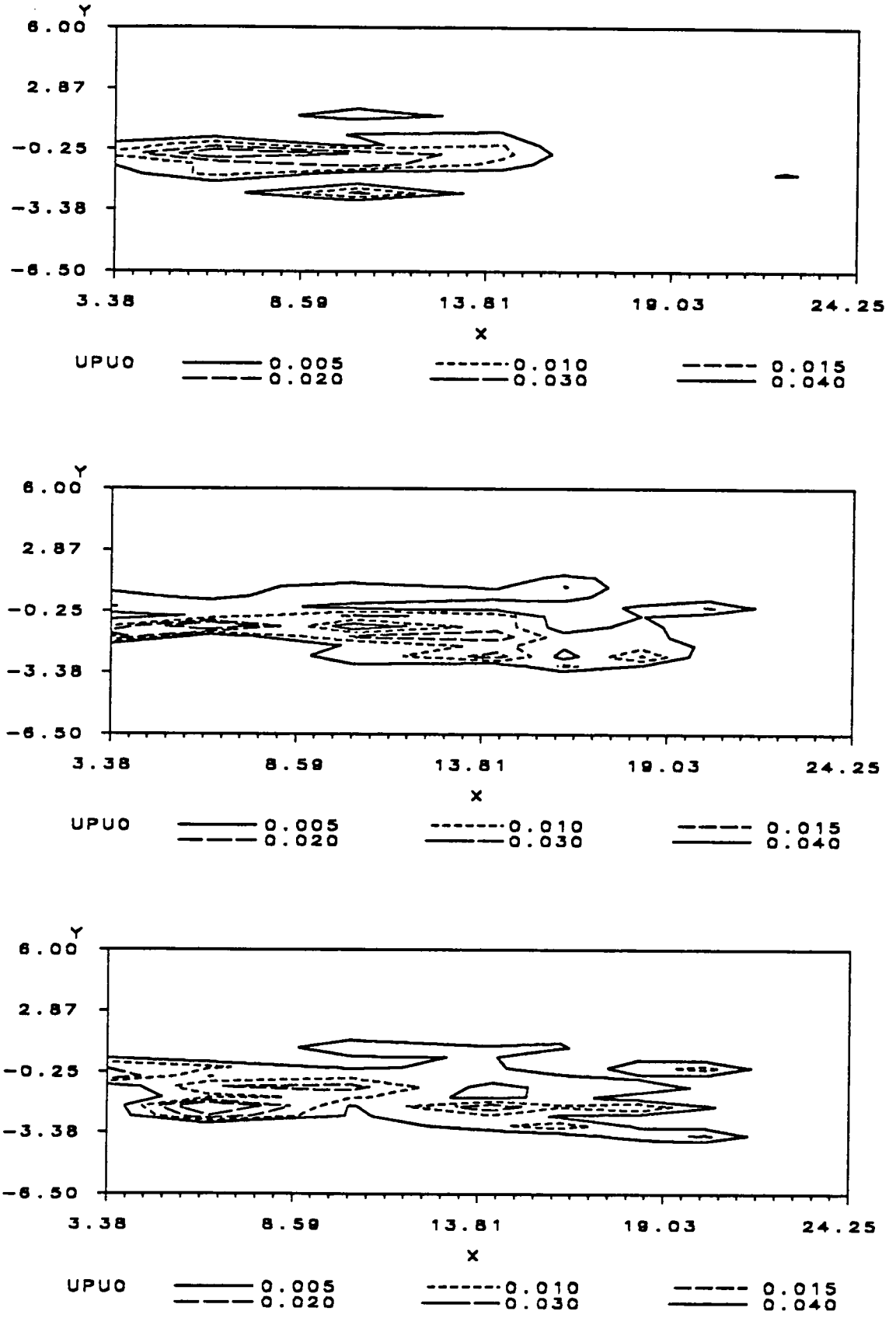

Figure 76. Axial turbulence contour plots for 4 Hz - 4 psig for bent tube inlet configuration. Top - t/T = 0.8750, center - t/T = 0.9167, bottom - t/T = 0.9583.

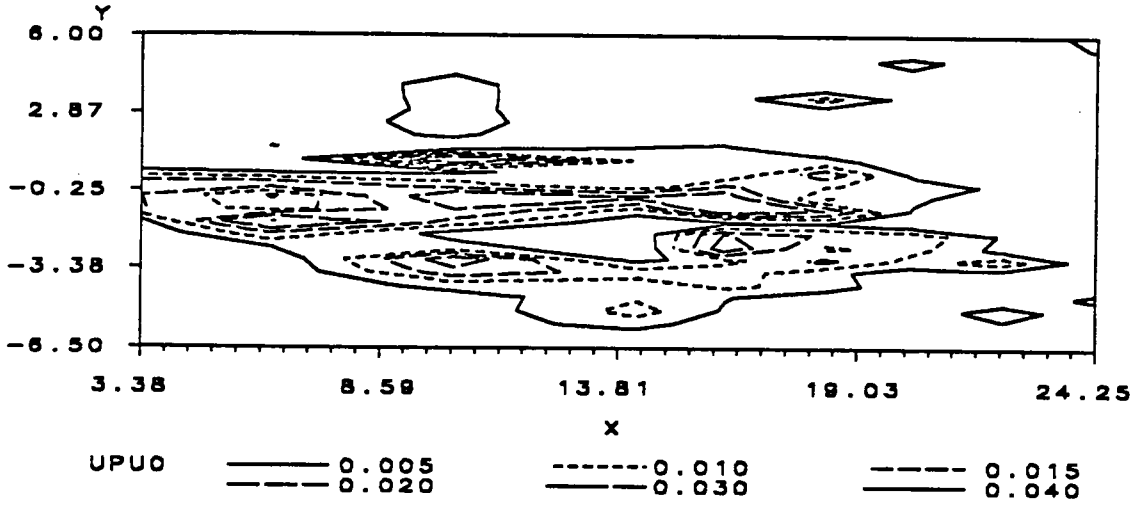

Figure 77. Axial turbulence contour plots for 4 Hz - 4 psig for bent tube inlet configuration. Top - t/T = 1.000.

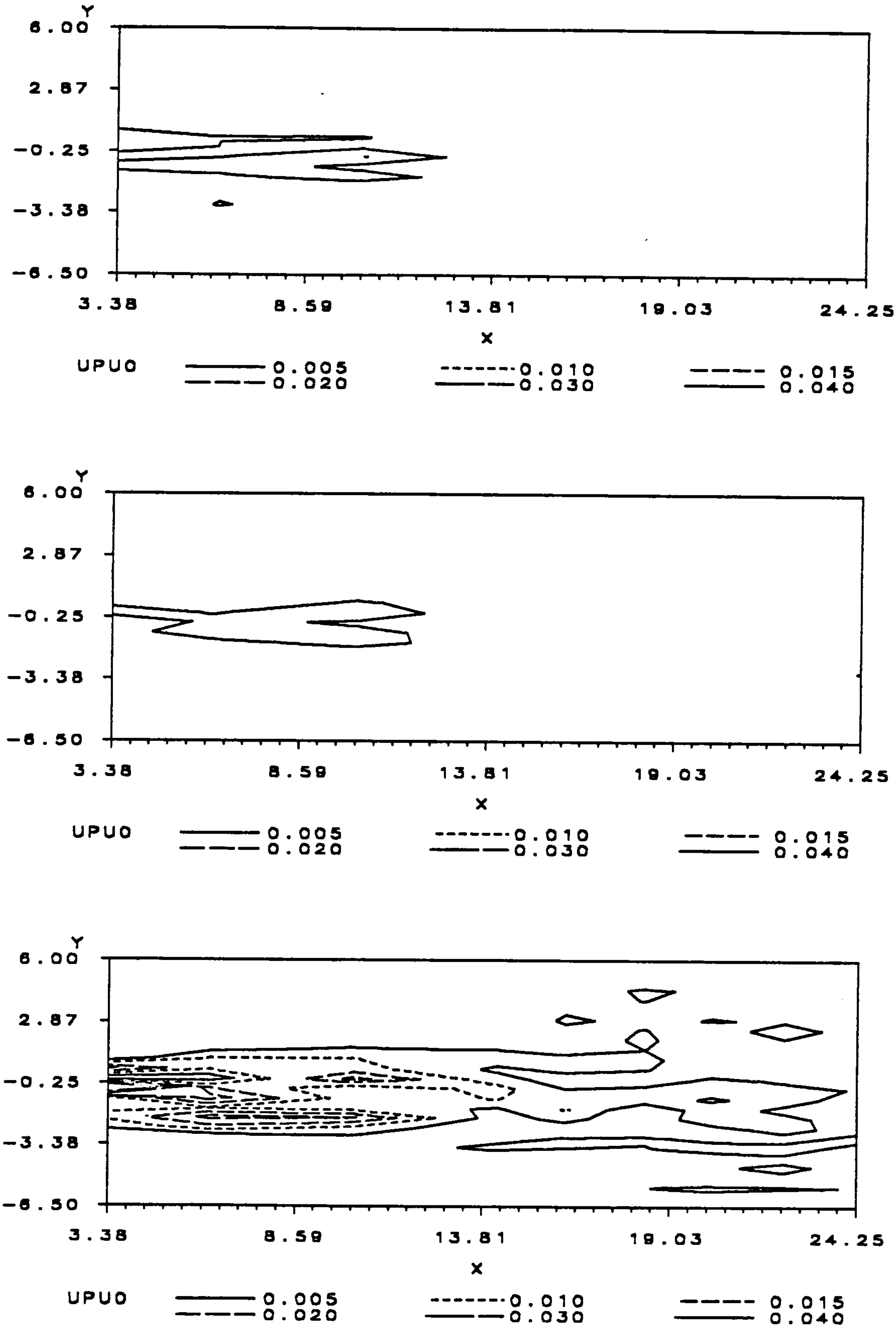

Figure 78. Axial turbulence contour plots for 8 Hz - 4 psig for bent tube inlet configuration. Top - t/T = 0.000, center - t/T = 0.091, bottom - t/T = 0.182.

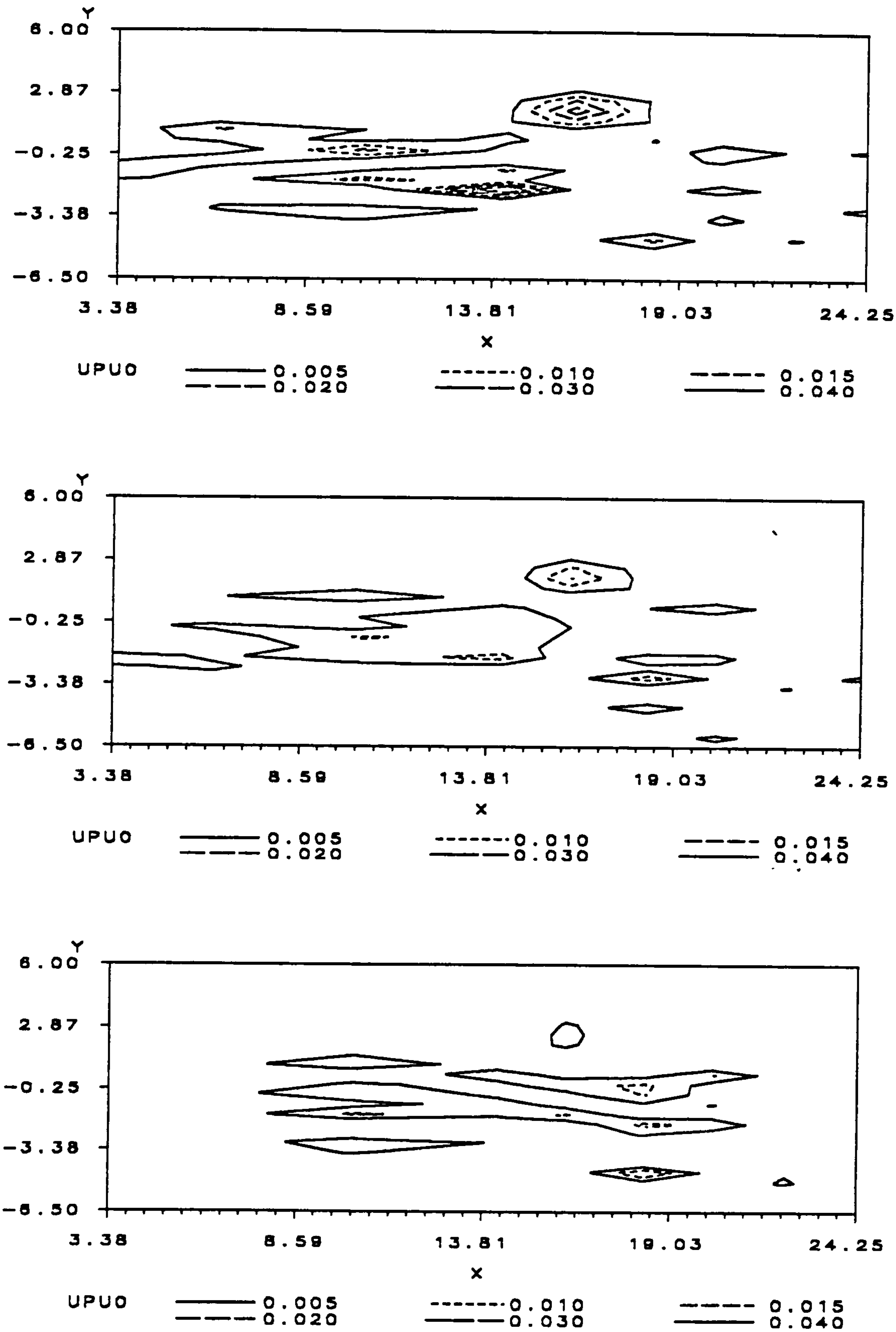

Figure 79. Axial turbulence contour plots for 8 Hz - 4 psig for bent tube inlet configuration. Top - t/T = 0.273, center - t/T = 0.364, bottom - t/T = 0.4545.

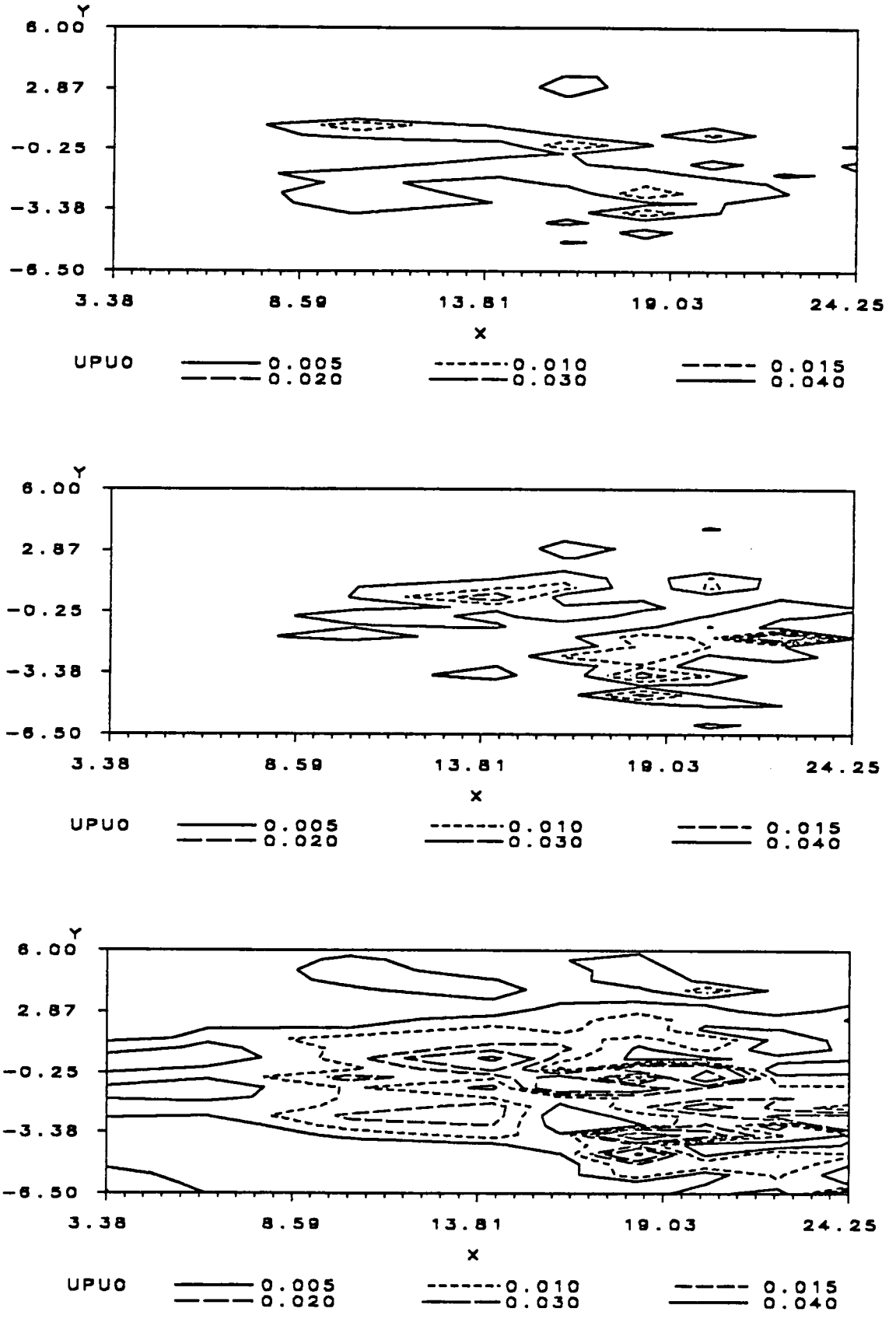

Figure 80. Axial turbulence contour plots for 8 Hz - 4 psig for bent tube inlet configuration. Top - t/T = 0.5454, center - t/T = 0.6364, bottom - t/T = 0.7273.

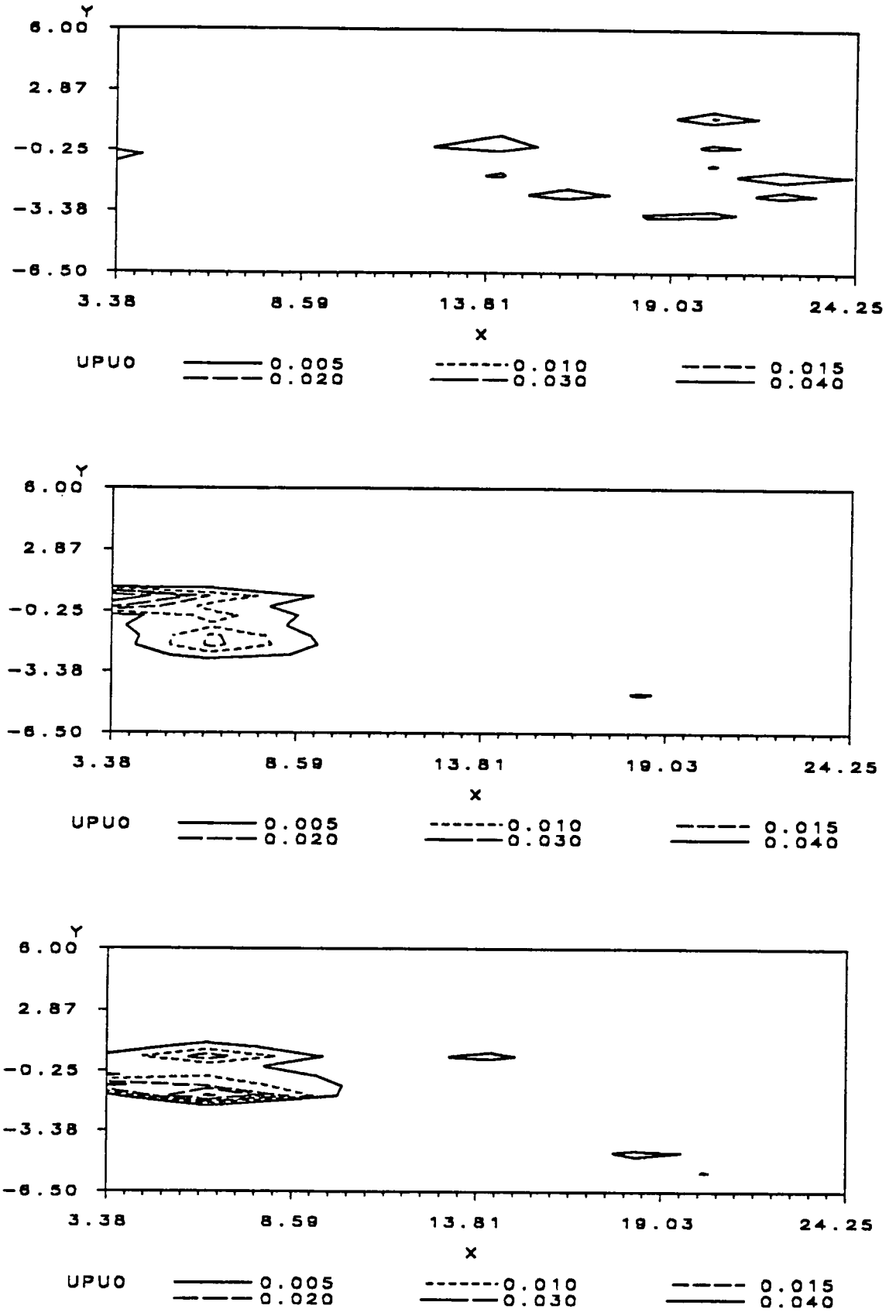

Figure 81. Axial turbulence contour plots for 8 Hz - 4 psig for bent tube inlet configuration. Top - t/T = 0.8182, center - t/T = 0.9091, bottom - t/T = 1.000.

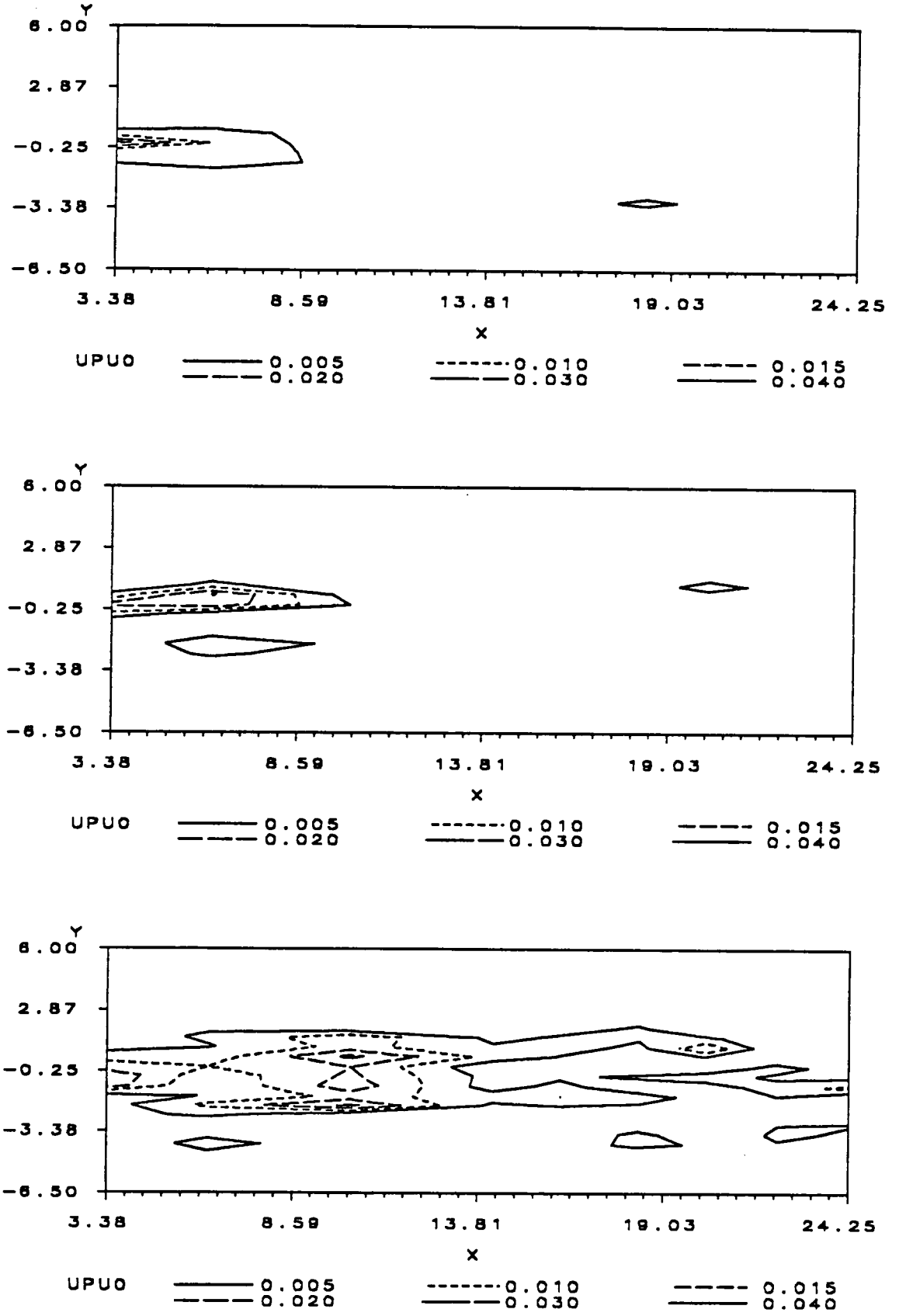

Figure 82. Axial turbulence contour plots for 12 Hz - 4 psig for bent tube inlet configuration. Top - t/T = 0.000, center - t/T = 0.143, bottom - t/T = 0.286.

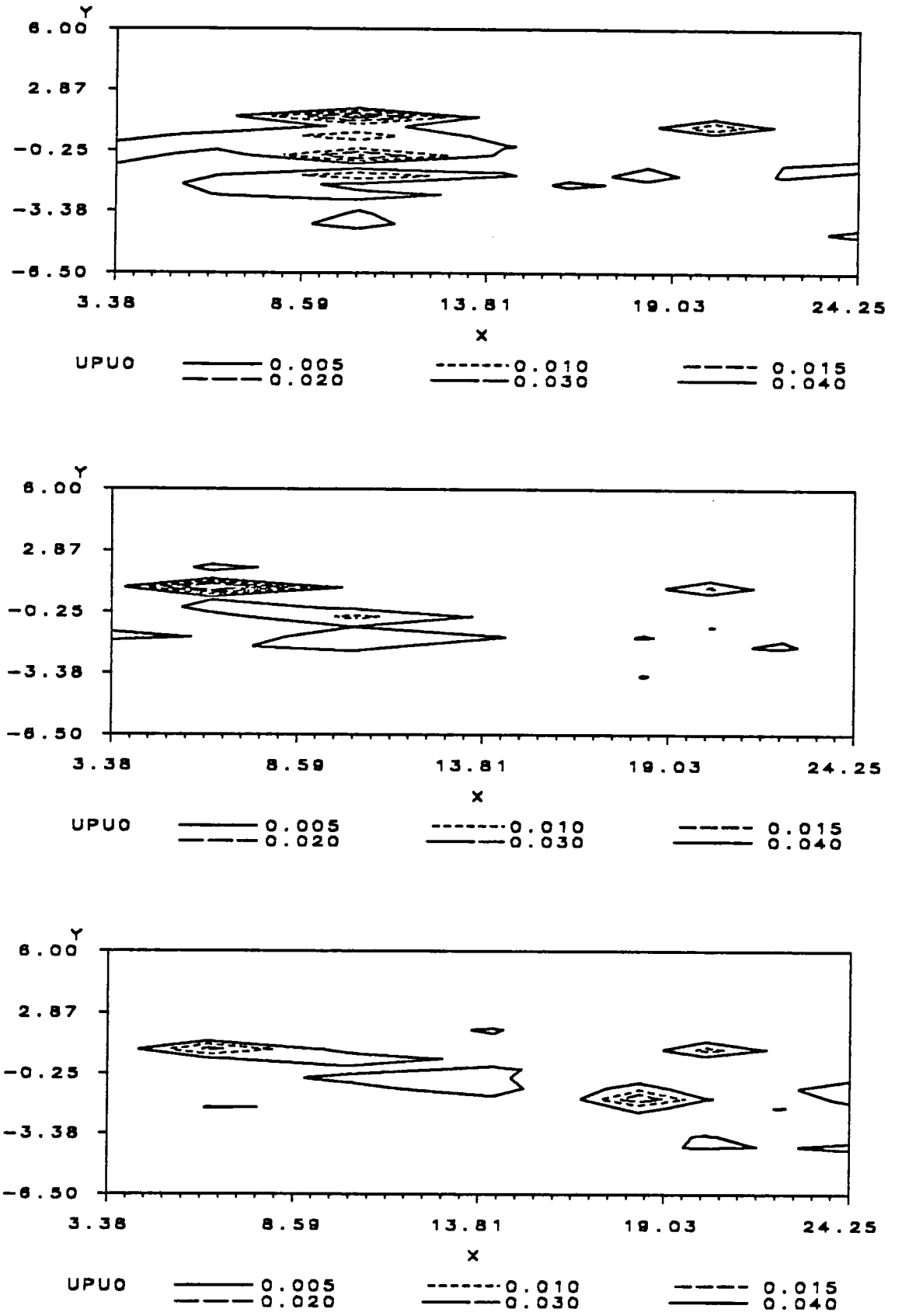

Figure 83. Axial turbulence contour plots for 12 Hz - 4 psig for bent tube inlet configuration. Top - t/T = 0.429, center - t/T = 0.571, bottom - t/T = 0.7143.

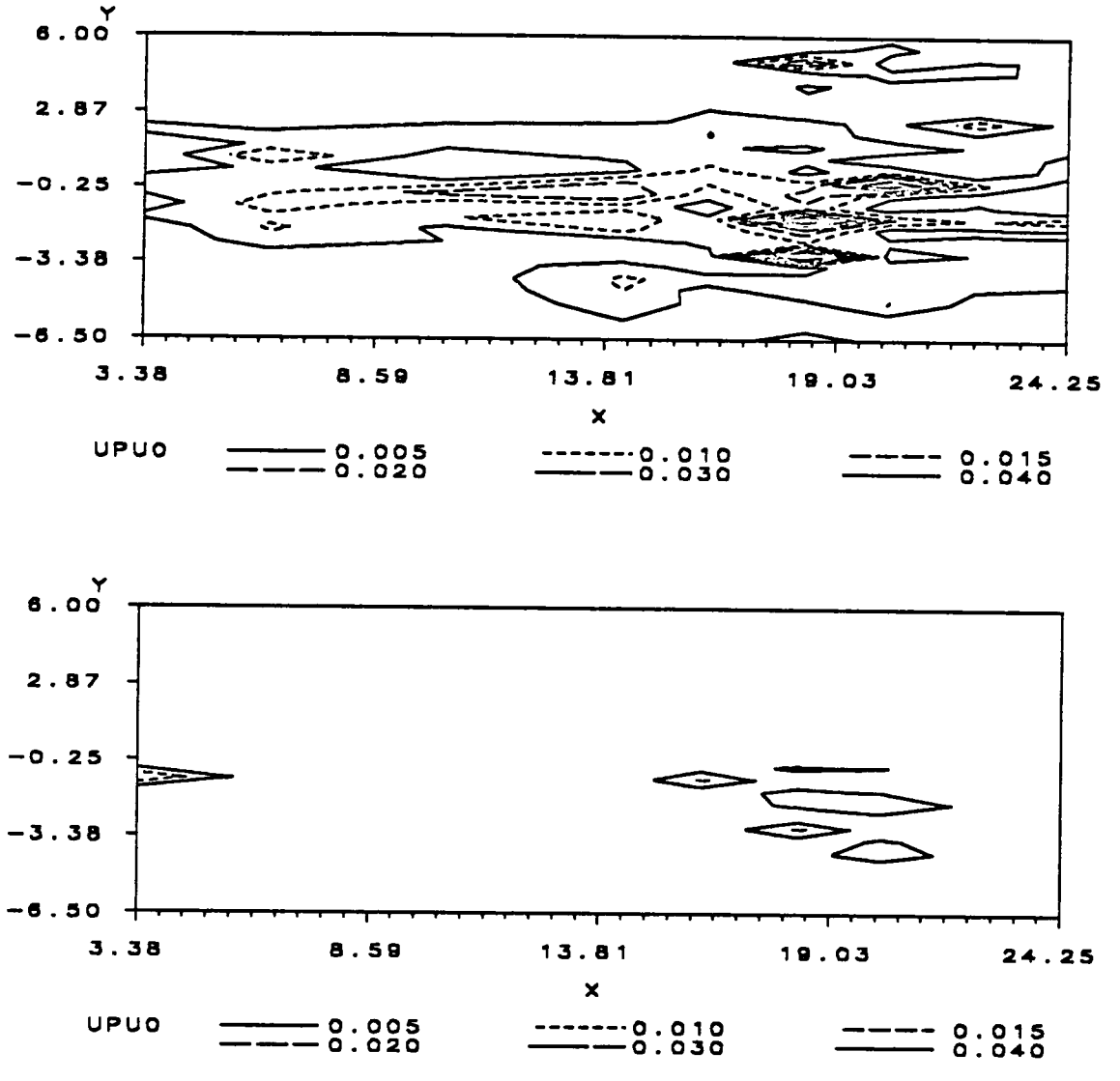

Figure 84. Axial turbulence contour plots for 12 Hz - 4 psig for bent tube inlet configuration. Top - t/T = 0.857, center - t/T = 1.000.

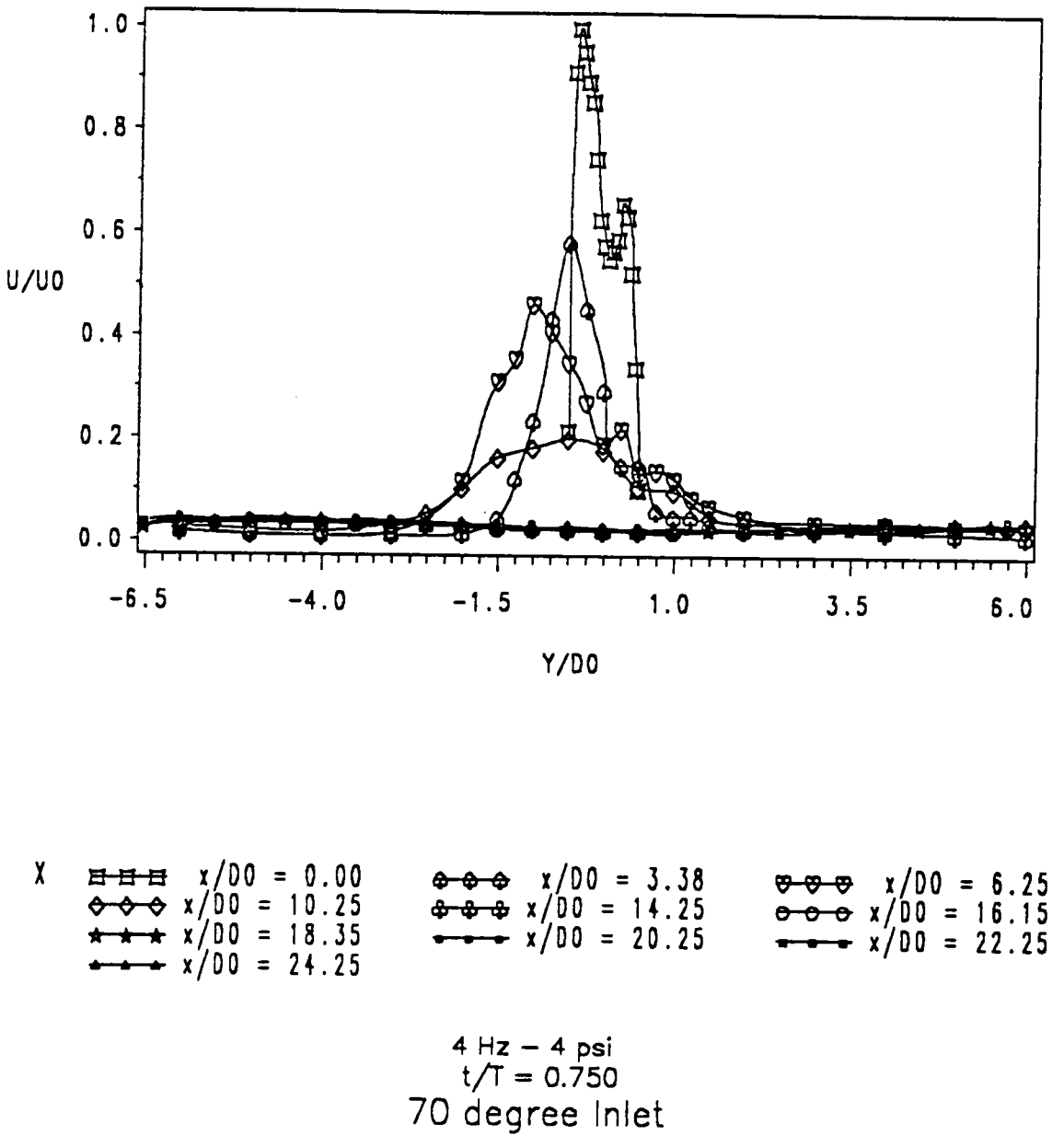

Figure 85. Phase-lock averaged mean velocity profiles for the bent tube case at 4 Hz and t/T = 0.750.

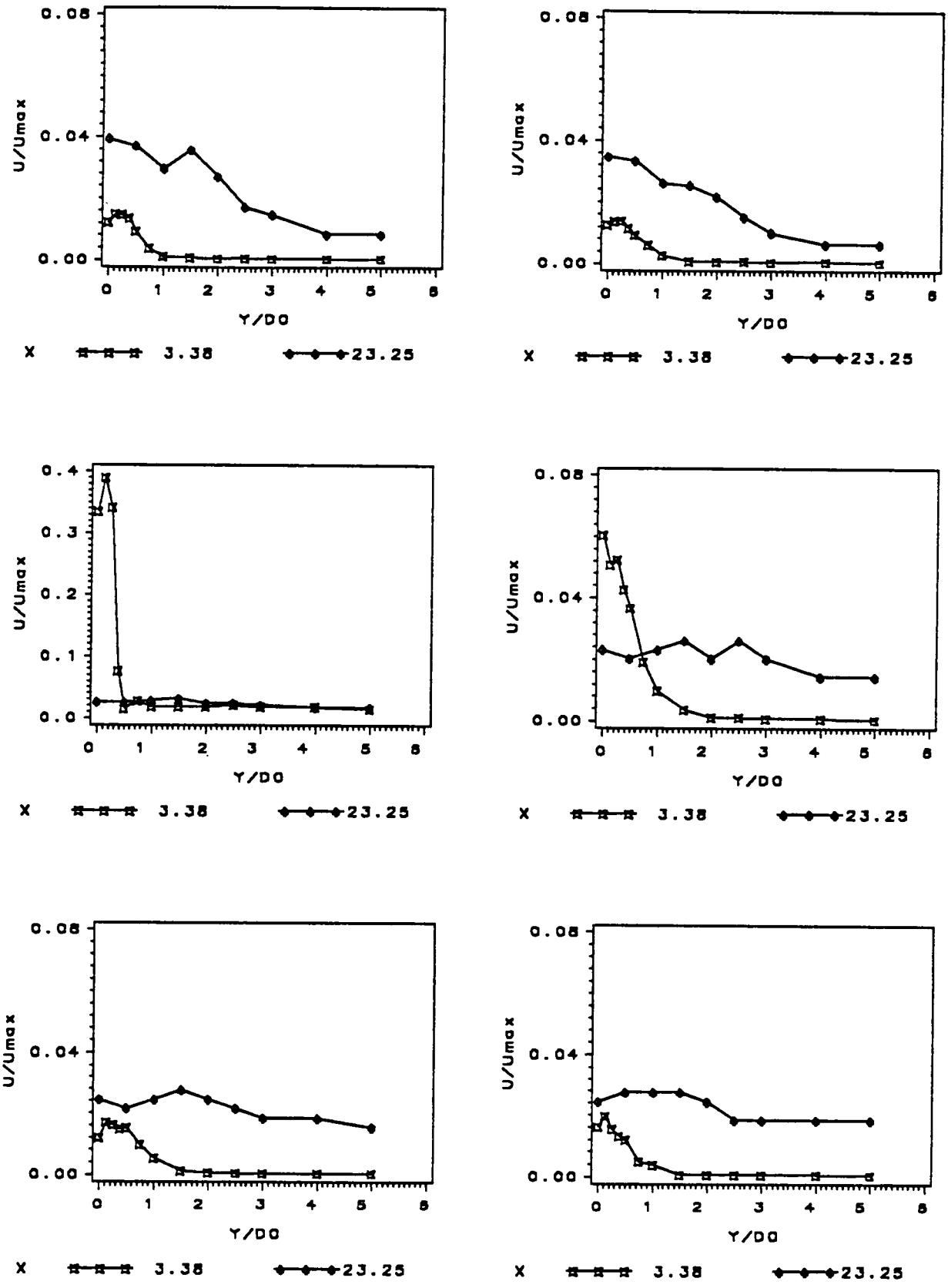

Figure 86. Axial turbulence plots for 4 Hz - 4 psig for straight tube inlet configuration during charging phases. Top - t/T = 0.000,0.041; center - t/T = 0.625,0.666; bottom - t/T = 0.708,0.750.

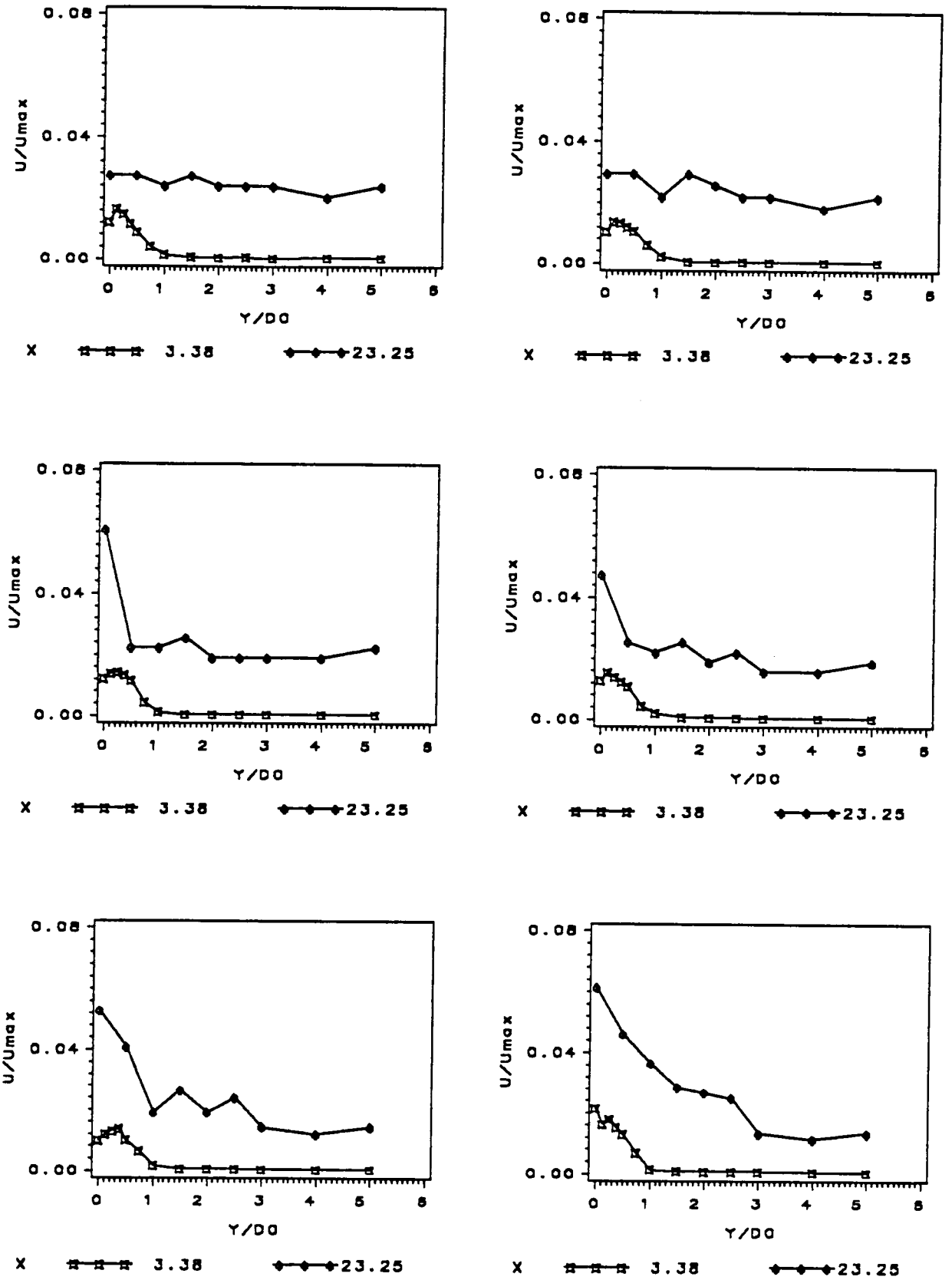

Figure 87. Axial turbulence plots for 4 Hz - 4 psig for straight tube inlet configuration during charging phases. Top - t/T = 0.791,0.833; center - t/T = 0.875,0.916; bottom - t/T = 0.958,1.000.

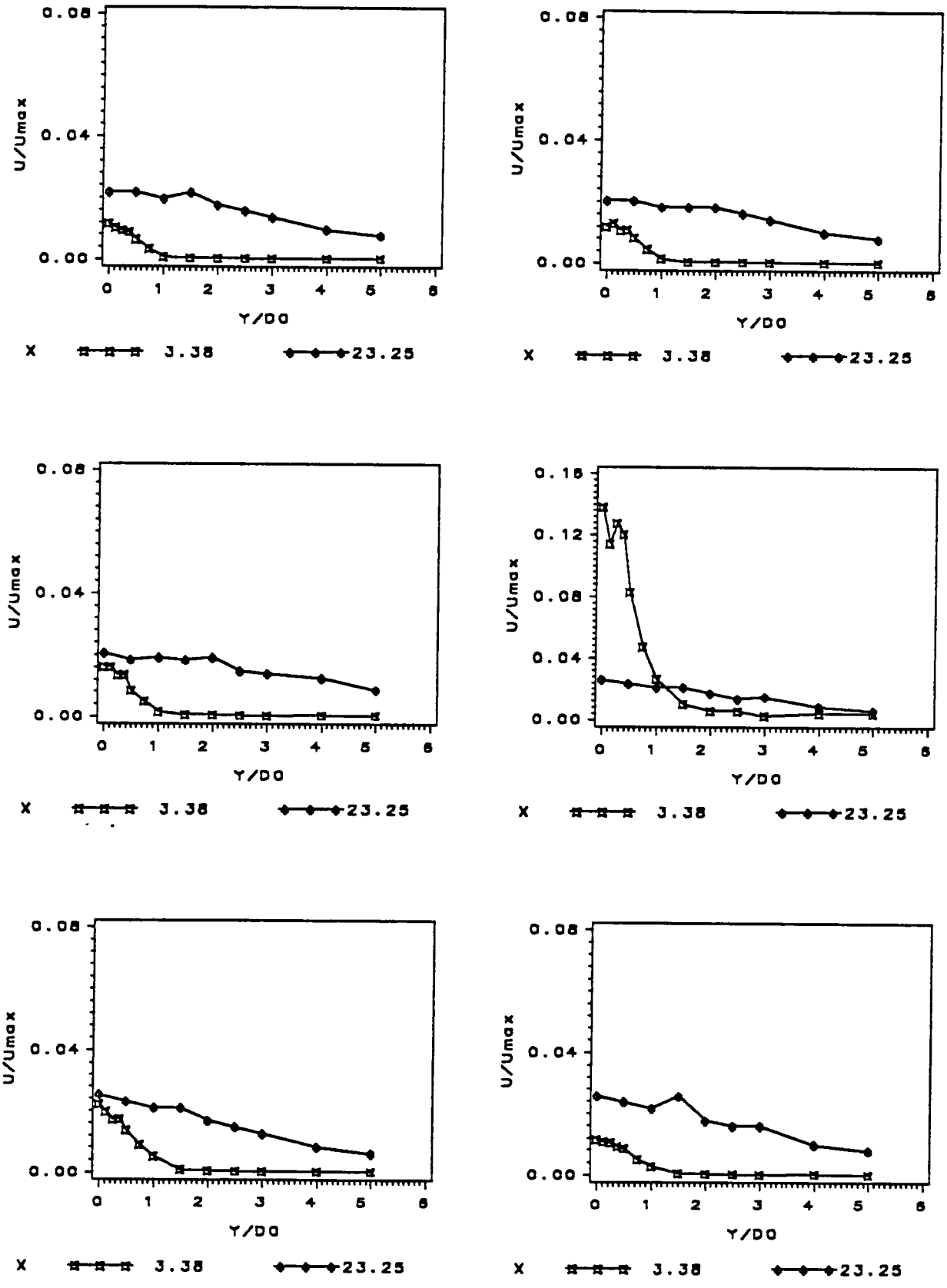

Figure 88. Axial turbulence plots for 8 Hz - 4 psig for straight tube inlet configuration during charging phases. Top - t/T = 0.000,0.091; center - t/T = 0.182,0.818; bottom - t/T = 0.909,1.000.

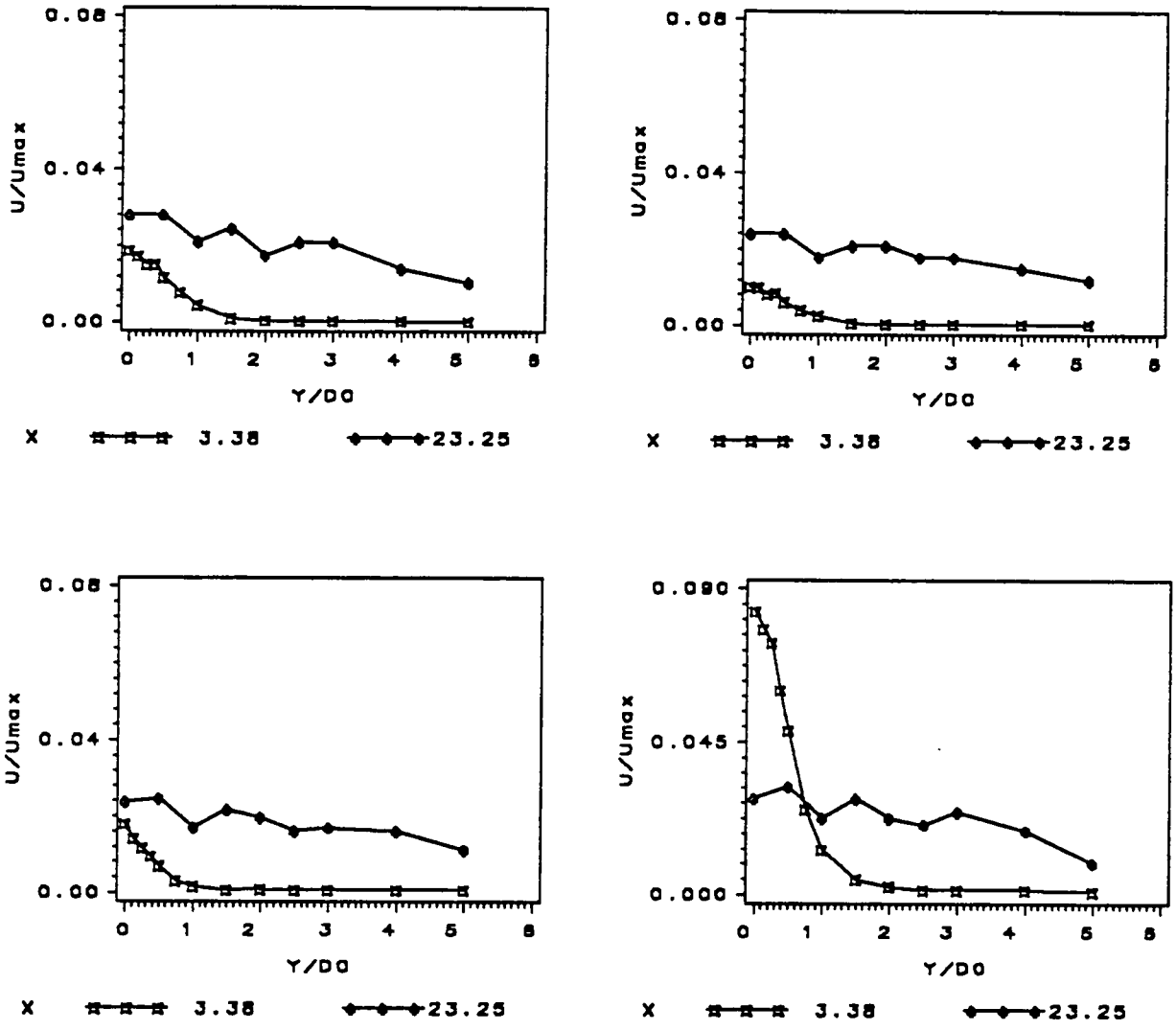

Figure 89. Axial turbulence plots for 12 Hz - 4 psig for straight tube inlet configuration during charging phases. Top - t/T = 0.000,0.143; center - t/T = 0.286,1.000.

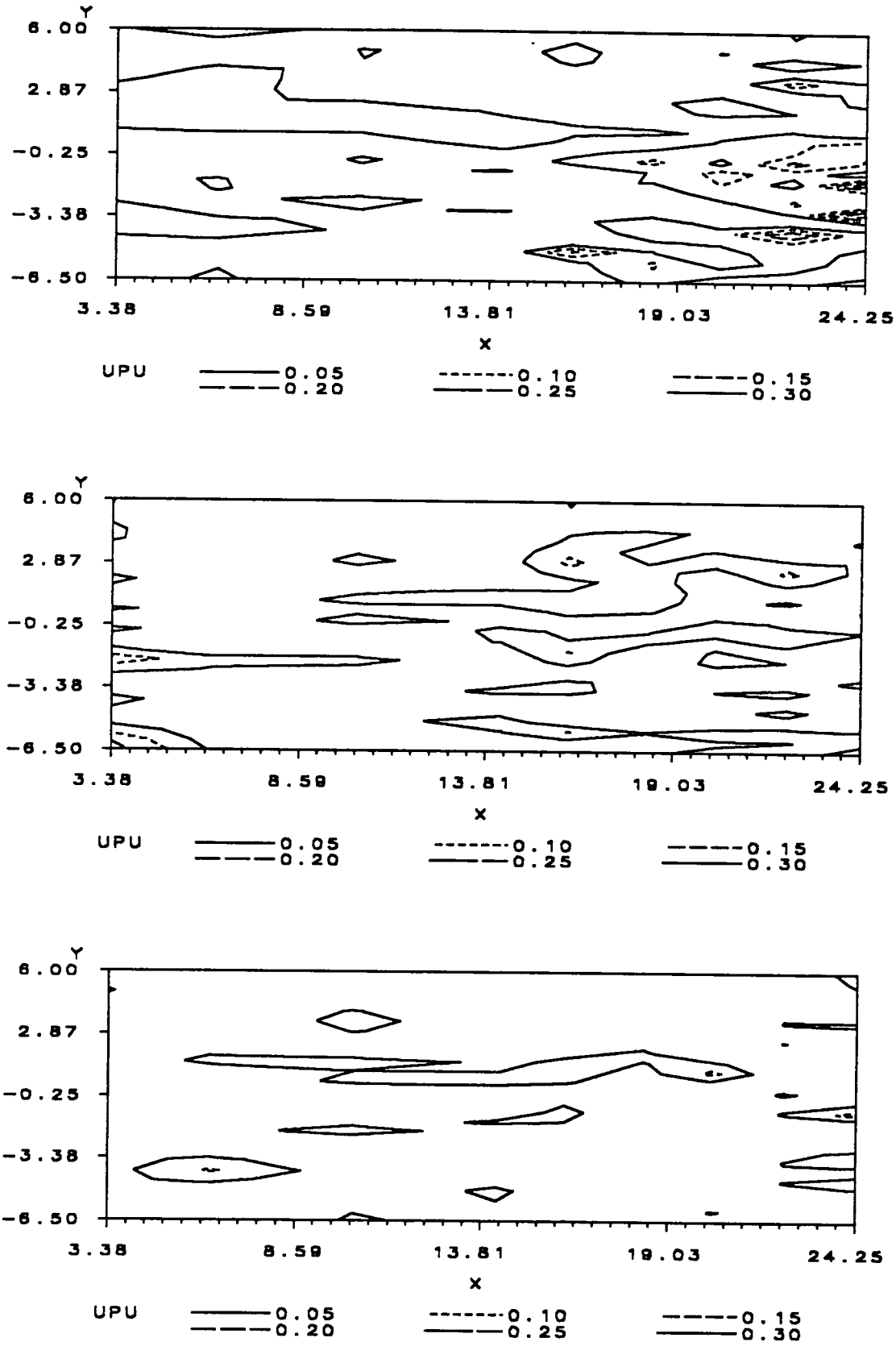

Figure 90. Axial turbulence contour plots for bent tube case for different frequencies. Normalized by local phase averaged velocity. Top - 4 Hz, t/T = 0.083; center - 8 Hz, t/T = 0.182; bottom - 12 Hz, t/T = 0.286.

The vita has been removed from the scanned document